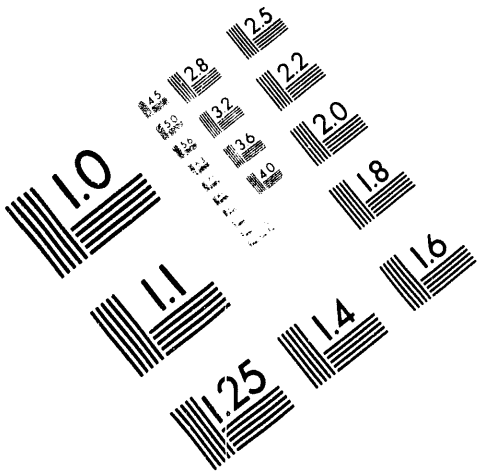

Association for Information and Image Management
1100 Wayne Avenue, Suite 1100
Silver Spring, Maryland 20910
301/587-8202

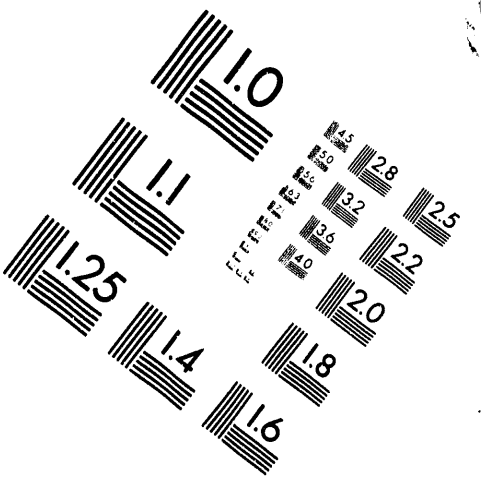

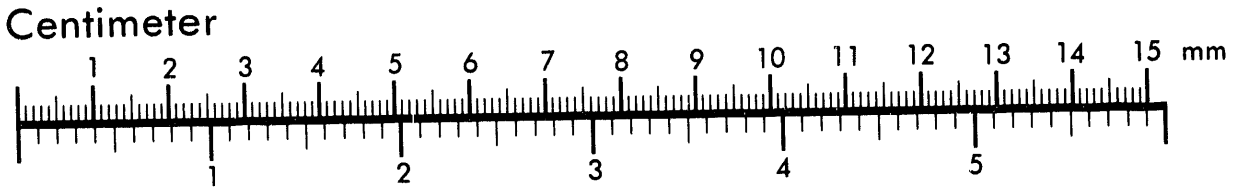

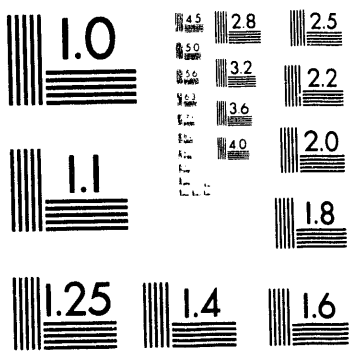

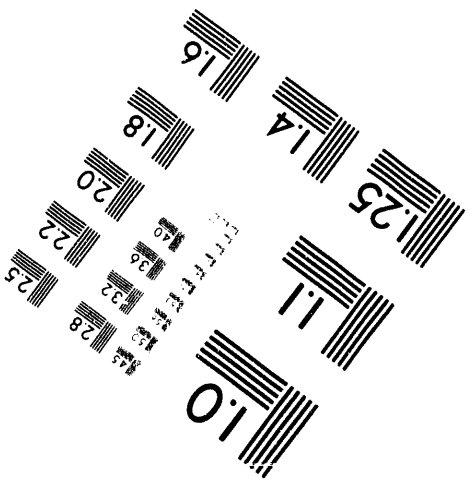

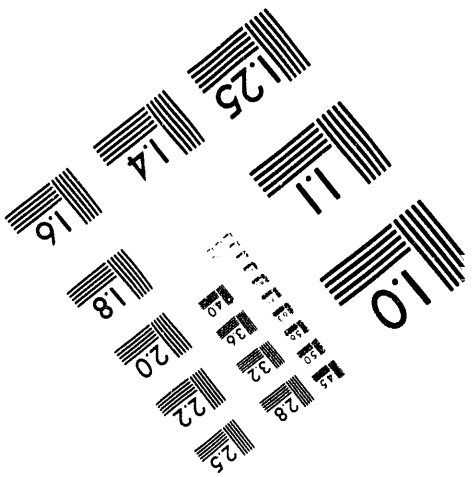

MANUFACTURED TO AIIM STANDARDS
BY APPLIED IMAGE, INC.

1 of 1

Lawrence Livermore National Laboratory

INERTIAL CONFINEMENT FUSION

ICF Quarterly Report

October – December 1992
Volume 3, Number 1

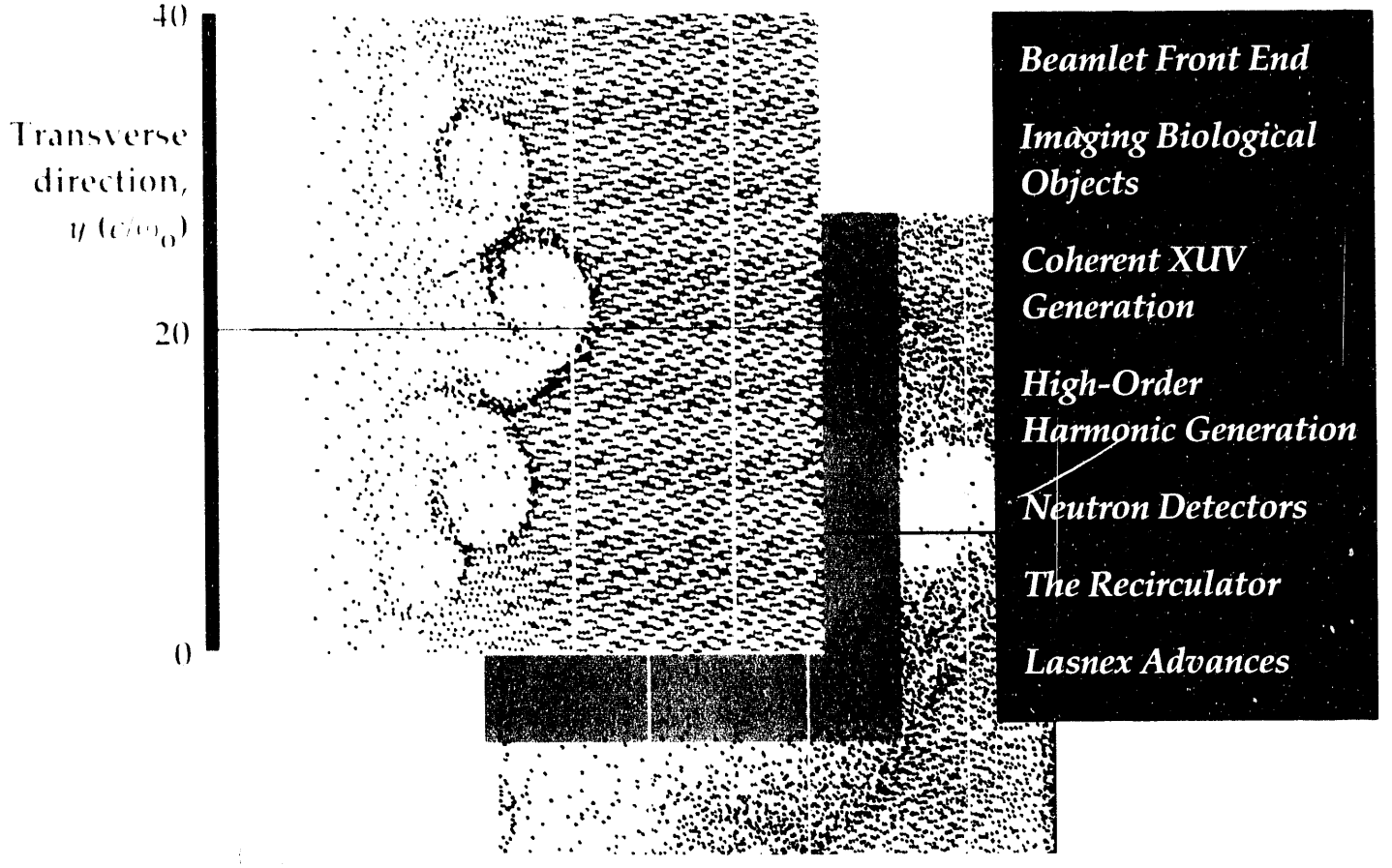

2-D Simulations of Ultra-Intense, Short-Pulse Laser Plasma Interactions

UCRL-LR-105821-93-1

The *ICF Quarterly Report* is published four times each fiscal year by the Inertial Confinement Fusion Program at the Lawrence Livermore National Laboratory. The journal reports selected current research within the ICF Program. Major areas of investigation presented here include fusion target theory and design, target fabrication, target experiments, and laser and optical science and technology. Questions and comments relating to the technical content of the journal should be addressed to the ICF Program Office, Lawrence Livermore National Laboratory, P.O. Box 5508, Livermore, CA 94551.

The Cover: The ions associated with a plasma that has been irradiated by an ultra-intense laser pulse are shown in two directions. The rippling of the critical surface is due to a Rayleigh-Taylor instability that develops as the laser (acting as the light fluid) pushes against the plasma at the critical surface (the heavy fluid). The bottom plot shows that eventually, since the light pressure associated with the central bubble is so large, a plasma void forms in the overdense plasma. This plasma-laser interaction can now be modeled and predicted by particle in cell (PIC) simulations. See the article, "Two-Dimensional Computer Simulations of Ultra-Intense, Short-Pulse Plasma Interactions," page 28.

UCRL-LR-105821-93-1
Distribution Category UC-712
October – December 1992

Work performed under the auspices of the U.S. Department of Energy by Lawrence Livermore National Laboratory under Contract W-7405-Eng-48.

Printed in the United States of America
Available from
National Technical Information Service
U.S. Department of Commerce
5285 Port Royal Road
Springfield, Virginia 22161
Price codes: printed copy A03, microfiche A01.

INERTIAL CONFINEMENT
FUSION

Quarterly Report

October – December 1992
Volume 3, Number 1

In this issue:

Foreword

This issue of *The ICF Quarterly* contains eight articles reporting on the progress on various activities within the Inertial Confinement Fusion Program.

The leading article, "The Beamlet Front End: Prototype of a New Pulse Generation System," discusses the system design and performance of the front end of the Beamlet Demonstration Project laser, which is being constructed as a testbed for future ICF laser systems. This laser system incorporates new technologies for spatial and temporal pulse shaping, bandwidth generation and amplification. The present performance of the front end has exceeded the requirements for achieving the full system milestone.

The second article, "Imaging Biological Objects with X-Ray Lasers," reports on the progress in developing x-ray lasers of ever shorter wavelengths and the advances in x-ray optics development for imaging of biological objects. The authors demonstrate imaging rat-sperm nuclei with resolution of about 500 Å with an x-ray laser at about 45 Å. The resolution is limited mainly by the limitations in the x-ray optics. Future improvements in x-ray optical technology should further improve this limit on resolution.

The next two articles, "Coherent XUV Generation via High-Order Harmonic Generation in Rare Gases" and "Theory of high-Order Harmonic Generation" present, respectively, the recent experimental and theoretical advances in the nonperturbative interaction of atoms with intense laser fields. Experimental results illustrate that high energy photons can be efficiently generated by very high-order harmonic emission by an atom subjected to an intense laser field. This process could have practical applications in developing sources of coherent XUV radiation. The theoretical article confirms the experimental observations and demonstrates how detailed, first-principle calculations can be used to determine optimal conditions for efficient harmonic generation.

The article "Two-dimensional Computer Simulations of Ultra-Intense, Short-Pulse Laser-Plasma Interactions," continues along the theme of theoretical investigations of interactions of intense laser with matter—in this case a preformed plasma. It is shown that the laser absorption can be very high and that MeV electrons can be produced because of the tremendous ponderomotive acceleration.

Recent progress in developing high-resolution, time-of-flight neutron detectors is reported in the article "Neutron Detectors for Measuring the Fusion Burn History of ICF Targets." Since neutrons escape the target without encountering collisions, a time resolved detection of neutrons provides an accurate "movie" of the target implosion. The 20-ps resolution, scintillator detector should prove to be a powerful diagnostic tool for characterizing target implosions.

The next article, "The Recirculator," provides an overview of a conceptual design and cost analysis for a heavy ion fusion reactor. The authors show that the use of recirculating induction accelerators to boost the energy of the heavy ions can lead to substantial cost savings. Several engineering and physics issues associated with this design are also discussed.

The last article, "Lasnex Evolves to Exploit Computer Industry Advances," briefly outlines the improvements made to the Lasnex codes to make them more powerful, user friendly, portable from machine to machine, and to conform to industry standards. The ability to do production runs on workstations, rather than on Cray supercomputers, has lead to substantial cost savings.

The issue concludes with the Nova facility report and a list of publications from within the ICF program.

Shamasundar N. Dixit
Scientific Editor

THE BEAMLET FRONT END: PROTOTYPE OF A NEW PULSE GENERATION SYSTEM

B. M. Van Wonterghem
D. R. Speck
M. J. Norman
V. Karpenko
R. B. Wilcox

Introduction

In conceptual designs[1] for new ICF facilities, multimegajoule Nd:glass-based laser systems irradiate targets. To achieve the required cost efficiency, extensive use is made of very high density multisegment amplifiers in a multipass configuration with high beam fill factors. Large aperture optical components in such facilities will experience very high fluences and require sufficient bandwidth to suppress the damage and energy loss caused by stimulated Brillouin scattering.[2,3] In addition, various target irradiating schemes require large bandwidth and flexible pulse shaping. With the technology employed in the Nova front end, it would be exceedingly expensive to build a pulse generation and distribution system that would satisfy the requirements of multimegajoule lasers. A front-end system with more flexibility, better stability and reliability, and lower initial and operating cost is needed.

The Beamlet Demonstration Project is being constructed as a testbed for the basic physical principles on which future ICF laser systems will be based.[4] For this project, we developed and finished the initial testing of an advanced front end. This front end system makes extensive use of new technologies to provide reliable operation and simultaneous flexible spatial beam shaping, temporal pulse shaping (200 ps to 10 ns), bandwidth generation (up to 30 GHz), and output pulse energies exceeding 10 J.

We produced 3-ns output pulses with energy up to 10.5 J and a flat-topped 5 × 5 cm beam profile. We also demonstrated amplification of shaped pulses with a 15:1 contrast and bandwidth exceeding 48 GHz. The present performance exceeds the expected input energy required for driving the Beamlet laser to its milestone shot (5 kJ at 3ω in a 3-ns pulse).

Here we describe the system components and performance, based upon over 100 full front end shots being completed since we achieved the assembly milestone in September 1992.

System Architecture

Figure 1 shows a schematic diagram of the front end and identifies five main subsystems. The master oscillator is a diode pumped Nd:YLF microchip laser operating in a single longitudinal mode. Its output is chopped, amplified and fed into a single mode optical fiber. The resulting 1-μs pulses are coupled into an optical integrated circuit that produces shaping and bandwidth. The temporally and spectrally shaped pulses are then sent out to the preamplifier section in the laser bay through a 60 m long optical fiber. Figure 2 provides a view of the amplifier system mounted on a space frame. A regenerative amplifier provides a large gain and feeds a spatial beam shaper that produces a square beam with smooth, but steep edges. The beam is magnified to its final size and preamplified in a novel 4-pass rod amplifier. The output beam is relayed into the Beamlet cavity through two transport spatial filters.

Oscillator and Pulse Forming System

The master oscillator is a diode pumped Nd:YLF microchip laser operating in a single longitudinal mode at 1053 nm. A Pockels cell reduces the duty factor by chopping the CW output into 1-μs pulses at a 1-kHz rate. These pulses are launched into a single mode,

polarization preserving optical fiber after being amplified by a diode laser pumped CW slab amplifier. The peak power is about 250 mW at this point. The fiber couples the pulses into an advanced optical integrated circuit that produces shaping and bandwidth. This $LiNbO_3$ waveguide circuit has two amplitude modulators and a phase modulator, which are driven by low voltage external circuitry. The present device has an insertion loss of less than 5 dB, while the combined extinction ratio of the modulators exceeds 50 dB. These are very important parameters because they ultimately determine the prepulse contrast of the shaped pulse and the signal-to-noise ratio of the following preamplifier. In contrast to the highly resonant discrete modulators being installed on Nova and the Optical Sciences Laser, the waveguide electro-optic phase modulator is a travelling wave device with a wide bandwidth up to 17 GHz. The π-modulation voltage remains however weakly frequency dependent. A detailed description of the oscillator and pulse forming system has been published previously.[5]

A significant operational advantage of this system is the provision of high-quality polarization preserving connectors for coupling between fibers and devices. These allow for repeatable and alignment free reconfiguration of components and diagnostics. Fiber-optic splitters and switches are being used to route optical signals to various diagnostics. Except for the master oscillator breadboard, all hardware is rack-mounted (Fig. 3).

Using the present master oscillator, the pulse delivered to the high bay preamplifier has a peak power of 5–8 mW, equivalent to an energy of 15–24 pJ in a 3-ns pulse. The 60-m length of the transport fiber to the high bay does not exceed critical lengths for dispersion L_D and self-phase modulation L_{nl} for normal operating conditions. For a 10-mW peak power and a 100-ps rise time, we calculate L_D to be 450 m and L_{nl} 43 km, assuming typical values for fiber and material dispersion.[6]

Regenerative Amplifier

Bringing the energy from picojoule to joule levels requires amplification by 12 orders of magnitude. The

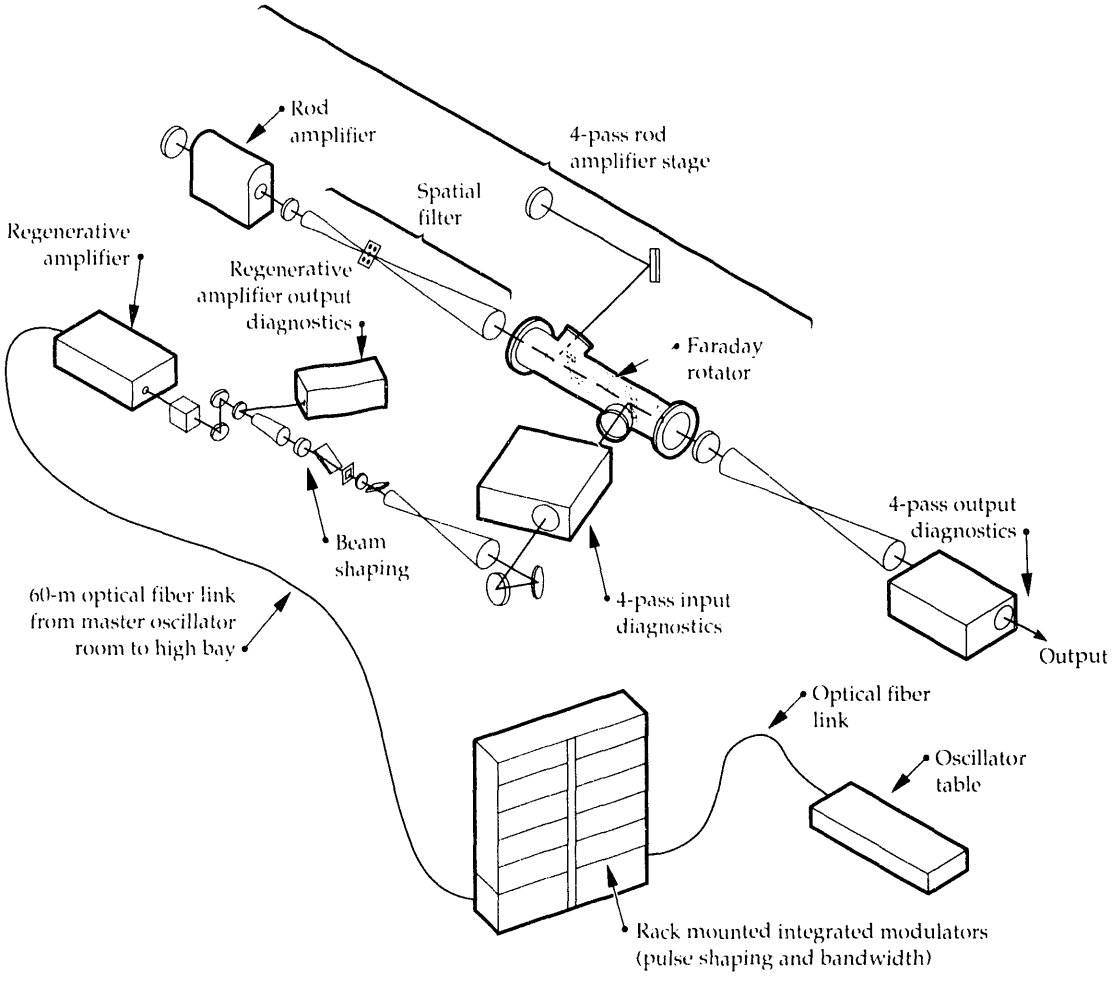

FIGURE 1. Schematic diagram of the Beamlet front end system, identifying the major subsystems: master oscillator, pulse forming system, regenerative amplifier, spatial beam shaping, and a 4-pass 5-cm-diam rod amplifier. A 60-m optical fiber transports the pulses from the oscillator room to the laser bay. The output transport filter relays the beam to the Beamlet cavity injection system. Diagnostic packages are located at the output of the regenerative amplifier, and the input and output of the 4-pass rod amplifier.

amplification process must maintain pulse shape within controlled limits, maintain the bandwidth while avoiding phase-to-amplitude-modulation conversion, and add minimal noise to maintain the high contrast. Conventional front-end technology applies the shaping and phase modulation to much stronger signals. The most convenient method to achieve high gain is to inject the pulse in a resonant cavity with a moderate gain rod amplifier ($1.5 < G < 6$).[7] To maintain the temporal shape, the amplifier must operate in its linear regime; the pulse must leave the cavity before gain depletion effects become important. This amplification system is known as a regenerative amplifier.[8]

We adapted the ring regenerative amplifier design currently used in chirped pulse amplifier systems.[9] Figure 4 shows a diagram of the amplifier. Two Faraday isolators prevent the return of amplified spontaneous emission pulses to the modulators. The ring cavity is made up using two thin film polarizers and two high reflectors. A KD*P Pockels cell is used as switching element in combination with a z-cut quartz 90° rotator. With no voltage applied to the Pockels cell, the pulses make one single round-trip through the ring before leaving through the exit polarizer. When the Pockels cell is switched to half-wave retardation, the pulse remains in the cavity and undergoes amplification until the half-wave voltage is switched off. Leakage through the exit polarizers (< 0.2%) is blocked by a pulse slicer. The cavity round trip time amounts to 13.4 ns, but the 1-ns rise and fall time of the Pockels cell limit the useful gain window to 10 ns.

We modified the ring cavity by introducing two lenses, each having a focal length $L/4$, where L is the total circumference (about 4 m). The input aperture is therefore image relayed onto itself after one round trip, while the second aperture acts as a spatial filter in the focal plane. The output beam has a symmetric, nearly Gaussian profile. The thermal relaxation time of the 4-mm-diam amplifier rods is 9.6 s. A 0.2-Hz repetition rate prevents undesirable build-up of thermal lensing and birefringence.

Two Nd:glass heads provide a combined small signal gain up to 6. The energy stored in the mode volume amounts to ~150 mJ. The amplifier operates in the linear operating region by switching out the pulse after approximately 14 round trips; this avoids pulse shape distortion (PSD) by gain depletion. At output energy levels between 5 and 7 mJ, the PSD is less than 10%. When operating in the linear gain regime, it is advantageous to keep the gain per round trip low, while maintaining sufficient stored energy and minimizing passive losses in the cavity. The use of two different athermal phosphate

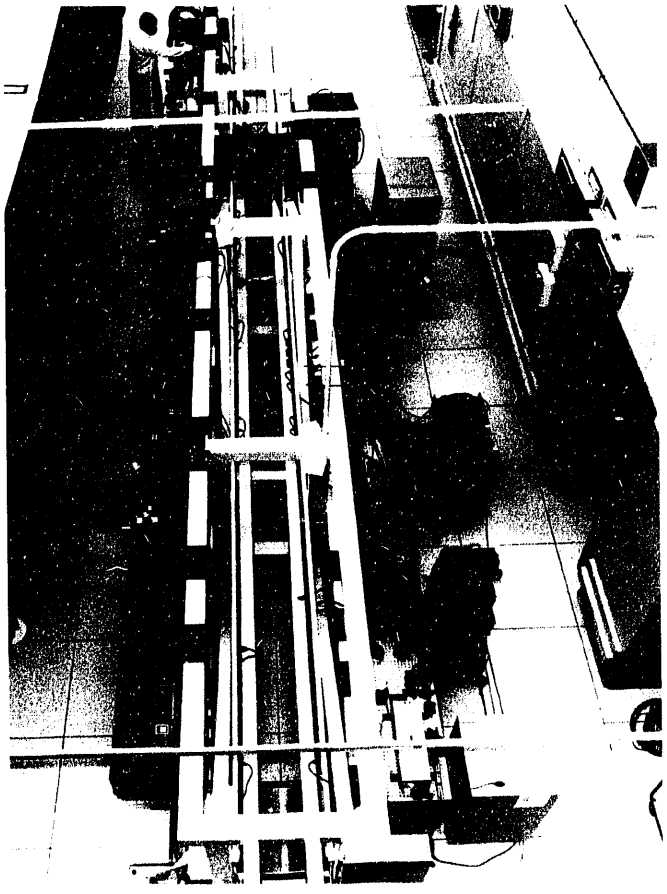

FIGURE 2. View of the front end preamplifier section in the laser bay. It consists of a regenerative amplifier, beam shaper, and 4-pass rod amplifier.

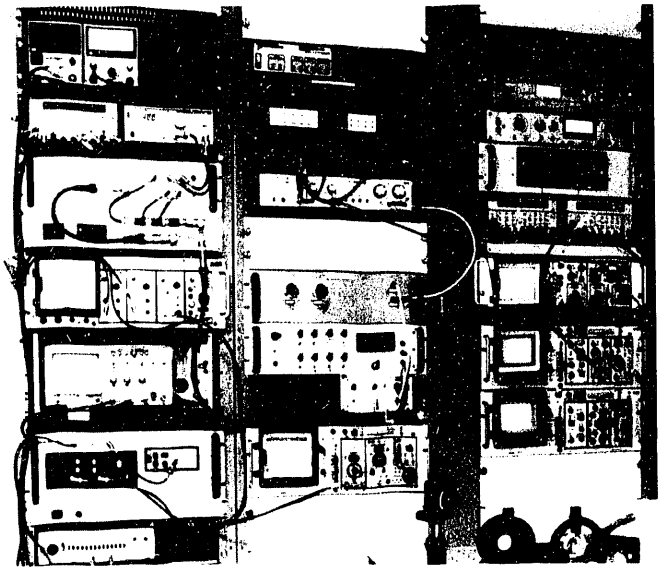

FIGURE 3. The Beamlet pulse forming system is completely rack mounted. Beam transport is accomplished using single mode optical fibers.

glass rods, APG-1 (Schott) and HAP-3 (Hoya), extends the gain bandwidth around the center Nd:YLF wavelength.[8] When operating the regenerative amplifier at a net gain of 10^{10}, we observed a gain bandwidth (FWHM) of 30 Å, sufficiently large to amplify phase modulated pulses with several Å bandwidth.

Output energy stability is an important issue for multipass amplifiers. The ratio of relative standard deviation of the output energy to that of the input energy in a multipass amplifier operating in the linear regime is given by the natural logarithm of the total gain. A reasonable output stability requires exceptional pump stability of the amplifier rods. We achieved pump stabilities on the order of 0.2% using low pressure flashlamps and optimized pulsed power supplies. However, stability degrades quickly as the lamps age, and alternative methods are being investigated.

Spatial Beam Shaping

The Gaussian beam from the regenerative amplifier needs to be converted to a square flat-topped beam for injection in the rod amplifier. Figure 5 illustrates the various steps in the beam shaping process. The regenerative amplifier output pulses are expanded in a 7.5× Galilean telescope to a collimated beam with radius of 10 mm. A combination of four quartz birefringent lenses imposes a radially varying retardation on the beam. In combination with a polarizer, it acts as a radially varying transmission filter.[10] While this can be done with a single birefringent lens, the four-lens combination provides for refractive power compensation and a wide range of input beam sizes. By rotating the inner pair of lenses together, while keeping the outer pair constant, the transmission through a polarizer can be made to vary on-axis, while the edge transmission remains maximum [Fig. 5(a)]. Thus the peak of a Gaussian beam can be flattened to any desired degree. Apodizing the beam using a 1-cm^2, square serrated aperture in combination with appropriate spatial filtering produces a beam with a 87% fill factor and Gaussian edges.[11] The serrated aperture is the primary relay plane of the laser system that will be relayed onto the final harmonic convertors.[12,13] The spatial filter magnifies the beam to 5 × 5 cm^2. The total transmission from the input telescope to beam shaper output is 27% for a flat-topped output profile, thus providing 1 to 2 mJ at the input of the next preamplifier stage. The transmitted energy is controlled by a half-wave plate in combination with a polarizer.

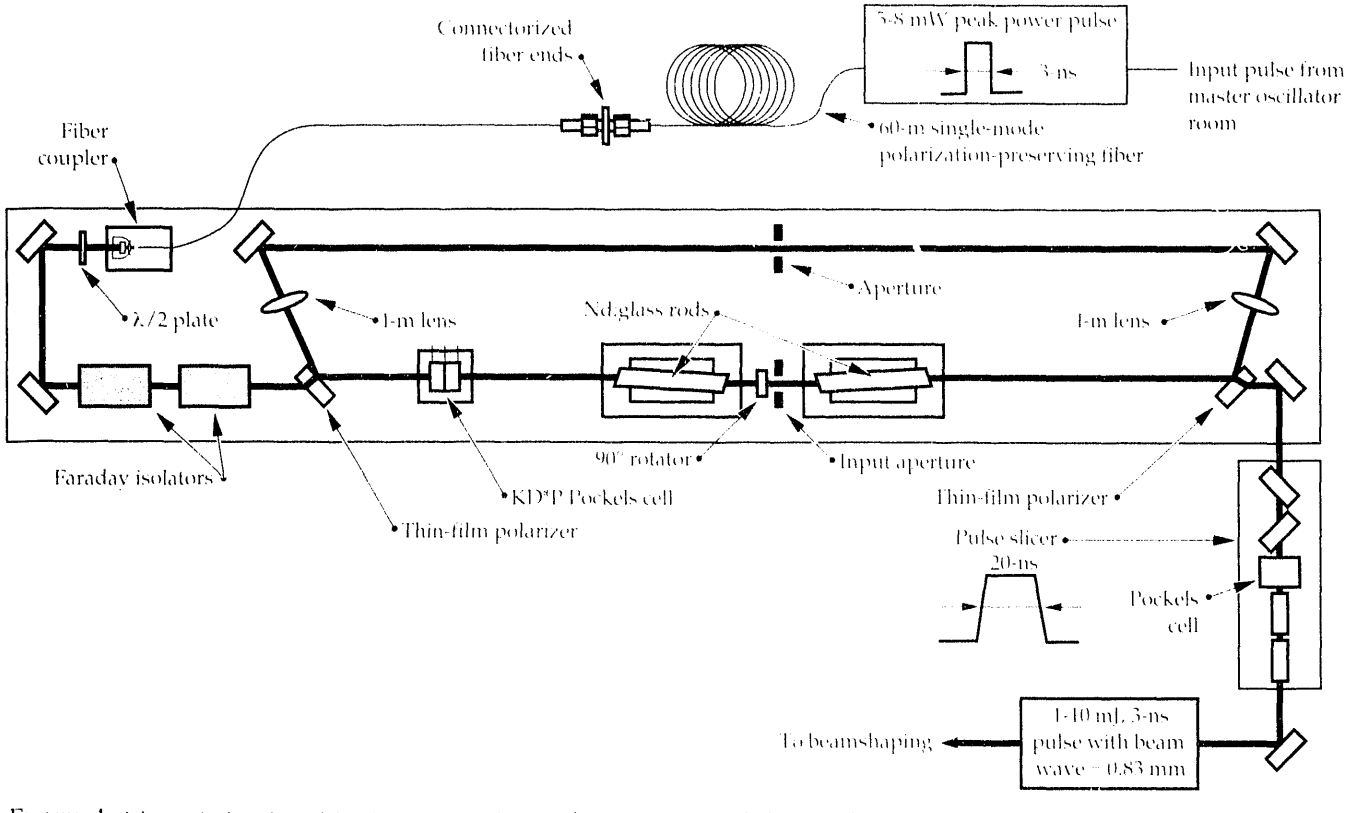

FIGURE 4. Schematic drawing of the ring regenerative amplifier using two Nd:glass amplifier heads in a self-imaging configuration. The input pulses from the MOR are delivered through an optical fiber. A pulse slicer blocks leakage through the cavity polarizers.

Multipass Rod Amplifier As Energy Booster

The remaining four orders of magnitude gain required to produce 10 J output energy are achieved using a standard Nova 5-cm-diam phosphate glass rod amplifier in a 4-pass configuration, as depicted in Fig. 6. The linearly polarized input beam is made circular by a quarter wave plate on its first pass through the rod. Returning through the rod and waveplate, the polarization of the second pass is rotated by 90°. The beam is therefore reflected by the second polarizer, and retroreflected by the second cavity mirror to make a third pass though the rod. The polarization of the 4th pass will be rotated by another 90° and become equal to the input beam polarization. Input and output beams are separated by a 10 cm aperture Faraday isolator. Figure 1 shows the actual layout of the preamplifier components on the space frame, while Fig. 2 presents a view of the space frame looking from the rod amplifier in the direction of the output beam.

The LHG-8 rod amplifier is operated at a small signal gain of 14.3. Since the double pass gain exceeds 200, extreme care was taken to avoid oscillations and parasitics in the cavity: lens surfaces and waveplates were tilted, and the rod was wedged.The pointing of the input beam is offset by 3 mrad such that the beams in the spatial filter focal plane are separated by 20 mm across. This reduces parasitic oscillations and crosstalk between the different passes.[14]

Unexpectedly, however, images of the spatial filter pinhole plane that was backlit by a reflection from the output spatial filter lens on the fourth pass, were amplified and appeared as small collimated beams in the output aperture. Increasing the tilt of the spatial filter lenses alleviated the problem. Moving the quarter wave plate to the other side of the spatial filter will eliminate it completely.

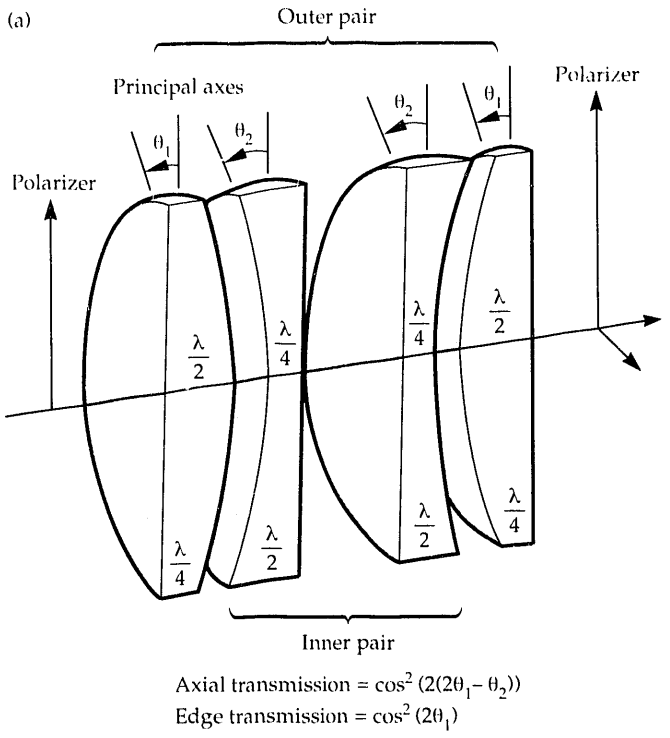

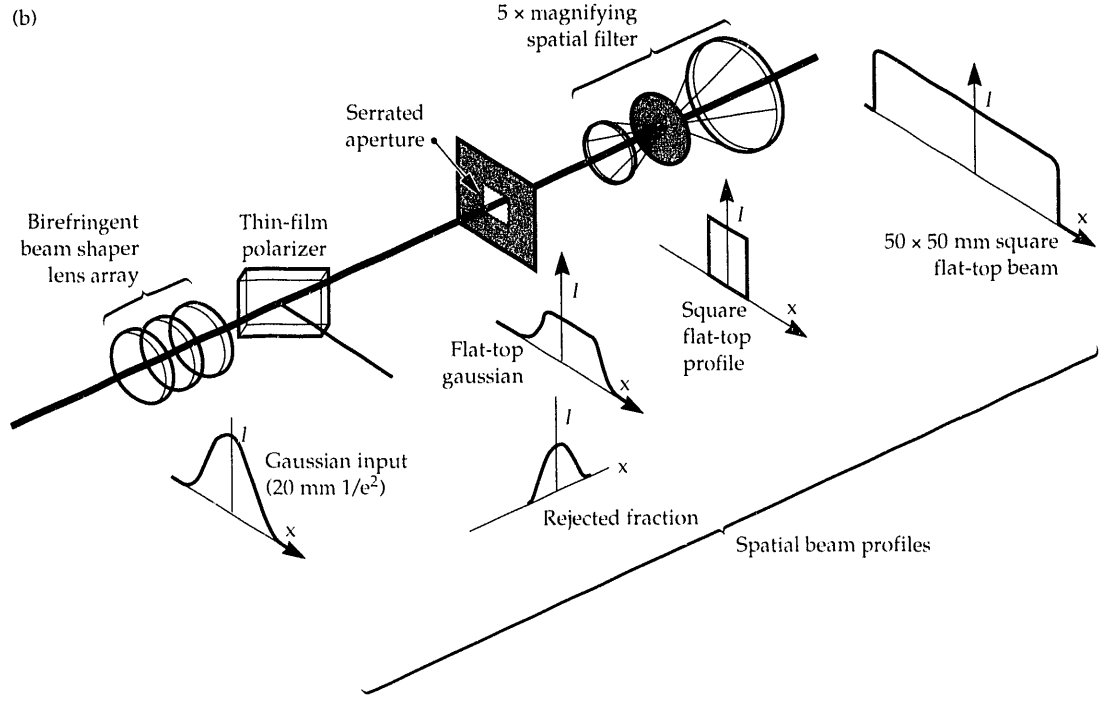

FIGURE 5. Layout of the beam shaping section. The magnified beam from the regenerative amplifier is shaped through a birefringent optical system. A square serrated aperture and spatial filter define the Gaussian edge profile of the beam.

The passive transmission of the 4-pass amplifier amounts to 53%. The extinction ratio of the Faraday isolator exceeds 2500. Residual leakage of the second pass through the isolator is blocked in the pinhole plane of the transport spatial filter following the amplifier. Transient thermal depolarization in the rod amplifier limits the repetition rate to 15–20 min.

Controls and Diagnostics

The master oscillator room (MOR) has a large number of fiber-coupled diagnostics to monitor power, pulse shape, modulator extinction and bandwidth. The extinction of the waveguide modulators is continuously optimized under computer control.

The preamplifier section (Fig. 1) is equipped with three diagnostic stations, located at the output of the regenerative amplifier, and the input and output of the 4-pass amplifier. Each has a near and far field viewing capability, an energy sensor, and a fast photodiode. The front end output sensor is being equipped with a radial shearing interferometer, streak camera and single shot bandwidth sensor, to allow a complete pulse characterization. Energy measurements were performed using a calibrated 4-in. full beam calorimeter. Two pinhole-plane-viewing cameras allow for easy alignment of the 4-pass amplifier cavity spatial filter. Over 52 stepper motors allow for remote alignment of the system.

System Performance

Output Energy

Figure 7 shows actual performance for 3-ns square input pulses, together with MALAPROP predicted values.[15] The calculations were based upon a small signal gain of 14.3 and a system transmission of 53%. The small deviation can be attributed to a small gain increase near the edges of the rod amplifier (discussed below). This data indicates that the regenerative amplifier operating at a nominal 5 mJ energy level provides plenty of energy to drive the rod amplifier to its maximum output energy, even taking into account beam shaping losses.

The energy output is limited to 12 J by Pt-inclusion damage in the LHG-8 glass of the rod amplifier; the damage fluence is 2.5 J/cm^2 for pulses with duration in the 1 to 5 ns range. MALAPROP calculations for a 3-ns square input pulse indicate acceptable values for the accumulated B-integral: 0.18 rad at 6 J output energy, and 0.4 at 12 J.

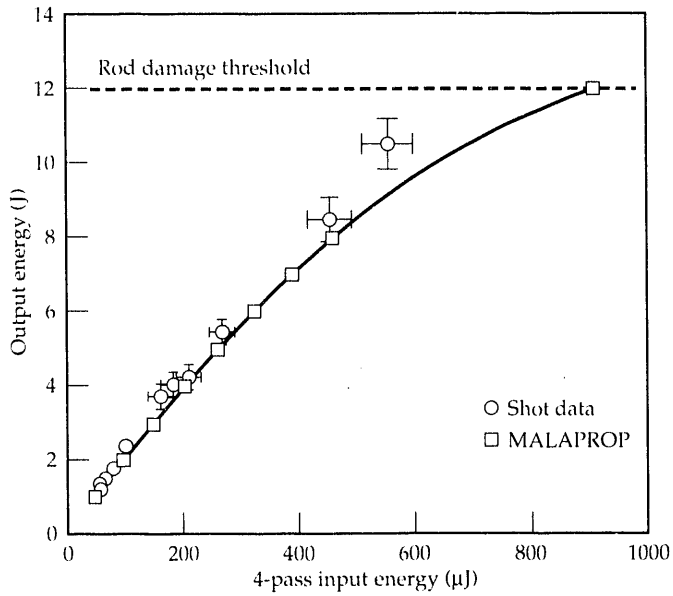

FIGURE 7. Performance curves of the 4-pass rod amplifier operating at a small signal gain G_0 = 14.3 measured with square 3-ns pulses. The passive cavity transmission equals 0.53. The solid curve is the performance predicted by the MALAPROP code.

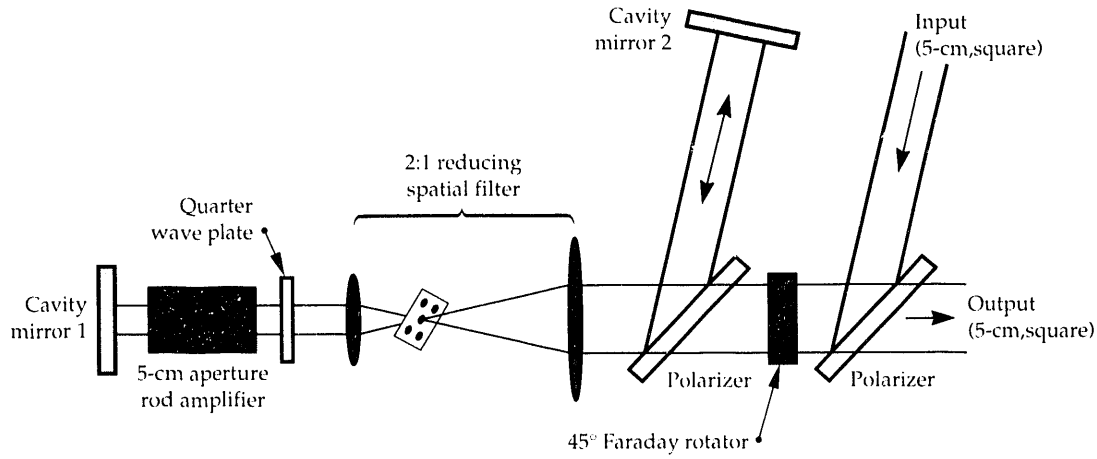

FIGURE 6. Schematic diagram of the 4-pass amplifier operation using a Faraday rotator and quarter wave plate. A 2:1 reducing spatial filter accommodates the 50 × 50 mm^2 beam to the 50-mm-diam rod.

The intensity contrast ratio is presently limited by the ratio of the peak power fed into the regenerative amplifier to its equivalent noise input power (< 0.3 μW)[16] and amounts to 2×10^4. A research effort is underway to develop a much higher power oscillator. The integrated amplified spontaneous emission output from the 4-pass amplifier is less than 12 mJ, leading to an intensity contrast exceeding 10^8.

Beam Uniformity and Wavefront Quality

We observed excellent near field quality in the 4-pass output beam, even at the highest energy levels. Figure 8(a) shows the near field of an 8.3-J output pulse obtained using an input pulse with a flat intensity profile. The parabolic shape of the lineout through the center (Fig. 9) indicates a 10% gain drop in the center of the beam, corresponding to a 1% reduction in gain coefficient in the rod amplifier. This excellent pumping uniformity results from the selection of a rod with low (0.4%) Nd^{3+} concentration and was further improved by grinding and edge-cladding the rod. The birefringent beam shaper was easily adjusted to obtain a flat output profile, as shown in Fig. 8(b). The peak to average uniformity deviation is less than 12%. For comparison, we superimposed a 36th order supergaussian profile on the line-outs in Fig. 9. Both images were actually obtained 2.2 m beyond the output relay plane and thus had lower fill factors and relatively sharp intensity peaks on the beam edge. Far-field images in the output sensor indicate that the beam divergence is better than 1.3 times the diffraction limit. Preliminary radial shearing interferograms of the output pulses indicate a peak-to-valley wavefront deformation of less than 0.25 waves. They verify the uniform energy deposition and pumping in the 5-cm rod amplifier. The accumulation of optical aberrations in the cavity does not seem to have a significant effect in the 4-pass amplifier.

Shaped Pulses

The PSD of the 4-pass amplifier is defined as the ratio of the gain at the beginning of the pulse to the gain at the end for a square input pulse. We measured a PSD of 2.2 at the highest recorded output energy of 10.5 J for a 3-ns square input pulse, as shown in Fig. 10. Four preset input pulse shapes are presently available: square, 1.6:1 contrast, 8:1, and 15:1. Additionally, a 100:1 contrast pulse has been demonstrated in the MOR. Figure 11 shows a 15:1 shaped pulse after the waveguide modulators, and the resulting 9:1 contrast (1.7 times reduced) pulse after amplification to 2.8 J.

Bandwidth Generation and Propagation

Figure 12 shows a frequency spectrum of pulses modulated by applying a 4-GHz RF signal (P = 20 W) to the waveguide phase modulator. The spectrum consists of a number of equally spaced sidebands. The amplitude of the nth sideband is given as $J_n(\delta)^2$, the square of the nth order N-Bessel function of the modulation index δ, which is defined as the amplitude of the phase

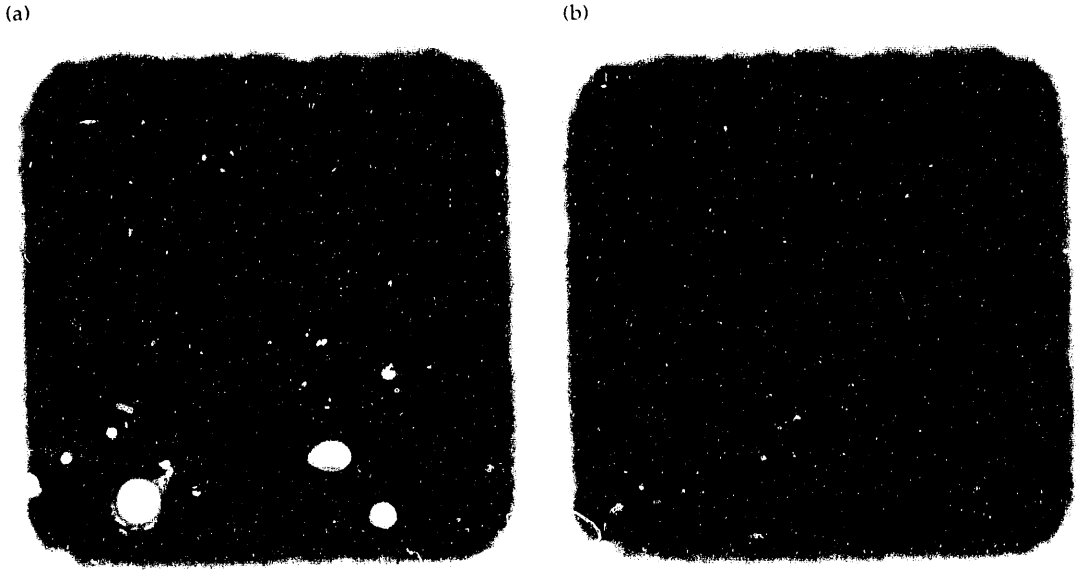

FIGURE 8. Near field images of the front-end output beam, observed 2.2 m beyond the relay plane. (a) Using a flat-topped input profile, we observe the a gain minimum near the amplifier axis (b) after adjusting the beam shaper to compensate for the non uniform gain. The slight fringe pattern visible on both images is inherent to the CCD camera response.

modulation. The total bandwidth is less important than the need to share energy among the greatest possible number of sidebands, separated in frequency by an amount exceeding the line width of the SBS gain.[3]

When the phase or amplitude relation of the sidebands are modified by dispersion or a frequency dependent gain and transmission, phase modulation will be converted into undesirable amplitude modulation. Etalon effects between parallel surfaces can be a serious problem in the regenerative amplifier. We now observe peak to average modulation below 4%. Figure 13 shows regenerative amplifier output pulses after 14 round trips for a 3-ns square input pulse with and without phase modulation (4 GHz), indicating little additional amplitude modulation in a pulse with 40-GHz bandwidth.

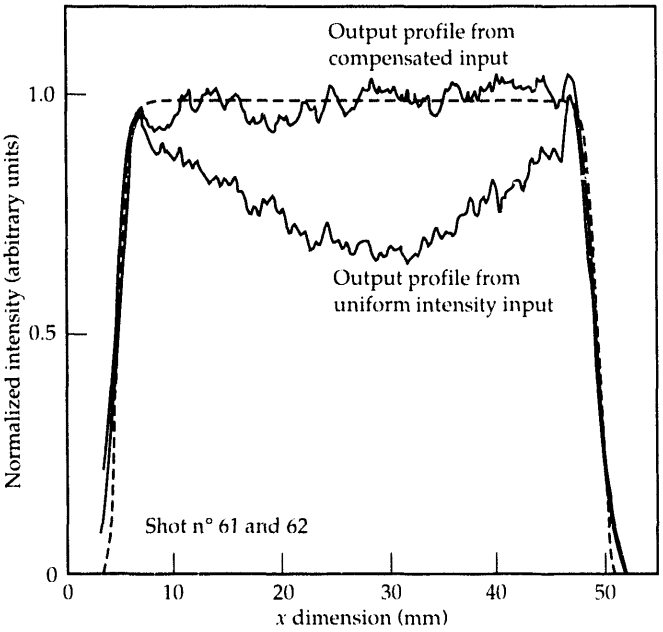

FIGURE 9. Line-outs of near field images of the front end output beam. The dotted line represents a supergaussian profile of order 36. A 1% gain coefficient reduction in the center of the 5-cm ø rod is responsible for the energy drop in the center of the beam.

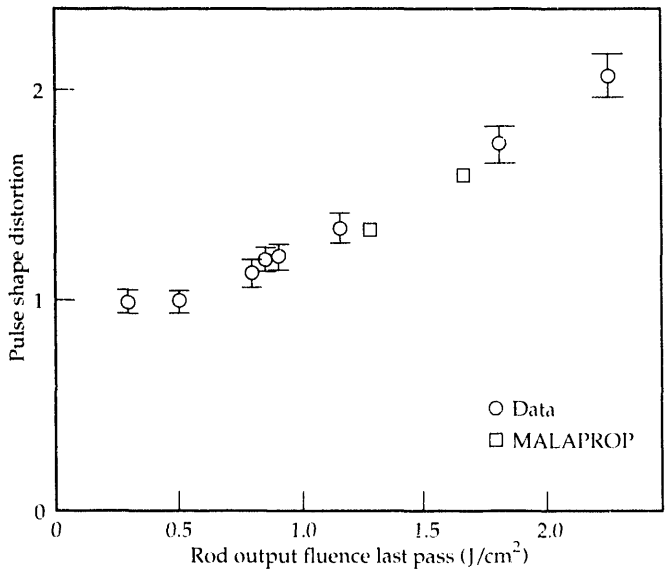

FIGURE 10. Pulse shape distortion for 3-ns square input pulses as a function of fluence at the output end of the rod amplifier.

Conclusion

We have successfully assembled and operated a new type of front-end pulse generation system that meets the system requirements for driving the Beamlet laser. The advanced optoelectronic technology applied in the oscillator and pulse shaping system is a viable alternative for

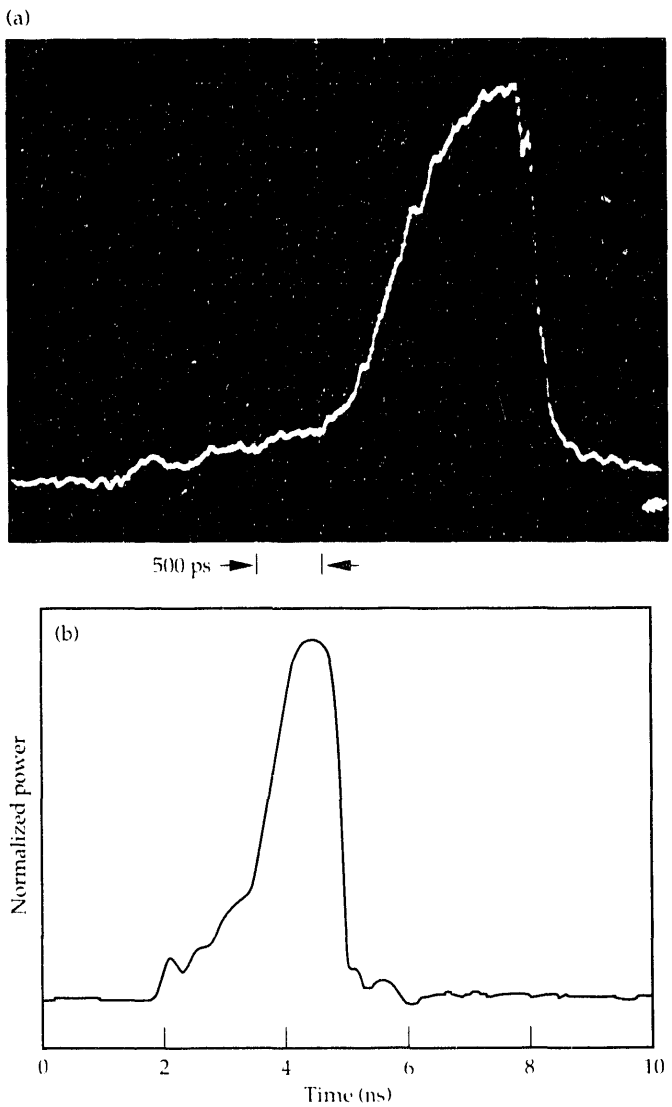

FIGURE 11. Time profile of (a) a 15:1 contrast shaped MOR pulse and (b) the resulting 9:1 contrast output pulse amplified to 2.6 J. Beamlet requires 6:1 contrast input pulses to obtain its milestone performance (5 kJ at 3ω in a 3-ns square pulse). The low peak power of the MOR pulses requires the use of an avalanche photodiode and sampling scope.

the conventional Nova pulse generation system. We operated a large aperture multipass amplifier based on a 5-cm-diam rod amplifier to obtain a 10-J, 3-ns shaped pulse with excellent wavefront quality. We believe carefully designed multipass amplifier schemes will provide performance equivalent to those of more complicated linear amplifier chains using two or three times as many rod amplifiers, without degradating the beam quality and signal to noise ratio.

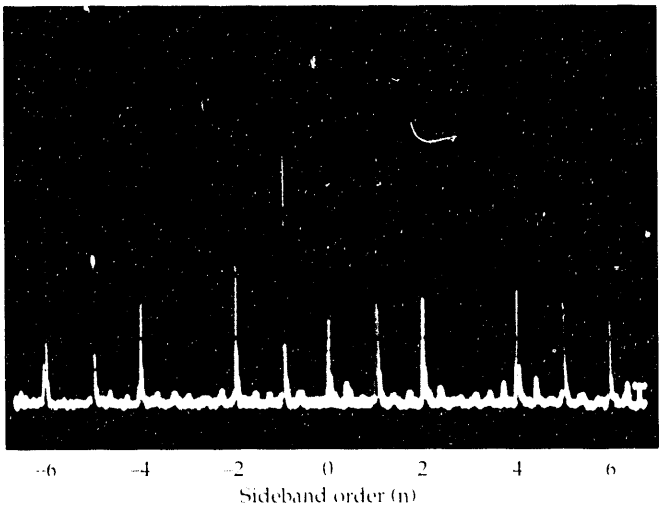

FIGURE 12. Frequency spectrum of the phase modulated MOR pulses, obtained by scanning etalon. The waveguide modulator was driven by 20 W of RF power at 4 GHz, which equals the separation of the various sidebands. We estimate a modulation index of 4.7 in this case.

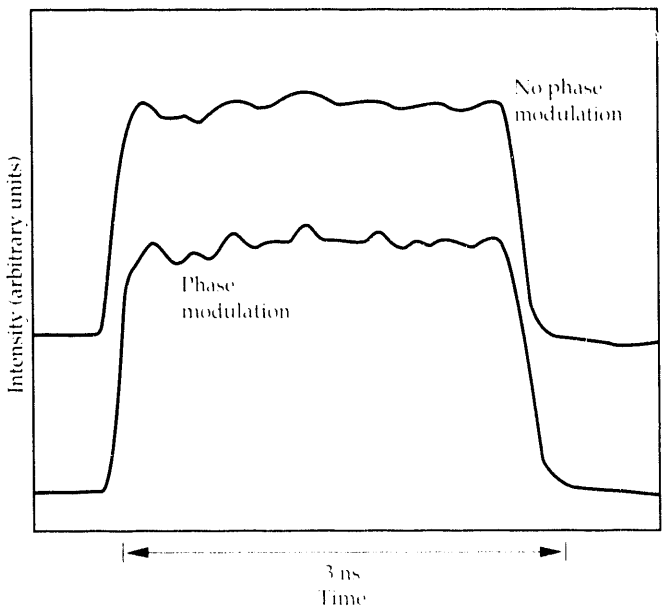

FIGURE 13. Regeneratively amplified MOR pulse shapes with and without phase modulation. A photodiode and 6 GHz oscilloscope were used for this measurement. The energy of the pulses was 3 mJ. The phase modulator was driven by a 10-W, 4-GHz RF signal (30-GHz bandwith).

Acknowledgments

We thank D. Browning and B. Behrendt for expert technical assistance, J. Richards, D. Larson, and G. Pollock for their important contributions to this project, and J. Auerbach for his extensive modeling efforts. The continuing support by J. Campbell and M. Campbell is greatly appreciated.

Notes and References

1. J. D. Lindl, R. L. McCrory, and E. M. Campbell, "Progress Toward Ignition and Burn Propagation in Inertial Confinement," *Physics Today*, **45** (9), 32 (1992).
2. J. R. Murray, J. R. Smith, R. B. Ehrlich, D. T. Kyrazis, C.E. Thompson, T. L. Weiland, and R.B. Wilcox, "Experimental Observation and Suppression of Transverse Stimulated Brillouin Scattering in Large Optical Components," *J. Opt. Soc. Am B* **5**, 2402 (1989).
3. S. N. Dixit, "Numerical modeling of the suppression of Stimulated Brillouin Scattering due to Finite Laser Bandwidth," *SPIE Proc.* **1626**, 254 (1992).
4. J. R. Murray, J. H. Campbell, D. N. Frank, J. T. Hunt, and J. B. Trenholme, "The Nova Upgrade Beamlet Demonstration Project," *ICF Quarterly Report* **1** (3) 89, Lawrence Livermore National Laboratory, Livermore, CA, UCRL-LR-105821-91-3 (1991).
5. R. B. Wilcox, "Oscillator and Pulse-Forming System for the Beamlet," *ICF Quarterly Report* **2** (3) 115, Lawrence Livermore National Laboratory, Livermore, CA, UCRL-LR-105821-92-3 (1992).
6. G. P. Agrawal, *Nonlinear Fiber Optics* (Academic Press, San Diego, 1989), pp. 51 ff.
7. J. E. Murray and W. H. Lowdermilk, "The Multi-Pass Amplifier: Theory and Numerical Analysis," *J. Appl. Phys.* **51**, 2436 (1980).
8. S. E. Swain and F. Rainer, "Many Pass Resonant Laser Amplifier," *IEEE J. Quant. Electr.* **QE-4**, 385 (1969).
9. F. G. Patterson and M. D. Perry, "Design and Performance of Multiterawatt Subpicosecond Neodymium:glass Laser," *J. Opt. Soc. Am B* **5**, 364 (1991).
10. J. M. Eggleston, G. Giuliani, and R. L. Byer, "Radial Intensity Filter Using Radial Birefringent Elements," *J. Opt. Soc. Am B* **11**, 1264 (1981).
11. The serrated aperture was designed by J. Auerbach, Lawrence Livermore National Laboratory.
12. R. J. Gelinas, J. M. Auerbach, S. K. Doss, R. G. Nelson, P. A. Renard, and J. B. Trenholme, "Optical Propagation Modeling for Nova and Beyond," *ICF Quarterly Report* **2** (1) 11, Lawrence Livermore National Laboratory, Livermore, CA, UCRL-LR-105821-92-1 (1991).
13. J. T. Hunt, P. A. Renard, and W.W. Simmons, "Improved Performance of Fusion Lasers Using the Imaging Properties of Multiple Spatial Filters," *Appl. Opt.* **16**, 779 (1977).
14. J. E. Murray, D. C. Downs, J. T. Hunt, G. L. Hermes, and W. E. Warren, "Off-axis Multipass Amplifier as a Large Aperture Driver Stage for Fusion Lasers," *Appl. Opt.* **20**, 826 (1981).
15. *Laser Program Annual Report 1976*, Lawrence Livermore National Laboratory, Livermore, CA, UCRL-LR-50021-76 (1976) pp. 2-344-ff.
16. H. Kogelnik and A. Yariv, "Considerations of Noise and Schemes for its Reduction in Laser Amplifiers," *Proc. IEEE* **52**, 165 (1964).

IMAGING BIOLOGICAL OBJECTS WITH X-RAY LASERS

L. B. Da Silva
J. E. Trebes
S. Mrowka
B. J. MacGowan
J. A. Koch
D. L. Matthews
T. W. Barbee, Jr.
R. Balhorn
J. Gray

Introduction

In recent years, substantial progress has been made in developing x-ray microscopy for biological applications.[1] This work has been motivated primarily by the possibility of producing images with resolutions superior to that obtainable with visible light microscopes while causing less radiation damage to the specimen than conventional electron microscopes.[2] Furthermore, in contrast to electron microscopy, x-ray microscopy has the potential to view organisms hydrated in physiologically normal environments, thus revealing their natural structure.

This article describes our effort to develop imaging with an x-ray laser[3] and presents recent results which have achieved near diffraction-limited resolution of dried rat sperm nuclei. These results will be a basis for comparison in future experiments with hydrated specimens.

Background

An early demonstration of x-ray imaging of unaltered and hydrated biological specimens was reported by Rothman et al.[4], who used a scanning microscope and x rays from an undulator beam line to view zymogen granules with a resolution of 750 Å. More recently, two groups working with imaging[5] and scanning[6] x-ray microscopes reported images with identifiable features as small as 300 Å. Their progress was facilitated by advances in x-ray optics technology[7] and by the development of high brightness x-ray sources.[8] In the area of optics, the successful manufacture of zone plates with outer zone widths as small as 300Å allows images with comparable spatial resolution to be achieved.[1,9] In the area of x-ray sources, new undulator beamlines on synchrotrons now permit the production of high-resolution images on timescales of minutes rather than several hours. Unfortunately, these exposures take longer than the timescales associated with natural motion, which are estimated (from Brownian motion theory) to be ~100 μs for resolutions better than 200 Å.[10] To eliminate the blurring effect of motion, the use of extremely high brightness pulsed sources is necessary.

The brightest pulsed x-ray sources currently available are laser-produced plasmas and x-ray lasers.[11] Laser-produced plasmas can achieve conversion efficiencies as high as 10–20% into the wavelength range of 23–45Å, which is considered optimal for biological imaging. These sources are well suited to contact microscopy, where a broad x-ray spectrum has a small effect on resolution. Such an x-ray source was recently used by Tomie et al.[12] to produce 0.5-ns flash contact x-ray images of a hydrated sperm cell with a spatial resolution of ~1000Å. Extending the use of these plasma sources in imaging microscopy, where chromatic aberrations necessitate the use of narrow bandpass optics, will significantly reduce signal levels. This is not the case for x-ray lasers, which have quasi-monochromatic emission and very high brightness.

X-ray lasers have been produced worldwide by a variety of approaches.[13] Most use electron collisional excitation pumping or recombination pumping in a long (1–5 cm), thin (30–1000 μm) laser-produced plasma. The x-ray laser output is typically subnanosecond in duration, has an angular divergence of ~10 mrad, has a narrow-bandwidth ($\lambda/\Delta\lambda \geq 10^4$) (Ref. 14), and has an energy of 0.01–10 mJ. A 182-Å x-ray laser was previously used to produce contact x-ray micrographs of dry cervical

cancer cells.[15] However, only recently have x-ray lasers with wavelengths near and inside of the "water window" (23–44Å) been developed[16] with sufficient output energy to view a wide range of biological objects. Operating inside the water window, which extends from the oxygen K-shell absorption edge to the carbon edge, is important for enhancing the contrast between organic material and water.

X-Ray Laser Imaging Microscope

Figure 1 shows a schematic of our x-ray imaging microscope. X-rays from a tantalum nickel-like collisionally pumped x-ray laser[17] operating at 44.83 Å are collected and focused onto a specimen. The x-ray laser was generated by irradiating a 3.5-cm-long, 2000-Å-thick plastic foil coated with 900 Å of Ta with two cylindrically focused laser beams operating at a wavelength of 0.53 μm. The heated foil explodes to form a high temperature plasma with low density gradients.[18] For our experiment, two optical beams from the Nova laser were used to generate a combined intensity on target of 3.0×10^{14} W/cm^2 for a duration of 500 ps.[17] Figure 2 shows the measured time history of the x-ray laser pulse; the short, ~200-ps FWHM pulse is characteristic of exploding foil amplifiers. The x-ray laser originates from a ~100-μm-diam gain region at the center of the plasma and has a beam divergence of 10 mrad (FWHM). The output energy is ~10 μJ, which gives a brightness of 10^{21} photons/(s-mrad^2-mm^2-0.01% bandwidth). This is four orders of magnitude brighter than the X-1A beam line at the National Synchrotron Light Source,[19] currently the world's brightest soft x-ray synchrotron beam line.

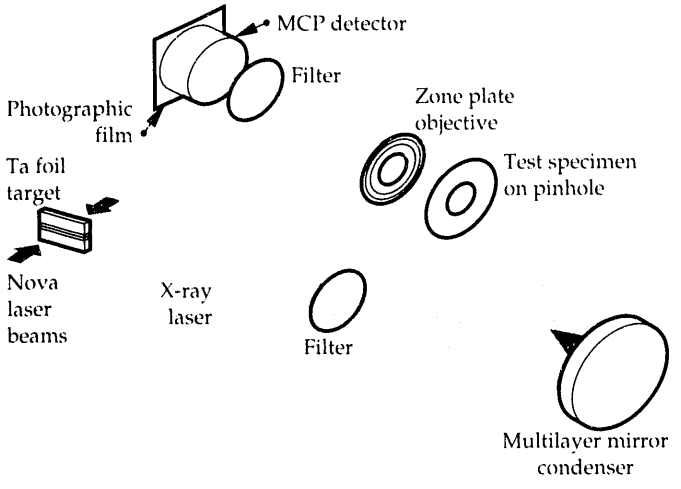

FIGURE 1. Schematic drawing of the x-ray microscope showing main components.

The x-ray laser beam is collected and focused onto the object with a spherical tungsten-carbide/carbon multilayer coated x-ray mirror.[20] The mirror has a measured normal incidence reflectivity of 5% and a bandpass of 1.5% at the x-ray laser wavelength of 44.83 Å. The multilayer mirror isolates the specimen from the harsh environment of the laser-produced plasma and also eliminates most of the background soft x-ray continuum. The mirror has a radius of curvature of 1 m and is operated slightly off-axis at an angle of 1.4°. The laser-to-mirror distance is 3.0 m, resulting in a 5× demagnification of the x-ray laser source region. A 10-mrad aperture limits the section of the mirror used to a 3-cm- region centered on the optic. A filter (2000 Å Ti on 2000 Å of lexan) placed between the mirror and the x-ray laser further protects the sample by eliminating scattered optical radiation. The zone plate[8] we used has 500 zones, an outer radius of 45 μm, an outer zone width of 450 Å, and a focal length of 900 μm at 44.83 Å. The Rayleigh resolution of the zone plate lens is calculated to be ~550 Å. The zone plate is operated at a magnification of 1000× which attempts to match the zone plate resolution to the microchannel plate resolution of ~40 μm. The low reflectivity of the condenser mirror precluded our use of a two mirror system (e.g. Schwarzschild) to fully illuminate the zone plate. As a result, the zone plate was partially illuminated, resulting in an astigmatic point spread function with a diffraction limited resolution in one direction (~550 Å) and a resolution of ~1000 Å in the perpendicular dimension.

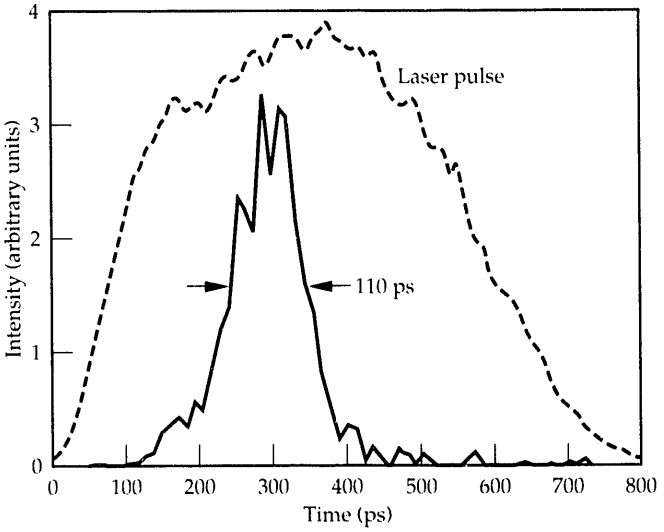

FIGURE 2. Measured time history of Ta Ni-like x-ray laser.

Sample Alignment and Positioning

In existing low repetition rate x-ray lasers, it is impractical to dynamically focus the object. For this reason, we implemented an off-line alignment procedure that accurately sets the zone plate and sample separation, as determined from the zone plate focal length and desired image magnification. The procedure uses two white light interferometers (Fig. 3) to define two planes in space with the desired separation. The sample and zone plate, both of which are mounted on 1000 Å silicon nitride windows, can then be accurately positioned and aligned using the interferometers. The sample and zone plate are glued together and the separation monitored during curing of the glue. In the initial separation, we must account for the 2 to 3 μm reduction in spacing which occurred during the curing. This procedure allows us to position the sample and zone plate separation to ±0.5 μm, which is within the focal depth of our $f/10$ system.

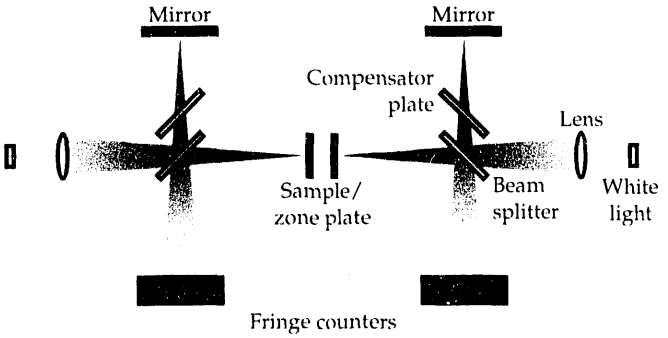

FIGURE 3. Double white light interferometer setup used for positioning sample and zone plate.

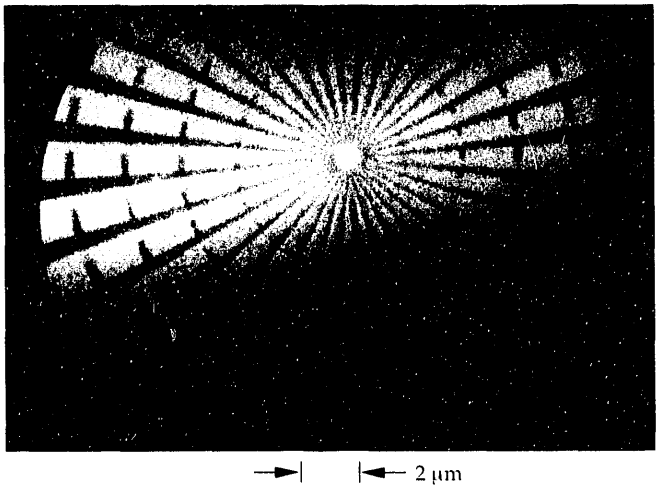

FIGURE 4. Image of resolution test pattern obtained with x-ray laser microscope.

Imaging Experiments

Figure 4 shows an image of a resolution test pattern consisting of radial gold bars that taper down to ~350 Å at the center. These 1000-Å thick bars are on a 1000 Å silicon nitride substrate. Features near the diffraction-limited resolution of ~550 Å are clearly observed. The nonuniform illumination pattern is due to the finite size of the x-ray laser source, which is demagnified onto the test pattern by the multilayer mirror collecting optic. The effective source size is estimated to be 50 × 80 μm.

Using this x-ray microscope, we imaged three specimens of rat sperm nuclei which had undergone different preparations. Our goals were to 1) investigate the advantages of gold labeling (an analog to isotopic tracing techniques), and 2) to assess the effects of the various preparation techniques on the nuclei. The nuclei were first prepared by treating sperm isolated from rat epididymides; a disulfide reducing agent and detergent[20] dissolves the tails, acrosome, and nuclear membranes thus exposing the DNA-protamine complex that comprises sperm chromatin. A droplet containing the amembraneous nuclei was deposited onto a silicon

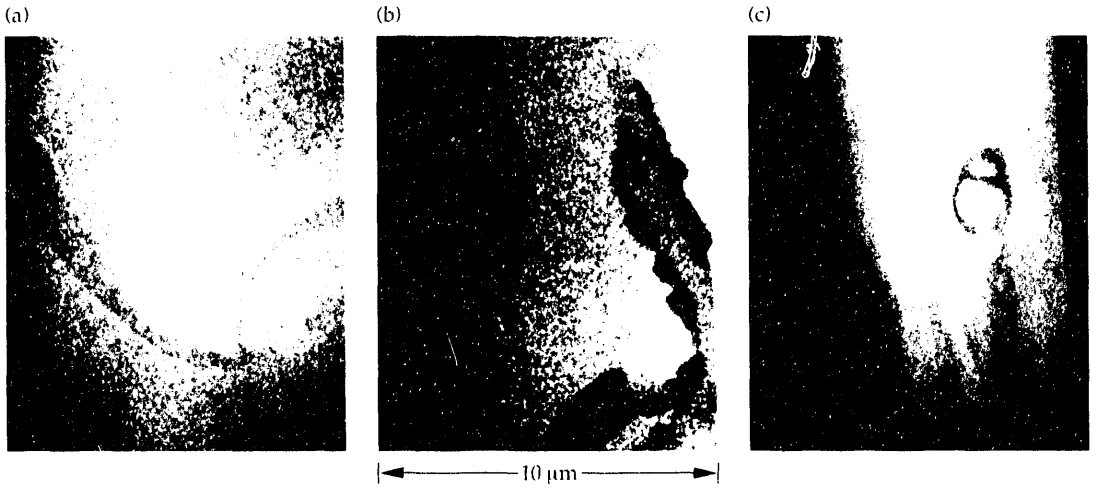

FIGURE 5. X-ray microscope images of rat sperm nuclei with (a) no gold labeling, (b) stained with antiprotamine 1 and gold labeled, and (c) stained with antiprotamine 2 and gold labeled.

nitride window (300 x 300 μm, 1000-Å thick) and the liquid containing unbound nuclei was removed after 30 s. Figure 5 shows images of (a) unstained rat sperm nuclei, (b) images stained with mouse antiprotamine 1, and (c) antiprotamine 2 antibodies tagged with 400-Å-diam gold. The images show distinct differences. The stained images show high concentrations of gold along the edge of the sperm nuclei and some evidence of individual 400-Å gold particles on the surface. The clumping of the gold particles is particularly evident in Fig. 5(b). The frame structures observed in Fig. 5(c) are a consequence of the preparation technique which unmasked internal sites for antibody binding. These images clearly show the value of gold labeling to enhance contrast but also show that unnecessary preparation techniques can lead to unwanted artifacts.

A unique advantage of x-ray microscopy which will prove useful in future studies is that it can also be used to obtain information about elemental density. By selecting an appropriate x-ray laser wavelength, the contrast between elements can be enhanced. Figure 6 shows the wavelengths of demonstrated Ni-like x-ray lasers along with the calculated transmission for 1 μm of water, DNA, protein ($C_{52}H_7$-$O_{22}N_{16}S$, r = 1.35 g/cm^2), and 500 Å of gold. The large change in absorption across the carbon absorption edge at 44.3 Å can be used to map out carbon abundance by taking two images of the specimen, one with the tantalum x-ray laser (44.83 Å) and one with the tungsten x-ray laser (43.8 Å). Plans to perfom such an experiment are currently underway.

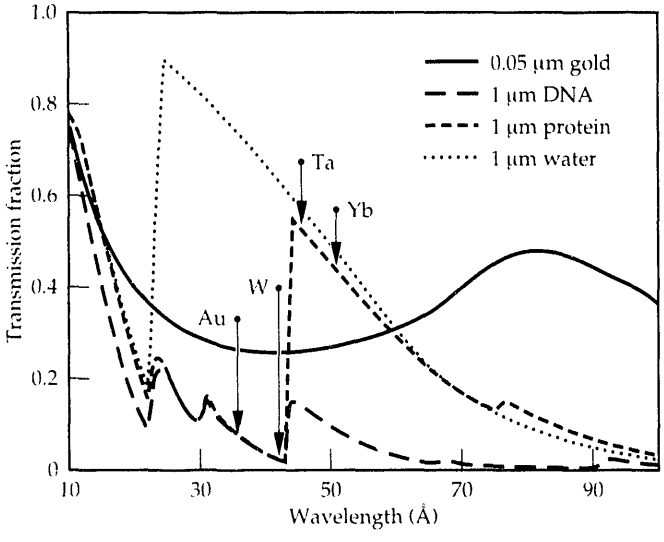

FIGURE 6. X-ray transmission through 1 μm of DNA, protein ($C_{52}H_7O_{22}N_{16}S$, r = 1.35 g/cm^2), water, and 0.05 μm of gold. The wavelength of demonstrated Ni-like x-ray lasers are indicated by an arrow and the corresponding element. By taking advantage of the sharp absorption edges and available x-ray lasers, elemental abundance can be mapped out.

Conclusions

These preliminary experiments illustrate the capability of existing x-ray laser microscopes to produce images of biological specimens with single 200-ps exposures. The Ni-like Ta x-ray laser operating at 44.83 Å is ideal for imaging biological specimens that have been immunogold-labeled to reduce the necessary dosage. The development of normal incidence, multilayer x-ray optics at wavelengths below the carbon K-edge (43.7 Å), where there is high contrast between proteins and water, will make short wavelength x-ray microscopes possible within a year. In addition, the use of multilayer mirrors to double-pass the gain region should lead to 100–1,000 times more output. The increased energy will improve the image quality; it will also allow several microscopes to be combined so that an object can be imaged from different lines of sight. The multiple frames can then be synchronized to obtain animated, three-dimensional images or time delayed to observe the effects of high dosage on specimens. Finally, recent advances in optical pump lasers will significantly reduce the size of x-ray lasers and increase their repetition rate, making x-ray laser based microscopes accessible to a wider community.

Notes and References

1. A. Michette, G. Morrison, and C. Buckley, *X-ray Microscopy III*, (Springer-Verlag, Berlin, 1991).
2. D. Sayre, J. Kirz, R. Feder, D. M. Kim, and E. Spiller, "Potential Operating Region for Ultrasoft X-ray Microscopy of Biological Materials," *Science* **196**, 1339 (1977).
3. L. B. Da Silva, J. E. Trebes, S. Mrowka, E. Anderson, D. T. Attwood, T. W. Barbee, J. Brase, J. A. Koch, D. Kern, R. A. London, B. J. MacGowan, D. L. Matthews, D. Minyard, G. Stone, and T. Yorkey, "Demonstration of X-ray Microscopy with an X-ray Laser Operating Near the Carbon K-edge," *Opt. Lett.* **17**, 754 (1992).
4. S. S. Rothman, N. Iskader, D. Attwood, Y. Vladimirsky, K. McQuaid, J. Grendell, J. Kirz, H. Ade, I. McNulty, D. Kern, T. H. P. Chang, and H. Rarback, "The interior of a whole and unmodified biological object—the zymogen granule—viewed with a high-resolution x-ray microscope," *Biochim. Biophys. Acta* **991**, 484 (1989).
5. W. Meyer-Ilse, P. Guttmann, J. Thieme, D. Rudolph, G. Schmahl, E. Anderson, P. Batson, D. Attwood, N. Iskander and D. Kern, in *X-ray Microscopy III*, A. Michette, G. Morrison and C. Buckley, Eds. (Springer-Verlag, Berlin, 1991) p. 284.
6. C. Jacobsen, S. Williams, E. Anderson, M. T. Browne, C. J. Buckley, D. Kern, J. Kirz, M. Rivers and X. Zhang, "Diffraction-Limited Imaging in a Scanning Transmission X-ray Microscope," *Optics Comm.* **86**, 351 (1991).
7. N. Ceglio, *X-ray Sci. and Tech.* **1**, 1 (1989).
8. D. Attwood, K. Halbach, and K. Kim, *Science* **288**, 1265 (1985).
9. E. Anderson and D. Kern, in *X-ray Microscopy III*, A. Michette, G. Morrison and C. Buckley, Eds. (Springer-Verlag, Berlin, 1991) p. 75.

10. D. Attwood, *Proceedings of the Conference on X-ray Microimaging for the life sciences*, Lawrence Berkeley Laboratory, Berkeley, CA, LBL-27660 (1989).
11. R. Kauffman, in *Handbook of Plasma Physics, Vol 3: Physics of Laser Plasmas* M. Rosenbluth and R. Sagdeev, Eds. (Elsevier Science, New York, NY, 1991).
12. T. Tomie, H. Shimizu, T. Majima, M. Yamada, T. Kanayama, H. Kondo, M. Yano and M. Ono, "Three-Dimensional Readout of Flash X-ray Images of Living Sperm in Water by Atomic-Force Microscopy," *Science* **252**, 691 (1991).
13. G. J. Tallents, *X-Ray Lasers 1990*, G. J. Tallents, Eds. (IOP Publishing Ltd., York, U.K., 1990) ps. 116, 381.
14. J. Koch, B. J. MacGowan, L. B. D. Silva, D. L. Matthews, J. H. Underwood, P. J. Batson and S. Mrowka, "Observation of gain-narrowing and saturation behavior in Se x-ray laser line profiles," *Phys. Rev. Lett.* **68**, 3291 (1992).
15. C. H. Skinner, D. S. DiCicco, D. Kim, R. J. Rosser, S. Suckewer, A. P. Gupta, and J. G. Hirschberg, *J. Microsc.* **159**, 51 (1990).
16. B. J. MacGowan, L. B. D. Silva, D. J. Fields, A. R. Fry, C. J. Keane, J. A. Koch, D. L. Matthews, S. Maxon, S. Mrowka, A. L. Osterheld, J. H. Scofield, and G. Shimkaveg, *X-ray Lasers 1990*, G. J. Tallents, Eds. (IOP Publishing Ltd., York, U.K., 1990) p. 221.
17. B. J. MacGowan, S. Maxon, L. B. D. Silva, D. J. Fields, C. J. Keane, D. L. Matthews, A. L. Osterheld, J. H. Scofield, G. Shimkaveg and G. F. Stone, "Demonstration of X-Ray Amplifiers near the Carbon K-edge," *Phys. Rev. Lett.* **65**, 420 (1990).
18. M. D. Rosen, P. L. Hagelstein, D. L. Matthews, E. M. Campbell, A. U. Hazi, B. L. Whitten, B. MacGowan, R. E. Turner, R. W. Lee, G. Charatis, G. E. Busch, C. L. Shepard and P. D. Rockett, "Exploding-Foil Technique for Achieving a Soft X-Ray Laser," *Phys. Rev. Lett.* **54**, 106 (1985).
19. T. W. Barbee, "Multilayers for x-ray optics," *Opt. Eng.* **29**, 581 (1990).
20. R. Balhorn, B. L. Gledhill, and A. Wyrobek, *Mouse Sperm Chromatin Proteins: Quantitative Isolation and Partial Characterization, Biochemistry* **16**, 4704 (1977).

Coherent XUV Generation via High-Order Harmonic Generation in Rare Gases

J. K. Crane
M. D. Perry
K. S. Budil
T. Ditmire
S. Herman
H. Nguyen
B. Adams

Introduction

Since the mid-80s, there has been a renaissance in short-pulse laser development that has included the application of chirp-pulse amplification to laser system design, and the development of new broad-band, near-IR, solid-state materials such as Ti-sapphire, Cr-alexandrite, and Cr-LiSAF. As a result, it has become possible to routinely generate focused laser intensities of 10^{14} W/cm^2 and, with some effort, to create intensities exceeding 10^{17} W/cm^2 in subpicosecond pulses.

Paralleling this renaissance in laser development is the emergence of a new area of laser science called strong-field physics that investigates laser-matter interactions at high electric-field strengths. At intensities exceeding 10^{14} W/cm^2 the laser field is no longer a small perturbation to the atomic Hamiltonian, but becomes comparable to the Coulombic field that binds the electrons to the nucleus. At these intensities the outer electron can be excited to energies well above the atom's field free ionization potential, whereupon the atom may photoionize and release its surplus energy via the exiting electron (above threshold ionization, or ATI), or couple back to the atomic ground state, emitting a photon with energy exceeding the ionization potential of the atom. Because the electron is driven by the laser field, the emission process is coherent, and the photon is an odd integral multiple of the laser frequency. This process, called high-order harmonic generation, can produce coherent radiation well into the soft x-ray region of the spectrum and shows promise as a short-pulse, coherent source of ultra-bright, extreme ultraviolet (XUV) radiation.

In this article, we discuss experiments to extend the short wavelength limit of harmonic generation to shorter wavelength or higher energy photons, and discuss the scaling of this XUV source to high conversion efficiency.

Experimental Setup

The laser used in these experiments has been described elsewhere.[1] It is a short-pulse Nd:glass system that provides 800-fs pulses at a wavelength of 1.053 μm, with energies up to 8 J. We can frequency double this light with a thin KD*P crystal to obtain 0.526-μm light (650 fs and 2 J).

We focus the laser light at the output of a pulsed, supersonic nozzle placed at the center of a vacuum chamber (Fig.1). The jet can generate local densities >10^{18} atoms/cm^3 (Ref. 2). The resulting emission is collected with a grazing-incidence x-ray spectrometer that produces a vertical, flat-field, dispersed image on the input cathode of a streak camera. Figure 2(a) shows a streak camera photograph of emission from a helium

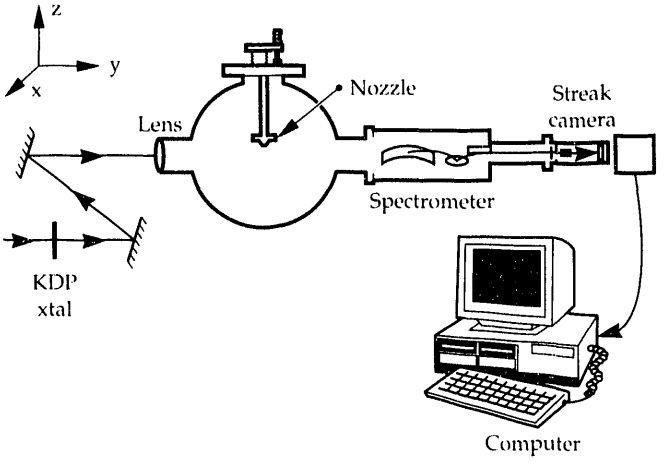

FIGURE 1. Experimental setup where we focus the laser light at the output of a pulsed supersonic nozzle placed at the center of a vacuum chamber.

plasma excited by 0.526-μm light.[3] The vertical direction spans the wavelength range from 14.5 nm at the bottom of the screen to 33 nm at the top. The horizontal time axis is 1 mm/ns or 23 ns full screen. The bright spots that form a vertical band are the harmonics 17-31 (30.9 to 17.0 nm). The horizontal stripes are emission produced by fluorescence from the Lyman series in He^+. We take lineouts in the vertical direction [Fig. 2(b)] to obtain spectra from a streak photograph or horizontal lineouts for time-resolved information at a fixed wavelength. Although the laser can only be fired once every few minutes, the streak camera produces a large amount of information for each shot.

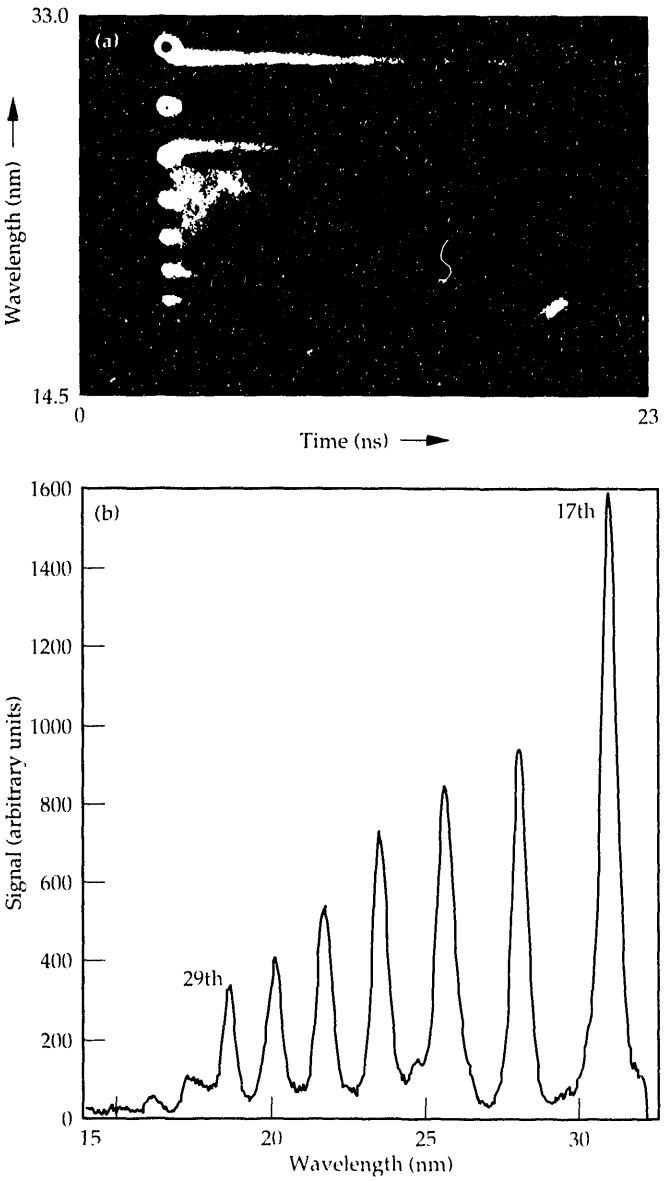

FIGURE 2. (a) Streak photograph in He showing harmonics of 0.526-μm light, harmonics 17-31, and recombination emission from He^+ transitions (Lyman series). (b) Lineout from streak photograph showing harmonic spectrum.

We use several diagnostics to characterize the laser and plasma. We measure the laser pulse width with a single-shot autocorrelator. We record the laser energy and the near-field spatial beam profile on every shot, and the far-field profile at regular intervals. Based upon the measured pulse width, laser energy and beam profile we determine the focused laser intensity. These values can be confirmed based on the observation of line emission from the plasma originating from different charge states of the ion. For example, the observation of Ar VIII lines implies an intensity exceeding 2×10^{16} W/cm^2 based on rates calculated from tunneling theory.[4]

To determine the electron and gas density of the plasma, we measure the backward-scattered Raman wave generated in the plasma by the intense laser pulse.[2] The frequency shift of the Stokes wave ω_s with respect to the laser ω_l equals the plasma frequency ω_p is $\omega_s = \omega_l - \omega_p$. The electron density is obtained from the plasma frequency, $n_e = \omega_p^2 m_e \varepsilon / e^2$, where m is the electron mass, ε is the vacuum permittivity, and e is the electronic charge.

Harmonic Generation-Short Wavelength Limit

Odd harmonics of the laser frequency are generated when a suitably intense pulse is focused in a dense gas. At laser intensities exceeding 10^{13} W/cm^2, the harmonics form a plateau, i.e., several orders of nearly constant intensity[5], in contrast to the rapid drop in harmonic intensity with increasing order that was first observed in the 1970s at much lower intensities (10^9–10^{11} W/cm^2). Figure 3 shows harmonic production in neon from the 3rd to the 19th harmonics of 527 nm measured in our laboratory[6]. One sees an initial decrease in harmonic intensity from the 3rd through 7th harmonics, followed by several orders of comparable level ending at the 19th, which corresponds to the cutoff of the normal incidence spectrometer used in this particular experiment.

The extent of the harmonic plateau is of great interest in scaling this phenomena as a useful XUV source. Harmonic generation is limited by competition with photoionization as the laser intensity is increased. At high intensity the photoionization rate becomes so rapid—shorter than the inverse laser pulse width—that all the atoms become ionized, and the nonlinear medium is depleted. Recently Krause et al.[7] proposed an empirical relationship for the harmonic cutoff (i.e., end of the plateau region). The harmonic cutoff for a particular atom is given by

$$E_c = IP(0) + nU_p(I_{sat}) \quad . \tag{1}$$

E_c is the cutoff in eV, $IP(0)$ is the atom's field-free ionization potential, and U_p is the quiver energy (also called the ponderomotive potential), given by

$U_p(eV)=9.33X10^{14}I[W/cm^2]\lambda^2[\mu m]$, where λ and I are the laser wavelength and intensity. As stated earlier, the maximum plateau extent for harmonics produced from the neutral will be limited by photoionization, which depletes the ground-state population; consequently, U_p is evaluated at the saturation intensity for photoionization. A constant multiplier n is added that Krause, et al., estimate to be between 3 and 3.5 based upon single atom calculations for several different atoms and model potentials.[7] In addition, this scaling relationship has been corroborated in measurements of the plateau cutoff in our laboratory.[3,8]

Based upon Eq. (1), there are several controllable parameters that affect the short wavelength limit for harmonic generation. By increasing the laser intensity, we increase the quiver energy U_p of the electron, causing the plateau to be extended. Figure 4 shows data in helium at three different intensities.The curves are from lineouts of streak photographs taken at a fixed spectrometer setting and corrected for photocathode and grating efficiency. At the lowest intensity, 1.0×10^{15} W/cm^2, we see the 23rd to 29th harmonics. At 5×10^{15} W/cm^2, we see harmonics out to the 35th. The 23rd to 33rd harmonics are part of the plateau region, while the 35th is an order of magnitude down from the other harmonics. At the highest intensity, 5×10^{16} W/cm^2, the plateau extends to the 33rd or 35th harmonic and the drop off after the 35th is more gradual. The data in the bottom curve were generated at a peak intensity slightly above I_{sat}; however, the volume of atoms exposed to I_{sat} was very small and most of the harmonic signal originated from atoms exposed to lower intensity laser light. The data in the middle curve represents harmonics generated at about $7I_{sat}$, extending the cutoff to the 33rd harmonic. The data in the top curve are signals produced from atoms exposed to about $70I_{sat}$. Again, the harmonic signal is approximately flat to the 33rd or 35th harmonics and decreases to the final harmonic, the 45th. Even though this intensity is well above I_{sat}, the plateau cutoff occurs at the same energy as predicted by Eq. (1). We believe that the harmonics 35–45 are produced from He^+. Although no neutral survives to an intensity $70I_{sat}$, there is an increase in harmonic signal because the volume of atoms exposed to an intensity $I>I_{sat}$ is much larger than for the other curves.

For the rare gases, both the ionization potential and the saturation intensity for ionization increase with decreasing atomic mass. As a result, the most dramatic increase in the harmonic plateau extent is seen in going from heavier-mass to lighter-mass rare gas atoms due to the increase in ionization potential and, consequently, the saturation intensity. Table 1 summarizes the predicted harmonic cutoffs based on Eq. (1) for a 1-ps laser pulse at 1.053 μm and 0.526 μm. Figure 5 shows experimental results with our glass laser at 0.526 μm. We show results for only the three lightest gases; the cutoffs in Xe and Kr at 0.526 μm are beyond the long wavelength limit

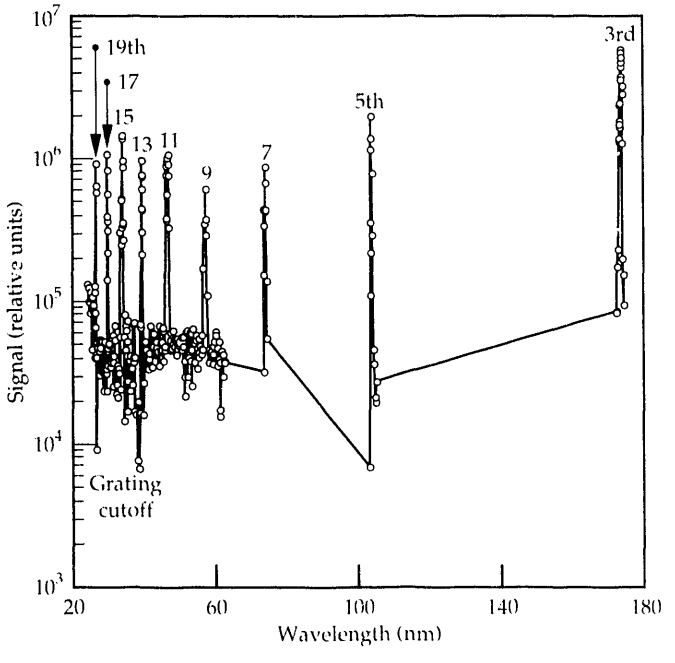

FIGURE 3. Neon spectra taken with normal incidence monochromator.

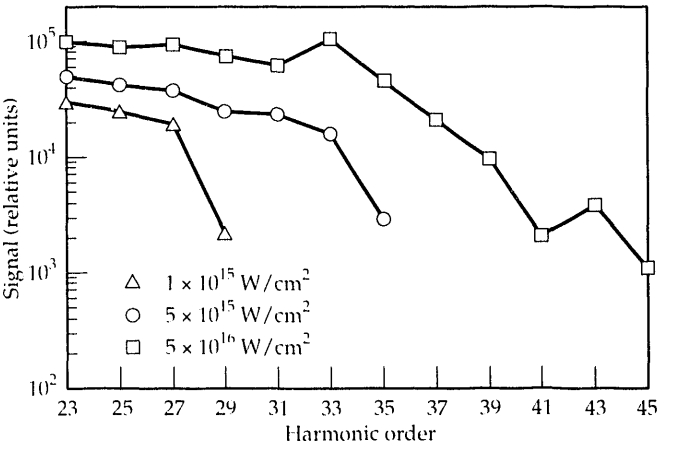

FIGURE 4. Harmonic signal vs order at three intensities in He at 0.526 μm.

TABLE 1. Harmonic cutoff for different rare gases.

Element	I_{sat} (W/cm2)	λ_c (1.05 μm)	$q(\lambda_c)$	λ_c (0.526 μm)	$q(\lambda_c)$
Xe	7×10^{13}	36.8 nm	29	70.7 nm	7
Kr	9×10^{13}	29.6	35	59.1	9
Ar	1.5×10^{14}	20.0	53	45.2	13
Ne	5.0×10^{14}	7.1	149	20.6	27
He	6.0×10^{14}	5.2	201	15.7	33

of our x-ray spectrometer. In the experiments we observe cutoffs in He at the 33rd harmonic, Ne at the 29th harmonic, and Ar at the 13th harmonic of 0.526 μm. These values agree with those predicted in Table 1 The weak harmonics in He and Ar that are beyond the predicted cutoffs may be from ions, i.e., He^+ and Ar^+. We are currently performing experiments to understand harmonic production from rare gas ions, which shows potential for extending the short wavelength limit much further.

A large increase in the energy of the plateau cutoff can be gained by going to longer wavelength as expected from the λ^2 dependence of the quiver energy term. We have observed the 71st harmonic[8] of the 1.053-μm glass laser, which is about the same cutoff as for 0.526 μm. The harmonics produced from 1.053 μm in our experiments are a factor of 50 weaker than the 0.526-μm harmonics. Recently two groups reported harmonics out to 150 eV[9,10], using more sensitive microchannel- plate detection: the group at Stanford used a Ti:sapphire system operating at 0.810 μm, while the laser system at Saclay operates at 1.05 μm. We suspect that harmonics from the 1.053-μm laser occur beyond our measured cutoff, but lie below the noise limit of the streak camera.

Conversion Efficiency

We are interested in developing a short-pulse, coherent XUV source based upon high-order harmonic generation. To promote such a system for potential applications, we must optimize and characterize its performance. Principal among the various source characteristics or specifications is the conversion efficiency from laser energy to harmonic energy. Recently we developed a model to determine the output and the various

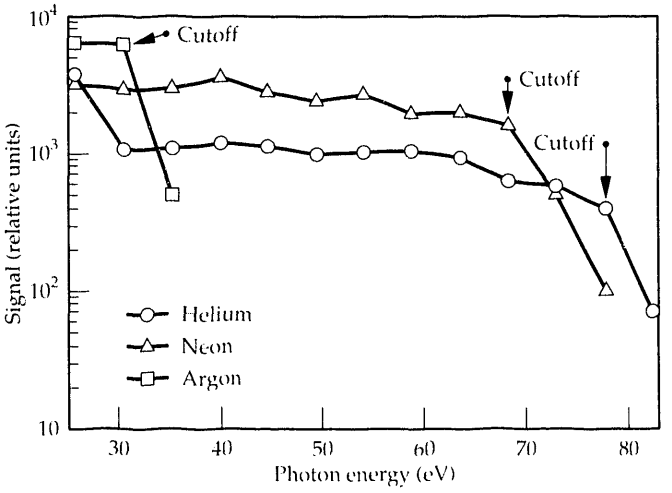

FIGURE 5. Harmonic signal vs photon energy in He, Ne, and Ar showing the location of the plateau cutoffs..

parametric dependences of our XUV source. The model and its development serve different purposes: to elucidate the physics of harmonic generation, especially the role of phase matching; to predict the upper limit of conversion efficiency for different harmonic orders (in different gases); and to understand the parametric dependences and their limitations in scaling the harmonic conversion to the maximum possible levels.

To derive the equations for the harmonic output of our source, one begins by solving the inhomogeneous wave equation with a source term that is the polarization field produced by the coherently driven dipoles. The nonlinear dipole moments used to calculate the polarization fields are obtained by solving Schrodinger's equation, including the laser-atom interaction. (See Kulander's article, "Theory of High-Order Harmonic Generation," in this issue for more details.) Once expressions for the electric fields of the different harmonics are obtained, energy, power, and efficiency can be determined by integrating the harmonic field expressions over time and space coordinates. This is a standard approach and is described in detail in Refs. 11–13. Rather than repeat the full calculations for the harmonic electric field, we start with the resulting expression for the number of photons.

The number of photons of a particular harmonic order is given by[12]

$$N_q = \frac{\pi^2 n^2 b^3 \tau |d_q|^2}{4h} \left|F_q(b,\Delta k)\right|^2 , \qquad (2)$$

where n is the atom density, τ_q is the pulse width of the harmonic, d_q is the dipole moment of the q-th harmonic, b is the confocal parameter of the focused laser, and $F_q(b,\Delta k)$ is the phase matching function.[11] For Gaussian beams, $F_q(b,\Delta k)$ is a complicated integral expression that must be solved numerically, therefore to identify the relevant physics, we consider a simpler form that applies to a square pulse[13]

$$\left|F_q(b,\Delta k)\right|^2 = \left(\frac{p}{q}\right)\left(\frac{2L}{b}\right)^2 \left\{\frac{\sin\left[\pi L / L_{coh}\right]}{\pi L / L_{coh}}\right\}^2 . \qquad (3)$$

In Eq. (3), p is the effective order of nonlinearity (~5–8), L is the length of the nonlinear medium, and L_{coh} is the coherence length–the distance over which the harmonic and driving fields become out of phase by π. The expression for the coherence length, $L_{coh}=\pi/[\Delta k+(2q/b)-(2q/pb)]$, includes a term, Δk, for the difference in dispersion between the driving and harmonic fields. In the

case of a plasma, the primary contribution to the dispersion is from free electrons n_e and $\Delta k = \lambda r_e n_e (q^2-1)/q$, where r_e is the classical electron radius.

The relationship between the medium length and the coherence length divides the expression for N_q into three regimes: $L<<L_{coh}$, $L\approx L_{coh}$, and $L>>L_{coh}$. To maximize conversion efficiency, the desired operating regime is where $L_{coh}>>L$. In this case, the harmonic field increases continuously over the length of the nonlinear medium because the harmonic field interferes constructively with the driving laser field. In contrast, for $L>>L_{coh}$, the polarization field and the harmonic field move in and out of phase with each other, and the output harmonic signal is produced in only the final coherence length of the medium. Figure 6(a) plots the number of harmonic photons vs confocal parameter calculated for the more rigorous Gaussian beam case. Figure 6(b) shows the harmonic conversion efficiency calculated for the same harmonic orders. (Harmonic conversion efficiencies are the number of harmonic photons at a particular order divided by the number of photons in the driving laser pulse.) In both plots, the three regimes are evident. For small b, $L_{coh}<<L$ and $N_q \sim b^3$. As b increases N_q goes through the transition region where $L_{coh}\approx L$ into the region where $L_{coh}>>L$ and $N_q \sim b$. This is the desired operating region for maximum conversion efficiency as can be seen from Fig. 6(b). This linear dependence of the number of harmonic photons on confocal parameter b in the region where $L_{coh}>>L$ can also be seen in Eqs. (2) and (3). When $L_{coh}>>L$, $|\mathbf{F}_q(b,\Delta k)|^2 \approx (p/q)(2L/b)^2$ and

$$N_q = \frac{\pi^2 n^2 b^3 \tau_q |d_q|^2}{4h} \left\{ \frac{p}{q} \left(\frac{2L}{b} \right)^2 \right\} . \quad (4)$$

This expression is shown as the flat-topped line in Fig. 6(a). From Eq. (4), one can see the relevant parametric dependences that describe the harmonic output in the region of desired operation ($L<<L_{coh}$), namely $N_q \sim (nL)^2 b$. The conversion efficiency, $\eta = N_q/N_1 \sim (nL)^2$ and is independent of the confocal parameter b, and so, to increase the conversion efficiency one must increase the column density nL. Eventually, absorption of the XUV photons or the reduction of the coherence length due to free electrons will set an upper limit to nL.

Coherent XUV Source

Our objective is to eventually produce an XUV source based upon harmonic generation that will be suitable for a variety of applications in areas such as spectroscopy, diagnostics, and molecular dynamics (or wherever short-pulse, coherent, XUV radiation is desired). An important feature of such a source is choosing the ideal laser system that will provide the source with its maximum capabilities. The ideal laser system should be tunable, for spectroscopic applications, short pulse (~100 fs, or less) for dynamic experiments that require ultrafast temporal resolution, have suitable pulse energy to operate in the regime $L<<L_{coh}$, and provide a reasonable repetition rate. Recently our group[14] built a 1-TW laser system based upon the new Cr-doped LiSAF (Cr:

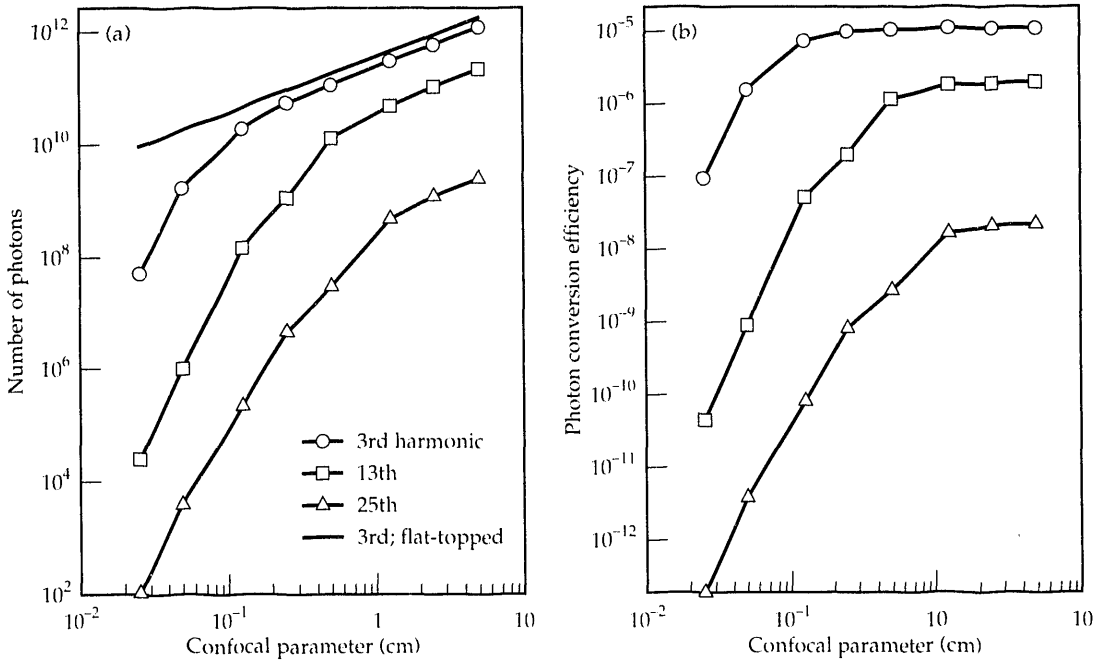

FIGURE 6.
(a) Calculated number of harmonic photons vs confocal parameter for 3rd, 13th and 25th harmonics of 0.526 μm, where the peak intensity is 6×10^{14} W/cm^2, L = 500 μm, n = 10^{19} cm^{-3}, and p = 5. The dotted line shows calculated results of the 3rd harmonic for a flat-topped beam.
(b) Conversion efficiency vs confocal parameter for 3rd, 13th, and 25th harmonics

$LiSrAlF_6$) material.[15] This laser has all of the desired features for producing coherent XUV radiation via high-order harmonics. The LiSAF laser system emits a 110-fs, 130-mJ pulse at a 5-Hz repetition rate. LiSAF is tunable from 0.75 to 0.95 μm. We will begin using this system for harmonic generation in the near future.

Summary

High-order harmonic generation is a source of high-energy (XUV-soft x-ray), short-pulse(~1ps), fully coherent radiation that is part of a larger class of high-intensity, laser-atom interaction phenomena that are seen above 10^{14} W/cm^2. The Short Pulse Laser Group is developing a source based upon high-order harmonic generation that can be used in a range of applications including atomic and molecular spectroscopy, molecular and solid state dynamics, pump-probe experiments in plasma physics, photoelectron spectroscopy, etc. Our current work is focused on understanding the short wavelength limits of this phenomena, optimizing and characterizing the output of an XUV source based on harmonic generation, and, finally, developing a useful XUV instrument using the short pulse, terawatt, Cr-doped LiSAF laser system.

Notes and References

1. F. G. Patterson, M. D. Perry, and J. T. Hunt, "Design and performance of a multiterawatt, subpicosecond neodymium: glass laser," *J. Opt. Soc. Am. B* **8**, 2384 (1991).
2. M. D. Perry, C. Darrow, C. Coverdale, and J. K. Crane, "Measurement of the local electron density by means of stimulated Raman scattering in a laser-produced gas jet plasma," *Opt. Lett.* **17**, 523 (1992).
3. J. K. Crane, M. D. Perry, S. Herman, and R. W. Falcone, "High-field harmonic generation in helium," *Opt. Lett.* **17**, 1256 (1992).
4. M. V. Ammosov, N. B. Delone, and V. P. Krainov, "Tunnel ionization of complex atoms and of atomic ions in an alternating electromagnetic field," *Sov. Phys. JETP* **64**, 1191 (1986).
5. A. McPherson, G. Gibson, H. Jara, U. Johann, T. S. Luk, I. McIntyre, K. Boyer, and C. K. Rhodes, "Studies of multiphoton production of vacuum-ultraviolet radiation in the rare gases," *J. Opt. Soc. Am. B* **4**, 595 (1987).
6. J. K. Crane, "High-order harmonic conversion efficiency in helium," Lawrence Livermore National Laboratory, Livermore, CA, UCRL-ID-108778, (1991).
7. J. L. Krause, K. J. Schafer, K. C. Kulander," High-order harmonic generation from atoms and ions in the high intensity regime,"*Phys. Rev. Lett.* **68**, 3535, (1992).
8. J. K. Crane, M. D. Perry, D. Strickland, S. Herman, and R. W. Falcone, "Coherent and incoherent XUV emission in helium and neon, laser-driven plasmas," Lawrence Livermore National Laboratory, Livermore, CA, UCRL-JC-111287 (1992).
9. J. J. Macklin, J. D. Kmetec, C. L. Gordon, "High-order harmonic generation in Ne," *Proc. Conf. on Quantum Electronics and Laser Science*, paper QPD10, May 1992.
10. A. L'Huillier and P. Balcou, "High-order harmonic generation in rare gases with a 1ps 1053 nm laser," submitted to *Phys. Rev Lett.* (1992).
11. J. F. Reintjes, "Nonlinear Parametric Processes in Gases and Liquids," (Academic Press, Inc., New York, 1984).
12. A. L'Huillier, Ph. Balcou, S. Candel, K. J. Schafer, and K. C. Kulander, "Calculations of high-order harmonic generation processes in xenon at 1064 nm," *Phys. Rev. A.* **46**, 2778, (1992).
13. A. L'Huillier, K. J. Schafer, and K. C. Kulander, *J. Phys. B* **24**, 3315 (1991).
14. T. Ditmire and M. D. Perry, "Terawatt Cr-doped LiSAF Laser System," *Opt. Lett.* (Jan 1993) (accepted).
15. S. A. Payne, L. L. Chase, L. K. Smith, W. L. Kway, and H. W. Newkirk, *J. Appl. Phys.* **66**, 1051 (1989).

THEORY OF HIGH-ORDER HARMONIC GENERATION

K. C. Kulander
K. J. Schafer
J. L. Krause

Introduction

Recent experiments employing short-pulse (<50 ps), high-intensity lasers to excite rare gas atoms have produced surprisingly strong x-ray ultraviolet (XUV) emission due to harmonic conversion of the pump radiation. This result is surprising for two reasons. First, the observed harmonics were of very high energy: up to the 67th order of 526 nm and the 133rd order of 1053 nm (>150 eV, in both cases). Second, the relative intensities of the harmonics dropped gradually up to a well-defined, high order after which they decline precipitously. This behavior is dramatically different from that observed in more traditional, long-pulse harmonic conversion studies. In that case, the atom does not experience very high intensities; the interaction remains perturbative as the atom ionizes. In the perturbative regime, higher order processes are less probable than lower orders so very high-energy photons cannot be produced in long-pulse experiments. In picosecond pulses, the neutral atom survives to intensities at which the atomic response becomes strongly nonperturbative. One characteristic of this response is the emission of harmonic photons of very high order.

It is expected that nonperturbative harmonic generation can be exploited to provide an inexpensive, flexible source of short wavelength, coherent, tunable, short-pulse radiation. The fundamental understanding of this process depends on the first principles calculation of the behavior of the individual atoms in strong, pulsed laser fields. From such studies, the properties of the radiation emitted from each atom in the field during the pulse can be determined. A second aspect of this process is the propagation of the generated harmonic fields through the excited medium. Therefore, a complete theoretical treatment of harmonic generation requires two equally important steps: (1) calculation of the polarization fields induced in the individual atoms by the driving laser and (2) determination of the macroscopic phase matching of these harmonic fields.

The objective of our theoretical efforts is to develop predictive capabilities that can establish, from first principles, the parameter space for optimum harmonic conversion using state-of-the-art, short-pulse optical lasers. To accomplish this goal we need to understand the dependence of the conversion efficiency on the atomic medium, laser pulse length, wavelength, peak intensity, the focal properties of the pump beam, and the gas density and spatial distribution.

Single-Atom Emission Spectrum

The problem of the behavior of an atom in an intense laser field has attracted a great deal of attention during the past few years because of the remarkable advances in short-pulse laser technology. LLNL has been one of the leaders in these advances, constructing the most powerful table-top laser system in the world.[1] This subpicosecond glass laser can produce more than 10 TW, with focused intensities above 10^{18} W/cm^2. It has been used for studies of emission rates of both electrons and photons from atoms and atomic ions, excited by this extremely intense radiation field.[2] The laser is capable of removing several electrons from the atoms during a pulse. The question arises whether the harmonic emission produced in these fields comes from the neutral atoms or from ions.

These experiments present a unique challenge for theoretical study because the electric field of the laser can equal or exceed electrostatic interactions within the atom. The nonperturbative response of the atomic electrons can be reproduced only with a formalism that can

handle these interactions on an equal footing. This means the traditional method of treating the electromagnetic field as a weak perturbation of the field-free atomic states is certainly invalid. During the past few years, we have developed such an intense field theory.[3–6] It requires the explicit solution of the time-dependent Schrödinger equation for the atom in the pulsed field. Because the field is extremely strong, it can be represented by a classical oscillating electric field, so that the resulting equation to be solved is given by

$$i(\partial/\partial t)\Psi(\vec{r},t) = \{H_0 + ezE_{max}f(t)\sin(\omega t)\}\Psi(\vec{r},t) \quad , \quad (1)$$

where H_0 is the atomic Hamiltonian which includes the kinetic energies and the Coulombic interactions. The atom-field interaction term corresponds to a linearly polarized laser field with a slowly varying envelope given by $f(t)$. Equation (1) is an initial value problem with the field-free ground state of the atom being the solution at $t = 0$.

It turns out that it is not possible to solve Eq. (1) exactly for a multi-electron atom using present computational capabilities. However, we have demonstrated that a sufficiently accurate solution for the rare gases can be obtained using a single-active-electron (SAE) model.[7] In this approximation, simultaneous, multiple excitations of the atomic electrons are neglected. We separately determine the response to the driving field of each valence-shell electron in the potential generated by the nuclear attraction and the remaining electrons, frozen in their initial orbitals. This results in solving an equation similar to Eq. (1) but with an appropriate single-particle effective potential[8] for the orbital of each "active" electron. From the evolution of the time-dependent orbitals, we can extract the rates and strengths of the desired electron and photon emission processes.

We determine the value of the time-dependent electronic orbitals on a grid of points defined in either a cylindrical or spherical coordinate system. The linear polarization of the laser field means the wave function has cylindrical symmetry, and therefore, only two spatial dimensions are involved. The kinetic energy operations are carried out using finite differences and the time propagation via a Peacemann-Rachford implicit scheme.[3] The development of the SAE model has been a very significant advance in this field as it has made possible the study of strongly nonperturbative processes with modest computational effort. Its success demonstrates that the ionization and polarization dynamics of the rare gases are dominated by single excitations in the strong field regime.

We follow the evolution of the time-dependent wave function for a pulse, $f(t)$, which rises over five to ten optical cycles, then is held constant over several additional cycles. During the constant intensity portion of the pulse, emission rates can be determined.[9] The photon emission strength is given by the square of the Fourier transform of the time-dependent dipole of the total electronic charge distribution

$$\sigma(\omega) \equiv \omega^3 |d(\omega)|^2$$

$$= \omega^3 \left| (T_2 - T_1)^{-1} \int_{T_1}^{T_2} dt e^{i\omega t} \int d\vec{r}\Psi^*(\vec{r},t) z \Psi(\vec{r},t) \right|^2 \quad , \quad (2a)$$

or equivalently

$$= \omega^{-1} \left| (T_2 - T_1)^{-1} \int_{T_1}^{T_2} dt e^{i\omega t} \int d\vec{r}\Psi^*(\vec{r},t) \ddot{z} \Psi(\vec{r},t) \right|^2 \quad , \quad (2b)$$

where $\ddot{z} = [H,[H,z]]$ is the acceleration form of the dipole. The latter choice is more tractable because it weights the value of the wave function near the origin, which is more likely to be uncontaminated by numerical errors.[10] The use of the acceleration form allows us to obtain converged harmonic emission spectra for much higher intensities than would have been possible with Eq. (2a). For the hydrogen atom, $\ddot{z}$ is simply $-z/r^3 + E_{max}f(t)\sin(\omega t)$. Because the entire multi-electron wave function appears in the dipole moment expressions, contributions from the individual active electrons add coherently.[11] The interval for the transform is chosen to be well after the turn-on to minimize transient effects. Equation (2) provides the emission spectrum for a given intensity and wavelength. Because the atoms within the laser focus experience a range of intensities during the pulse, these calculations must be repeated for many intensities. For driving laser pulses shorter than 50 fs, the transform in Eq. (2) is taken over the entire pulse because under these circumstances the transient effects are real and can be significant.

The same calculations also provide the ionization rates of the atom for these wavelengths and intensities. Harmonic generation from a neutral atom decreases dramatically when the atom ionizes because the polarizability of the remaining ion is substantially lower than the neutral. Therefore, it is important to determine the lifetime of an atom in the field in order to evaluate the total emission during the pulse. Of course, ions subjected to much higher intensities will become polarized, emitting harmonic photons up to the point when they themselves become ionized. The ionization rates are determined by calculating the flux of probability through a surface well removed from the atom.[3] In Fig. 1, we show the calculated[12] ionization rates for neutral and singly ionized helium as functions of laser intensity for the two wavelengths used in the harmonic generation studies of Crane et al.[2] From these results, it is clear that, in a 1-ps pulse, the peak intensity in which helium will survive is

approximately 6×10^{14} W/cm^2 and for the ion is 5×10^{15} W/cm^2. Also, we note that the rates at these intensities are only weakly dependent on the wavelength, even though it requires at least 21 1053-nm photons as compared to 11 of the 527-nm photons to ionize helium. This is a clear manifestation of the nonperturbative nature of the dynamics under these conditions.

Figure 2 shows the emission spectrum for helium at an intensity of 3×10^{14} W/cm^2 at 527 nm. The spectrum shows the characteristic structure of emission in the nonperturbative regime.[10] There is a broad background on which there are narrow peaks at frequencies corresponding to odd multiples of the incident photon energy. Because of the inversion symmetry of an atom in a linearly polarized field, even harmonics are forbidden. The harmonic strengths exhibit the following pattern: a rather rapid decline for the first few orders, then a broad plateau of approximately constant intensity, followed by an abrupt cutoff. The width of the harmonic peaks is determined by the shorter of the ionization lifetime, or the pulse length. If we consider only the harmonic strengths as functions of intensity, we see the plateau rises and broadens with increasing intensity. This is shown in Fig. 3, where emission strengths for three different intensities are displayed. From extensive calculations on many realistic and model systems, we have identified a simple scaling law for the cutoff in the plateau[12] that depends only on the field-free ionization potential I_0 the wavelength and the intensity I. The plateau is found to end at approximately

$$E_{max} \cong I_0 + 3U_p \quad , \tag{3}$$

where U_p, which is given by $I/4\omega^2$ in atomic units, is the ponderomotive (or quiver) energy of a free electron in the field. We indicate this predicted cutoff by the arrows in Figs. 3 and 4. For a given pulse length, the atom will experience a maximum intensity before ionizing, which is called the saturation intensity, I_{sat}. If the peak intensity in the pulse exceeds I_{sat}, the cutoff will be defined by the ponderomotive energy at the saturation intensity.

As a result of this scaling law, we can identify a number of important factors in maximizing high-energy harmonic production. First, for a given pulse length, we want to work near the saturation intensity for the species

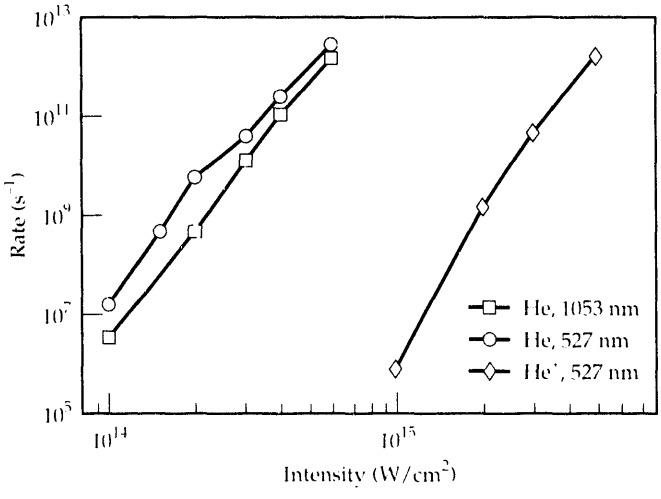

FIGURE 1. Calculated ionization rates for helium atom and ion as functions of laser intensity. The peak-intensity that helium will survive in a 1-ps pulse is approximately 6×10^{14} W/cm^2 and for ion is 5×10^{15} W/cm^2.

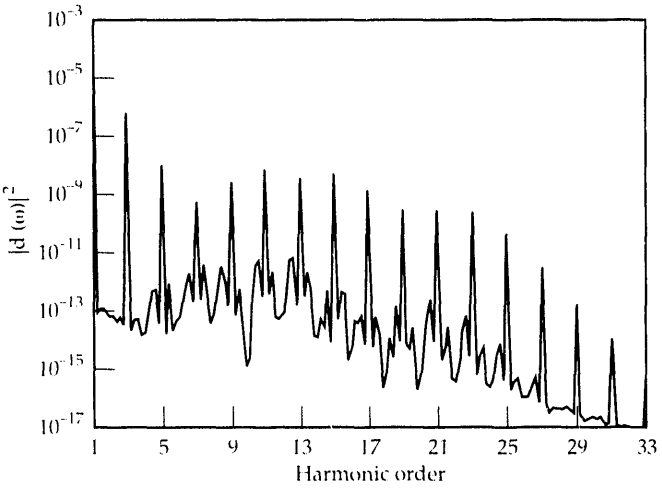

FIGURE 2. Calculated single atom photoemission spectrum in helium for an incident intensity of 3×10^{14} W/cm^2 at 527 nm. The spectrum shows the characteristic structure of emission in the nonperturbative regime. There is a broad background on which there are narrow peaks at frequencies corresponding to odd multiples of the incident photon energy.

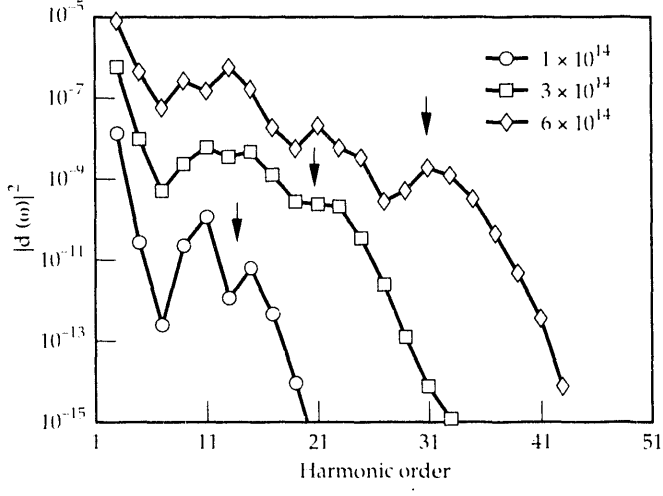

FIGURE 3. Calculated emission strengths at the harmonic frequencies for helium at three different incident intensities at 527 nm. The plateau in the spectrum rises and broadens with increasing intensity. We have identified a simple scaling law for the cutoff in the plateau that depends only on field ionization potential, the wavelength, and the intensity. The arrows indicate our predicted cutoff.

of interest. This will result in the highest conversion efficiency and highest energy harmonics. For peak intensities higher than the saturation intensity, the source will be destroyed during the rise of the pulse. Second by using shorter pulses, higher peak intensities can be employed, again leading to more and stronger harmonics. Also atoms with higher ionization potentials can survive to higher intensities producing broader plateaus. This leads to the question as to whether it is more desirable to generate harmonics from ions rather than neutrals because of the higher ionization potentials for ions. This is clearly the case.[12] In Fig. 4(a), we show that the helium ion, whose saturation intensity for a 1-ps pulse is approximately 5×10^{15} W/cm^2, will emit harmonic photons with energies above 400 eV (less than 3 nm). Figure 4(b) shows the advantage of using longer pump wavelengths as predicted by Eq. (3) to produce high-energy harmonics by comparing results in neutral helium for 1053 and 527 nm. Although the emission strength for the shorter wavelength pump is higher for the harmonics within its plateau, the cutoff is much higher for the longer wavelength.

Phase-Matching Calculations

From the results of the previous section in which we considered only the emission strengths of individual atoms, it appears that longer wavelengths are superior for high-energy harmonic production as is the use of ions as the active medium. However, there is a second, equally important factor in the macroscopic conversion efficiency. This is the propagation of the generated harmonic fields.[13,14] The phase of the high-order polarization field of each atom is set by the phase of the driving field at the atom. As these macroscopic fields propagate through the medium, their phases are modified by the indices of refraction at the harmonic wavelengths. This is also true for the pump field. The refractive indices are different at different wavelengths and are time dependent because of the changing excitation of the atoms and the creation of free electrons. The effect on the harmonic fields is generally stronger than for the pump. As a result, there will be both constructive and destructive interference possible during propagation. To study the interference, we also developed the capability to calculate the effects of phase matching in the nonperturbative regime. This has allowed us to obtain as complete a picture as possible of the factors that lead to optimization of harmonic conversion. This part of our work has been in collaboration with A. L' Huillier, who is the author of the phase-matching code we are now using.[14–16]

We solve the usual paraxial wave equation[15] for E_q, the envelope of the qth harmonic

$$\nabla_\perp^2 E_q + 2ik_q \frac{\partial E_q}{\partial z} = -4\pi(q\omega/c)^2 P_q \exp\left\{-i\int_{-\infty}^{z} \Delta k_q(z')dz'\right\} \quad (4)$$

in terms of P_q, the atomic polarization field at $q\omega$. The propagation is carried out using a finite difference scheme.[16] The solution of Eq. (4) provides the instantaneous harmonic field amplitude. We obtain the number of harmonic photons along with their spatial, temporal and spectral characteristics by solving Eq. (4) for several time increments that span the pulse. P_q and Δk_q ($= k_q - qk_1$), the phase mismatch, depend on time because of the temporal variation of the laser intensity, the depletion of the atomic (or ionic) medium through ionization, and because of the change in the indices of refraction due to the appearance of free electrons.

It is widely accepted, based on experiments on weak field harmonic conversion, that high-order fields produced by a focused laser cannot phase-match in a dispersive medium. The reason for this is that the coherence length, the distance over which the phase

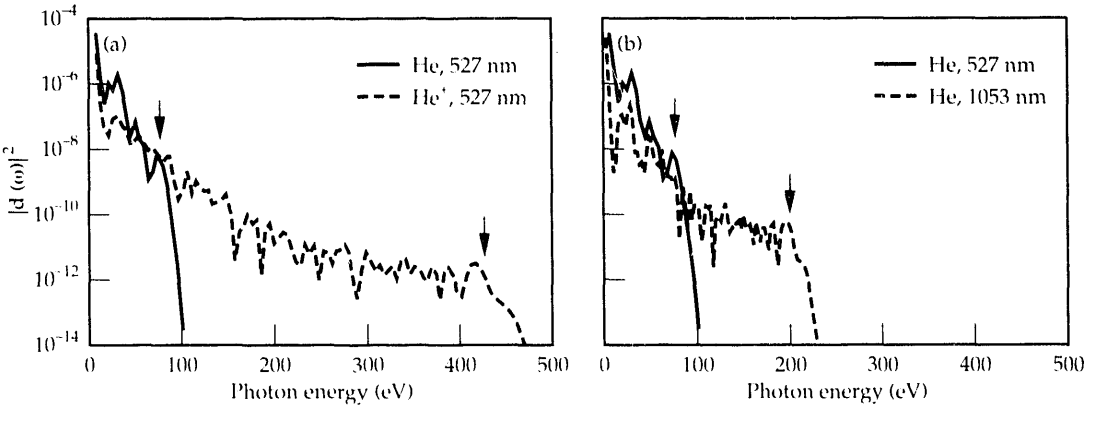

FIGURE 4. Calculated harmonic emission rates at the saturation intensities. (a) Comparison between emission from neutral helium and the ion at 527 nm. (b) Comparison between spectra for neutral helium at different incident wavelengths at 527 nm vs 1053 nm. The arrows indicate our predicted cutoffs.

between the pump and harmonic field, increases by π, exactly matches to the distance over which the polarization, induced by the laser, has appreciable amplitude. This coincidence occurs only when the polarization component for the qth harmonic scales as the incident electric field to the qth power, i. e., according to the lowest-order perturbation theory.[15] In the nonperturbative regime, the single-atom harmonic strengths vary much more slowly with incident intensity. Therefore, the distance over which there is appreciable amplitude in the high-order polarizations can be many times the coherence length. Since the single-atom harmonic spectrum exhibits a plateau, the intensity dependences of the emission strengths within the plateau must all be similar. The emission strengths are found to scale approximately as a power of the incident field intensity with the exponent in the range of 5–10 depending on the atom. This effective order slowly decreases with increasing intensity.

In Fig. 5, we compare the 13th harmonic field produced by a perturbative polarization to that from a polarization field that varies as the fifth power of the field ($|P_q| \equiv N_0 |d(\omega)| \sim |E_1|^5$). On the left side of this figure, we show the dipole amplitudes, and on the right, the amplitude of the resultant harmonic field. The laser propagation direction is left to right, and the fields shown are for a constant density distribution of width equal to the horizontal dimension plotted. In the perturbative case, both fields are strongly localized in the center of the medium at the point of peak intensity and have a width equal to the coherence length. The harmonic yield is given by the total amplitude at the far side of the active medium. This is negligibly small because of the destructive interference after the peak. On the other hand, in the nonperturbative case, the harmonic field shows the expected destructive interference over each coherence length, but because the amplitude of the source is more extended, the harmonic propagates out of the medium. One of the most surprising and felicitous results of nonperturbative harmonic generation is that reasonable phase matching can be achieved for a focused pump, even in a dispersive medium. This makes possible the development of strong XUV sources with quite modest laser drivers. The laser can be focused in order to achieve the intensity needed for the nonperturbative atomic response and the harmonic fields will still be able to propagate through the medium.

A second aspect of the effective orders of the plateau harmonics being similar is that the phase-matching factors are also comparable for the different orders. This results in the macroscopic, phase-matched spectrum having a very similar appearance to that of the individual atoms. Therefore, while we can predict the structure of the emission spectrum from the atomic calculations alone, we need to solve Eq. (4) in order to obtain the absolute conversion efficiency.

One of the most thoroughly studied cases of nonperturbative harmonic generation is the conversion in xenon of a 40-ps Nd:YAG laser (1.064 μm).[9,14–17] The group at Saclay, France has done a parameter study of the conversion efficiency, varying the intensity, confocal parameter, the position of the focus relative to the center of the gas jet, and the gas density.[18] We have collaborated with them on a complete calculation of the emission spectrum, combining the single-active-electron polarizabilities and a calculation of the propagation for the relevant experimental parameters. In Fig. 6, we compare our calculated harmonic photon yields and their experimental results for four different peak-laser intensities.[16] The total number of photons is given by

$$n_q = (c/4\hbar q\omega)\int\int |E_q(r,z',t)|^2 \, r\,dr\,dt \quad , \tag{5}$$

where z' is at the far edge of the active medium. The density of xenon atoms was $5 \times 10^{17}/\mathrm{cm}^3$, the confocal parameter is 1.5 mm and the width of the jet is 1 mm. The intensities considered in Fig. 6 range almost down to the perturbative regime up to twice the saturation intensity. The fall off with order for the lowest incident intensity is reminiscent of earlier long-pulse results, where higher orders were never expected to be observable. In the highest intensity case, most of the atoms in

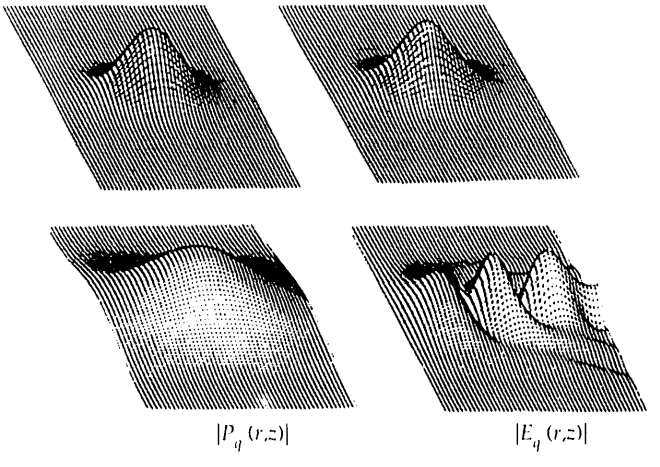

FIGURE 5. Perturbative (upper plots) and nonperturbative (lower plots) polarization field (left side) and propagated harmonic field amplitudes (right side). The polarization field for the latter case is assumed to vary as the amplitude of the incident laser field to the fifth power.

the center of the focus are ionized well before the laser reaches its peak. Therefore, the generated harmonics come mostly from the rising edge of the pulse and are weakly defocused by the electrons being produced. The effect of ionization for this density is mostly in depleting the active medium, not in reducing the output because of the increased dispersion. For higher densities, the role of electrons will become much more profound, affecting not only the harmonic phase matching but also the propagation of the pump beam itself. The agreement between the calculated and measured yields indicates both that we have a good understanding of phase matching for these conditions and that our single-active-electron approximation is valid for the ionization and photon emission rates.

The experiments of Crane et al.[2] in helium show a plateau that extends up to the 45rd harmonic when excited by a 650-fs pulse at 526 nm with a peak intensity above 10^{17} W/cm^2. From Fig. 1, we conclude the saturation intensity of neutral helium is approximately 6×10^{14} W/cm^2 and of the ion is 5×10^{15} W/cm^2. Therefore, there is plenty of intensity to polarize either the atoms or ions in the focal volume. Our calculations predict that the harmonics from the neutral should cut off after the 35th, so that we believe the higher orders observed are because of the emission from ions. We also predict the ion emission should extend up to 177th order [Fig. 4(a)]. In more recent experiments, harmonics up to 67th order have been seen. The difficulty in seeing these very high orders is most likely the result of the poor phase matching in the presence of the electrons that must accompany the production of an ionic medium.[16]

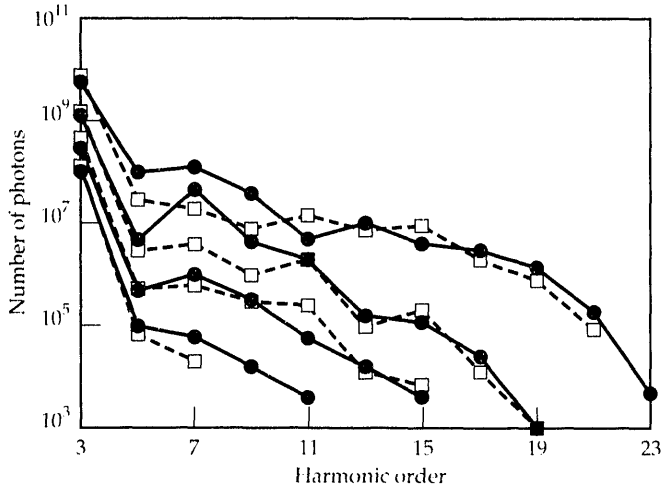

FIGURE 6. Absolute comparison between the measured and calculated harmonic yields in xenon for a 40-ps Nd:YAG pump laser. The intensites considered here range almost down to the perturbative regime up to twice the saturation intensity. The fall-off with order for the lowest incident intensity is reminiscent of earlier long-pulse results, where higher orders were never observed.

Additional experiments have shown the reliability of the scaling law for the maximum harmonic order given by Eq. (3). Macklin et al.[19] from Stanford have seen up to the 109th order of an 806-nm, 125-fs pulse in neon. They report that these harmonics are all from the neutrals, as predicted by our scaling law. L' Huillier and coworkers[20] observed the 133rd harmonic from a 1-ps, 1053-nm laser, also in neon. They did not see a cutoff because of detector limitations, but we would predict the plateau of the neutral would extend above the 153rd harmonic. This result, combined with the 526-nm result of Crane et al.[2] (in helium) shows the benefit of using longer pump wavelengths to reach very high-energy harmonics. Again we note the conversion efficiency is generally higher when the incident wavelength is shorter, but, of course, the number of harmonics is lower. From these studies, we found that most harmonic photons observed to date come from neutral atoms, but some harmonics from ions are beginning to be obtained. In either case, the emission process involves transitions from states well above the ionization limit. This is clearly a very different physical regime from that encountered previously in the field of laser-atom interactions.

Summary

We have presented an overview of recent developments in the theory of harmonic conversion of short-pulse, high-intensity optical lasers in atomic gases. The effort included both the determination of the single-atom emission spectrum and the phase matching of the harmonic fields as they propagate through the excited medium. Because the atomic (ionic) excitation dynamics are dominated by single-particle excitations, accurate calculations are feasible with moderate computational effort. We extended the theory of phase matching into a new physical regime where traditional beliefs about the efficacy of the process were found to be incorrect.

The physical process of high-order harmonic generation benefits from two fortunate factors present in the nonperturbative regime. First, the atomic spectrum exhibits a broad, surprisingly strong plateau of harmonics. This means that, in the nonperturbative regime, processes of varying orders are found to be comparable in strength. The decrease with order of nonlinear processes expected from the perturbative limit is violated much to our advantage. The second beneficial phenomenon is that the slow variation of the harmonic emission strengths with incident intensity results in unexpectedly strong phase matching. As a result of these two factors, we expect this process will be widely exploited as a relatively inexpensive source of high-brightness, coherent, short-pulse XUV radiation. The development of solid-state pump lasers

means the repetition rate can increase to the several Hertz to kiloHertz regime, and the photons emitted can be tuned to any desired wavelengths. We are now exploring the utility and advantages of such a source.

Acknowledgments

We wish to acknowledge the several contributions to this work by B. Shore and A. L' Huillier. Conversations with our experimental colleagues, especially M. Perry, J. Crane, S. Allendorf, and J. Macklin, have been very important in defining the directions the research has taken. Finally, we must acknowledge the contributions of very significant amounts of computer time from many friends and colleagues outside of the Laboratory without which this work would certainly have been impossible.

Notes and References

1. F. G. Patterson and M. D. Perry, "Compact 10 TW subpicosecond Nd:Glass laser," *Optics Letters* **16**, 972 (1991).
2. J. K. Crane, M. D. Perry, S. Herman, and R. W. Falcone, "High-field harmonic generation in helium," *Optics Letters* **18**, 1256 (1992).
3. K. C. Kulander, "Multiphoton ionization of hydrogen: A time-dependent theory," *Phys. Rev. A* **36**, 445 (1987).
4. K. C. Kulander, "Time-dependent Hartree-Fock theory of multiphoton ionization: Helium," *Phys. Rev. A* **38**, 778 (1988).
5. K. C. Kulander, K. J. Schafer and J. L. Krause, "Time-dependent numerical studies of multiphoton processes," in *Atoms in Intense Radiation Fields*, M. Gavrila, Ed., (Academic Press, New York, 1992) pp. 247–300.
6. K. J. Schafer, J. L. Krause, and K. C. Kulander, "Nonlinear effects in electron and photon emission from atoms in intense laser fields," *Int. J. Nonlin. Opt. Phys.* **1**, 245 (1992).
7. K. C. Kulander, K. J. Schafer, and J. L. Krause, "Single-active-electron calculations of multiphoton processes in krypton," *Intl. J. Quant. Chem.: Quant. Chem. Symp.* **25**, 415 (1991).
8. K. C. Kulander and T. N. Rescigno, "Effective potentials for time-dependent calculations of multiphoton processes in atoms," *Comp. Phys. Comm.* **63**, 523 (1991).
9. K. C. Kulander and B. W. Shore, "Calculations of multiple-harmonic conversion of 1064 nm radiation in Xe," *Phys. Rev. Letters* **62**, 524 (1989).
10. J. L. Krause, K. J. Schafer, and K. C. Kulander, "Calculation of photoemission from atoms subject to intense laser fields," *Phys. Rev. A* **45**, 4998 (1992).
11. K. C. Kulander, J. L. Krause, K. J. Schafer, S. W. Allendorf, J. K. Crane, K. S. Budil, and M. D. Perry, "Time-dependent dynamics of an atom in an intense laser field," in *Time-Dependent Quantum Molecular Dynamics: Experiment and Theory*, J. Broekhove, Ed., (Plenum, New York, 1992).
12. J. K. Krause, K. J. Schafer, and K. C. Kulander, "High-order harmonic generation processes from atoms and ions in the high intensity regime," *Phys. Rev. Letters* **68**, 3535 (1992).
13. B. W. Shore and K. C. Kulander, "Generation of optical harmonics by intense laser radiation: I. Propagation effects," *J. Mod. Opt.* **36**, 857 (1989).
14. A. L' Huillier, K. J. Schafer, and K. C. Kulander, "High-order harmonic generation in xenon at 1064 nm: The role of phase matching," *Phys. Rev. Letters* **66**, 2200 (1991).
15. A. L' Huillier, K. J. Schafer, and K. C. Kulander, "Theoretical aspects of intense field harmonic generation," (Topical Review) *J. Phys. B* **24**, 3315 (1991).
16. A. L' Huillier, K. J. Schafer, and K. C. Kulander, "Calculations of high-order harmonic generation in xenon at 1064 nm," *Phys. Rev. A* **46**, 2778 (1992).
17. K. C. Kulander and B. W. Shore, "Generation of optical harmonics by intense laser radiation: II. Single atom spectrum for Xe," *J. Opt. Soc. Am. B* **7**, 502 (1990).
18. P. Balcou and A. L' Huillier, "Phase matching effects in strong field harmonic generation," *Phys. Rev. A*, **47**, 1447 (1993) and references therein.
19. J. J. Macklin, J. D. Kmetic, and C. L. Gordon III, "Short-pulse tunneling limit of high-order harmonic generation," *Phys. Rev. Letters*, **70**, 766 (1993).
20. A. L' Huillier and P. Balcou "High-order harmonic generation in rare gases with a 1-ps 1053-nm laser," *Phys. Rev. Letters*, **70**, 774 (1993).

Two-Dimensional Computer Simulations of Ultra-Intense, Short-Pulse Laser-Plasma Interactions

S. C. Wilks
W. L. Kruer
A. B. Langdon

Introduction

One of the most exciting frontiers in physics today is the interaction of ultrashort, ultra-intense ($I > 10^{17}$ W/cm^2) laser pulses with dense plasmas. Short pulse lasers open up new avenues of research which enable experimenters to access a strongly nonlinear regime of laser-plasma interactions. This regime is characterized by relativistic effects and large light pressures. For many years, there was only incremental progress towards achieving peak powers and focused irradiances for pulses less than or equal to a picosecond (10^{-12} s). The first high-power lasers were typically CO_2 lasers with wavelengths of 10 μm, maximum intensity of 10^{16} W/cm^2, and pulse lengths measured in nanoseconds (10^{-9} s). However, these lasers were expensive and were exclusively research lasers. Carmen et al.[1] and Bach et al.[2] determined many properties of intense laser-plasma interactions, such as super hot electrons and enhanced absorption.[3]

Recently, however, a fundamental discovery enabled experimenters to stretch short laser pulses, amplify these stretched pulses, and recompress them to the original length.[4] This development, known as chirped-pulse amplification, made the recent progress in the development of relatively inexpensive ultra-intense ($I\lambda^2 > 10^{18}$ W · μm^2/cm^2), short-pulse (< 1 ps) lasers[5] possible. This progress led to a dramatic increase in two important laser parameters: (1) peak power, which is a measure of how much energy can be delivered in a given time, and (2) focused irradiance or $I\lambda^2$, which is a measure of the laser intensity in a focused spot. In fact, experiments using table-top terrawatt-class lasers (capable of producing more than 10^{18} W · μm^2/cm^2) are now being performed in the ultrahigh intensity, short pulse regime in many laboratories around the world. Possible applications for these lasers are currently under investigation. Some examples are: drivers for x-ray lasers,[6,7] harmonic generation,[8] and the laser wakefield accelerator.[9] Successful implementation of these applications requires the knowledge of laser-plasma interactions of such pulses.

This article will focus on a particular type of laser-plasma interaction: we will characterize the interaction of intense pulses of light with a preformed plasma which may have a scale length greater than or equal to a laser wavelength. The scale length is a measure of the slope of the plasma density at a particular point in the plasma. We will see that collective electron motion can give rise to intensely driven instabilities in the underdense plasma, and in resonantly driven plasma waves near the critical density. The critical density is defined as the density in the plasma at which the laser light frequency ω_0 equals the plasma frequency ω_p, where $\omega_p = (4\pi ne^2/m_e)^{1/2}$. Here n is the electron density and m_e is the electron mass. These two mechanisms allow for efficient laser light absorption by the plasma, and for the production of MeV electrons.

We will report on a variety of computer simulation results for this new laser-plasma interaction regime. We find that even for normal incidence (i.e., the propagation direction of the laser is at 90° to the surface of the target), the absorption of ultra-intense laser light by plasma electrons near critical surface of the plasma can be as high as 60%. We also find that we can predict the temperature of the hot electrons produced near the critical surface by simply knowing the associated ponderomotive potential of the incident laser. Of particular importance is the laser's ability to bore a hole deep into the overdense plasma, and steepen up the critical surface of the plasma to much less than a wavelength of the incident light. We then discuss the results of some simulations that provide insight to current experiments by C. Darrow, D. Klem, and S. Lane here at LLNL. By comparing the simulation results and experimental results, we can infer a range for the scale lengths present in the experiment. We conclude with a brief description of the role of Raman instability and various self-focusing mechanisms that occur in the underdense plasma.

Computer Simulation Set-Up

We used ZOHAR,[10] a 2-D particle-in-cell (PIC), electromagnetic, relativistic electron, mobile ion code to study this complex interaction regime. First, a large number of particles, typically on the order of one million, are laid down on a two-dimensional grid, about $10 \times 50\ \lambda_0$ (where λ_0 is a laser wavelength). The particles are assigned some initial velocity distribution, usually a Maxwellian, corresponding to some initial temperature for the plasma. The charge and current densities associated with the particles are then computed. The electric and magnetic fields are calculated according to Maxwell's equations using the charge and current densities as sources. The particles are then moved, according to the relativistically correct Lorentz force equation, depending on the electric and magnetic fields obtained. New charge and current densities are then calculated, and this process is repeated. Mobile ions, with a realistic mass of 2000 times the mass of an electron are pushed with a nonrelativistic mover. The electric field of the laser which is launched from the left boundary can either be in the plane of motion of the particles (p-polarization), or out of the plane (s-polarization). Assuming that the laser light has a wavelength of 1 μm, the runs can typically be carried out for up to a picosecond.

The main advantage of using PIC in studying plasma processes is that many nonlinearities that would otherwise require tremendous effort to include in analytical solutions are inherent in the PIC simulation method. PIC simulations are traditionally used to gain insight into long pulse, laser-plasma interactions. The equations are solved on a time scale dictated by the plasma frequency ω_p. A plasma period $T = 2\pi/\omega_p$ is typically on the order of a femtosecond so only a few picoseconds can be simulated before computer time becomes prohibitively long. Since until recently, most laser systems had pulse lengths on the order of nanoseconds, it was necessary to extrapolate the results of the simulation to the true laser plasma conditions in a realistic experiment. It is now possible to actually simulate the entire laser pulse, as pulse lengths are now measured in hundreds of femtoseconds.

Simulation Results

The parameter space we explore is an extension of previous laser-plasma physics critical to understanding direct-drive fusion. We begin by examining an interesting form of laser light absorption which occurs when a laser is normally incident onto an overdense plasma (Fig. 1). Kruer and Estabrook,[11] studied this absorption mechanism for irradiances up to 10^{18} W · μm^2/cm^2, and found that absorption caused by the **J** × **B** heating could become significant as the intensity of the laser increases. In fact, for oblique incidence this heating can be significant even in addition to resonance absorption for sufficiently intense laser pulses. For even higher intensities, the electron motion in the field of the light wave becomes strongly relativistic when the irradiance of the laser exceeds $I\lambda_\mu^2 > 10^{18}$ W · μm^2/cm^2. The momentum associated with the oscillatory motion of the electron in the light wave, given by $p_{osc}/m_e c$, is a measure of how relativistic the electron motion gets. This momentum is the relativistic extension of the oscillatory velocity of an electron in a light wave, $v_{osc} = 25.6\ (I\lambda_\mu^2)^{1/2}$, where $I\lambda_\mu^2$ is in W · μm^2/cm^2. A number of interesting effects arise when we began to study this extremely nonlinear regime.

The first set of simulations will concentrate on light that is normally incident onto an overdense plasma ($n = 2n_{cr}$). We assume the laser to have a finite spot, corresponding to a focused beam with half-width $2.5\ \lambda_0$. The plasma has initial dimensions of 5 × 6.75 μm. Immediately, a very strong, high-frequency electrostatic field is set up at the vacuum-plasma interface. This field is the relativistic equivalent of the **J** × **B** force discussed above, and the associated force on the electrons at the interface is given by $f_p = V(\gamma - 1)m_e c^2$, where $\gamma^2 = (1 + p^2/m_e^2 c^2)$. Although generally nonresonant, this field can still accelerate electrons near the

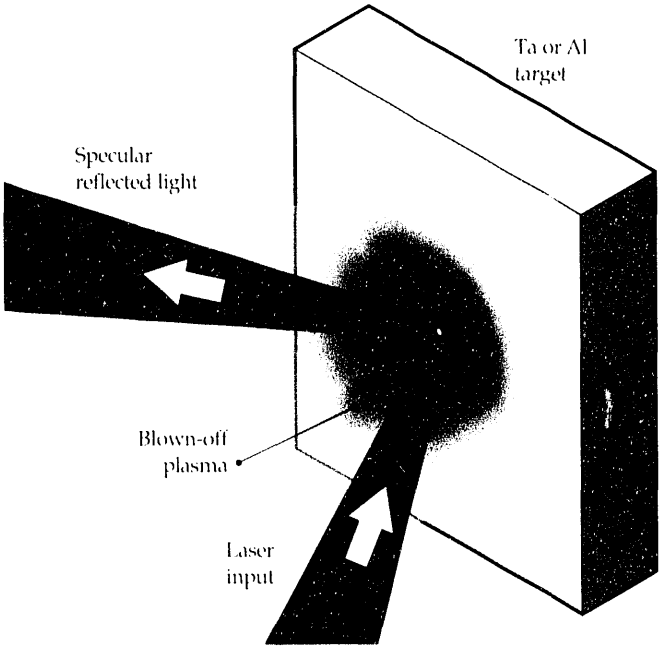

FIGURE 1. An intense, short pulse laser incident onto a preformed plasma. In a fraction of a picosecond, the ions in the underdense plasma which lie in the path of the laser are ejected transversely. Most of the laser's energy then goes into generating hot (MeV) electrons at the steepened critical surface. Because of the large ponderomotive force associated with the laser at this surface, most of the surface will be accelerated into the overdense plasma region. We simulated this region for this work.

vacuum-plasma interface. The frequency of this wave is $2\omega_0$, which means that twice every cycle, a group of electrons will be accelerated into the plasma by this ponderomotive force. This motion will show up as short "bursts" of high-energy electrons, separated by a distance of half of a laser wavelength, or $\pi c/\omega_0$ in the p_x vs x plots (Fig. 2). This absorption mechanism is similar to Brunel's not-so-resonant, resonance absorption[12] (to be discussed later), though it differs in that here, the electrostatic field associated with the ponderomotive force, not the electric field of the laser, drives electrons across the vacuum-plasma interface. Because the maximum amount of energy that the electrons can gain in this interaction is on the order of the ponderomotive potential, it is not surprising that the temperature associated with these accelerated electrons is essentially given by the ponderomotive potential. We find that the temperature of hot electrons injected into the overdense plasma can be estimated by

$$T_{hot} = [(1 + I\lambda_\mu^2/1.4 \times 10^{18})^{1/2} - 1] \times 511 \text{ keV} \quad . \qquad (1)$$

We can see from Eq. (1) that for irradiance over 10^{18} W · μm²/cm², electron temperatures of greater than 100 keV are possible, and for irradiance of 10^{19} W · μm²/cm², MeV temperatures are obtained. A number of simulations were done at these high intensities, and the results are shown in Fig. 3 along with the above estimate for T_{hot}, which is based on the ponderomotive potential of the laser. As expected, when we take an average of the results for the two different electric field polarizations (s and p), we can obtain reasonable agreement with the estimate for T_{hot} given above. Some experimental results are also included for comparison (Fig. 3).[2,13,14]

One of the most interesting aspects of this interaction is that the light pressure is sufficiently strong that it actually bores a hole into and past the critical surface. This interaction is a variation on the steepening seen in the strongly driven resonance absorption cases. However, since the light is now focused, a hole forms as the critical surface is pushed back, its depth increasing with time (Fig. 4). This process occurs because the light pressure p_L, of the laser light is extremely high: $p_L = 2I/c \approx 6 \times 10^3$ Mbar for $I = 10^{19}$ W/cm². The velocity of the steepened front moving into the overdense plasma can be estimated by balancing the momentum flux of the mass flow with the light pressure. The front velocity is given by

$$u/c = [(n_{cr}/2n_{pe})(Zm_e/M)(I\lambda^2/1.37 \times 10^{18})]^{1/2} \quad . \qquad (2)$$

Here n_{pe} is the electron density, u is the ion front velocity, M is the ion mass, and Z the charge state. For the example, a simulation with parameters $n_{pe}/n_{cr} = 4$, $Zm_e/M = 1/2000$, and $I\lambda^2 = 10^{19}$ W · μm²/cm² gave a front velocity of $u = 0.025c$, which is in good agreement with the above estimate. Note that this inward acceleration produces energetic ions with energies of about 10^{-3} Mc². The inward acceleration of the critical surface can be experimentally verified by observing a red shifting in the frequency of the reflected light. In fact the expected blue shifting of the reflected light caused by ponderomotive effects at the critical surface decreases[15] in experiments with lower intensity lasers ($I\lambda^2 = 10^{15}$ W · μm²/cm²).

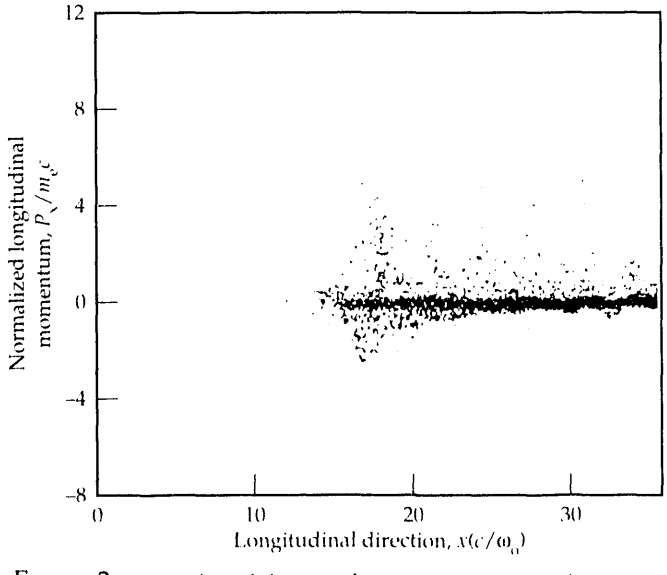

FIGURE 2. A snapshot of electron phase space (p_x vs x) at time $\omega_0 t = 180$. In this 2-D simulation, the intensity would be 10^{19} W/cm², for a 1-μm laser.

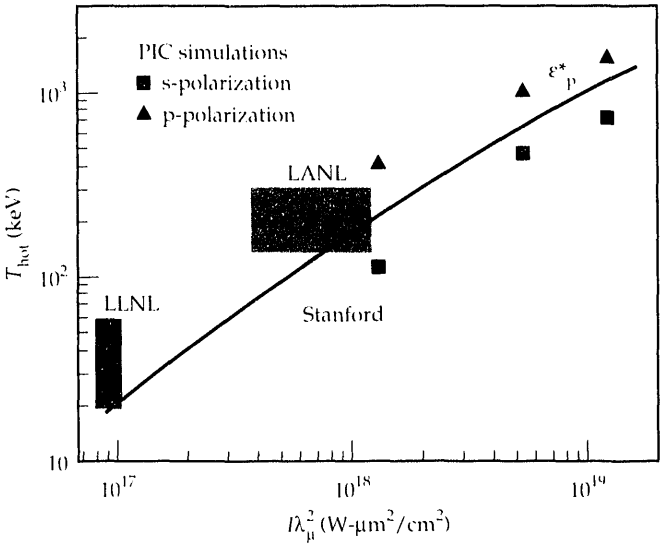

FIGURE 3. Simulation results for the heated electron temperature vs irradiance along with the estimate of the temperature ε_p, which is based on the ponderomotive potential of the laser. High-intensity experimental results from Stanford, LLNL, and LANL are also included for comparison.

As the hole forms, the absorption increases because the electric field associated with the laser can now drive electrons on the wall of the channel, first pulling them into the channel and then ejecting them laterally into the plasma. This type of absorption is like that discussed by Brunel,[12] which is similar to resonant absorption in a steep density gradient. In addition, the absorption caused by $\mathbf{J} \times \mathbf{B}$ heating continues at the deepest part of the hole. Eventually, the hole becomes so deep that almost all of the laser light is absorbed either at the deepest part of the channel, or along the sides. This process was confirmed by simulations that show an increase in the absorption relative to time, with the increase in the p-polarization cases being more dramatic than the s-polarization cases. In the case of p-polarization, the electrons can be directly driven by the laser in the x-y plane, across the density gradient. In an experiment, there would be no difference between the two cases, for this normally incident case.

Another interesting effect is the generation of extremely large magnetic fields in the overdense region of the plasma around the channel. Figure 4 shows magnetic field contours at $\omega_0 t = 600$ on the plane where the particles move (x-y plane). The periodic structure in the vacuum region to the left of the vacuum-plasma boundary (the dark line) is associated with the incident light wave. The contours inside the plasma denote an intense, nonoscillatory magnetic field generated by electron heating around the laser spot. In Fig. 4, the irradiance is $I\lambda^2 = 10^{19}\ \mathrm{W} \cdot \mu\mathrm{m}^2/\mathrm{cm}^2$, and the resulting static magnetic field has a value of about 250 Megagauss. The generation of large magnetic fields was noted in a number of related studies,[3,12,16] but they differ from the present result in the following ways. In the Helios experiment, similar magnetic fields were generated in the underdense plasma.[6] Additionally, for oblique incidence of intense lasers onto sharp vacuum-plasma interfaces, a large static B-field along the surface of the interface was noted by both Brunel[12] and Estabrook.[16]

Related simulations with scale lengths greater than or on the order of a wavelength of the incident light wave were performed. The scale length of the plasma, $L = n(dn/dx)^{-1}$, is essentially a measure of the steepness of the slope of the plasma density near the critical density. These simulations show what happens when the intense pulse is incident onto a vacuum-plasma interface formed by a prepulse, and the plasma is expanding into the vacuum from the surface of a solid target. These simulations begin with a plasma density that is ramped from 0 to 4 n_{cr}, over a distance of $4\lambda_0$, with an additional amount of plasma at 4 n_{cr} behind the ramp. The incident laser is focused as above, with a peak intensity of $I\lambda^2 = 5 \times 10^{18}\ \mathrm{W} \cdot \mu\mathrm{m}^2/\mathrm{cm}^2$, and is s-polarized. As the laser light enters the system from the left and begins to interact with the critical surface near the middle of the simulation box, a corrugated surface develops (Fig. 5a). Although the interaction of the light with the critical surface is similar to the "bubble" formation studied by Estabrook and Valeo[17], and by Kindel et al.[18], the interaction differs in two respects. First, the pressure associated with the central bubble is so intense, that it is accelerated into the overdense plasma (Fig. 5b). Secondly, the perturbation is actually seeded by the motion of the electrons due to the ponderomotive force of the light in the underdense portion of the plasma, well before the ions have a chance to move. The Rayleigh-Taylor-like instability, which develops on the critical surface, is caused by the photons (the light fluid) effectively accelerating the critical surface of the plasma (the heavy fluid). Similar to the sharp interface case discussed above, as the pulse continues to propagate, the absorption increases as the central hole deepens. Other simulations, with various scale lengths and intensities show similar behavior.

Comparison with Current LLNL Experiment

Ongoing experiments here at LLNL[13] focus a Nd:glass laser at 1.0 μm to a few times the diffraction-limited spot to produce intensities up to 10^{18} W/cm^2. The laser pulse has a full width at half maximum of about 1 ps, and is focused onto a solid target (typically either tantalum or aluminum) at an angle of 22° from the normal of the target. This short, picosecond pulse

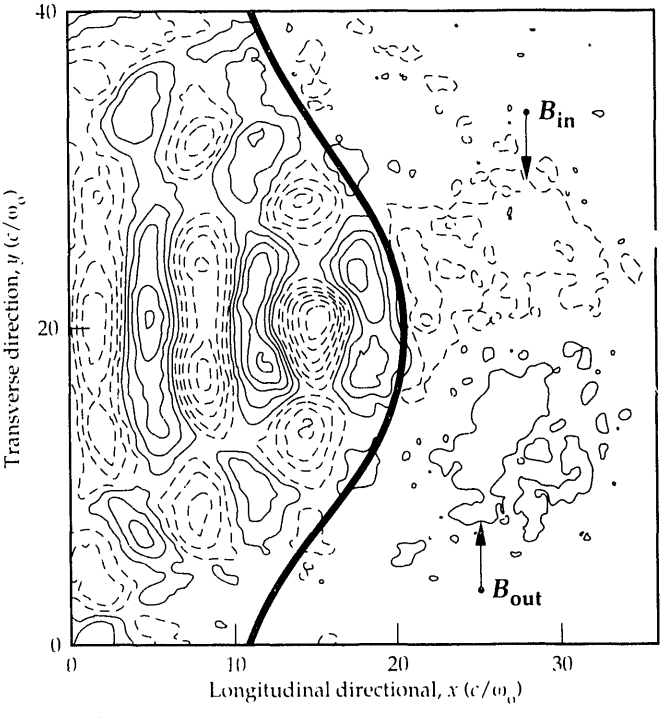

FIGURE 4. Spatial contours of the magnitude of the magnetic field B, present in the overdense plasma. The incident intensity was 6×10^{18} W/cm^2.

is actually riding on top of another lower intensity pulse, called the pedestal which is typically a few hundred picoseconds long. Although the intensity of the pedestal is roughly 3 orders of magnitude lower than the main pulse, it is still capable of creating a preformed plasma. The intense picosecond pulse interacts with this preformed plasma which has an estimated scale length of between 1 and 30 μm near the critical surface, depending on whether the pedestal is intense enough to steepen up the plasma density near critical.

The initial stage of the above interaction occurs when the intense, 1-ps pulse hits the critical surface. The pressure associated with the picosecond pulse is so intense, that it literally "pushes" the critical surface into the solid. The pressure allows for even more steepening of the critical surface as the pulse continues to interact with the critical surface. This interaction soon makes the scale length less than a laser wavelength of the incident laser light, and a hydrodynamical equilibrium may be set up. However, this process may take a significant fraction of the picosecond pulse. In the early CO_2 laser experiments, a hydrodynamical equilibrium was quickly set up in the first few picoseconds of the pulse. Since the pulses were nanoseconds long, the interaction was considered to be steady state because the laser pressure balances the plasma pressure for essentially the entire duration of the pulse. Our work studies the transition to equilibrium, as well as the final equilibrium state of a steepened profile. The equal importance of both the transition to, and final state of hydrodynamic equilibrium sets this work apart from previous long pulse, intense laser-plasma studies.

To model the transition from a long scale length plasma to one in hydrodynamical equilibrium, we will begin with a slightly steepened profile to find out what happens as the ultra-intense laser pulse is incident on this density gradient. A series of simulations were done for a linearly ramped plasma density with a scale length of 2 μm. The laser intensity was varied between $2 \times 10^{16} < I\lambda^2 < 10^{18}$ W · μm^2/cm^2, and was directed at an angle of 22° with respect to the normal of the target. The plasma density was ramped up to a maximum density of $2n_{cr}$.

Initially, we observe an intense form of resonance absorption placing near critical. This phenomenon was studied for lower intensities in the early days of laser fusion by many researchers.[18,19] Briefly described, when p-polarized light is incident at an angle to a density gradient, the laser is reflected at a density of $n_{cr}\cos^2\theta$. However, the electric field of the laser tunnels the distance to critical, where it resonantly drives up a plasma oscillation. Electrons can then be accelerated by this plasma oscillation down the gradient, thus absorbing a large fraction of the energy present in the laser. Figure 6(a) is a plot of the longitudinal momentum vs longitudinal position. We see that a large plasma wave has resonantly built up near the critical surface, and the associated electric field is accelerating electrons down the gradient. In contrast to experiments at lower intensities, these electrons can easily reach energies of 1–4 MeV, depending on the intensity of the incident laser (Fig. 3). When these electrons exit the plasma, they are attracted back into the plasma due to the ion charge left behind. The more massive ions are essentially stationary on the time scale of the electrons. The electrons are then accelerated back into the dense plasma with essentially the same energy they had when they were accelerated down the gradient. Evidence for electrons with these energies have been inferred in recent ultra-intense, laser-plasma interaction experiments.[14]

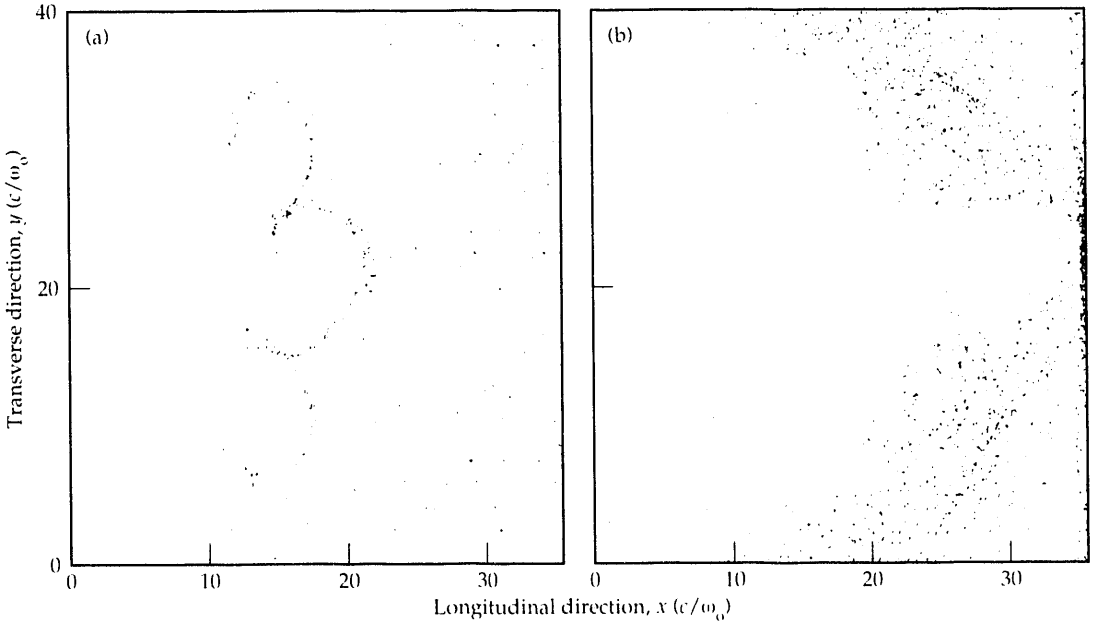

FIGURE 5. (a) Ion real space at $\omega_0 t$ = 800, showing Rayleigh-Taylor-like rippling of the critical surface. (b) The central bubble bored through the plasma at time $\omega_0 t$ = 1200.

Another mechanism that may lead to MeV electrons is the Raman instability in the underdense plasma. Stimulated Raman scattering is a process where an incident light wave decays into a plasma wave and a scattered light wave. For ultra-intense lasers, the spatial growth length for the instability can be just a few wavelengths of light long. A large plasma wave builds up in the plasma in a time much less than a picosecond. Electrons trapped in this wave can be accelerated to MeV energies for the forward Raman case.

Once the picosecond pulse steepens up the density near critical, a slightly different interaction occurs. Since we are also interested in what happens when the pulse is nearly in hydrodynamical equilibrium, we now begin the simulation with a very steep profile. Here, the plasma is ramped up to 5 n_{cr} over a distance of 1/2 laser wavelength. Figure 6(b) shows the longitudinal momentum phase space of the interaction when the density has steepened up to a scale length, $L << 1$ μm, for an intensity of 10^{18} W · μm^2/cm^2. The interaction is now considered to be a modified form of resonance absorption, the so-called "not-so-resonant, resonance absorption."[12] In this interaction, the scale length is so steep, that no tunneling of the laser electric field occurs, but the electric field of the laser directly drives the plasma oscillation at the critical surface. This interaction can also create hot electrons, but the temperature decreases somewhat from original resonance absorption, as the absorption of the laser light itself. Figure 6(b) confirms that the electrons are not as hot when the interaction occurs in a density where $L << 1$ μm, as expected from the above discussion of not-so-resonant resonance absorption.

An important experimental measurement is the absorption of laser light, and Fig. 7 shows the absorption for the two sets of simulations described above. The squares represent the absorption for very steep gradients ($L << 1$ μm) near the critical surface, whereas the circles represent the absorption when $L > 1$ μm. Our experimental data falls between these two extreme cases because experimentally, both conditions will be present during the interaction at different times.

An interesting feature of simulations that study the interaction of the laser in the underdense plasma can be found in the frequency spectrum of the reflected light. As expected, most of the reflected light is at the original frequency of the laser. However, there is a broad peak between 1/4 and 1/2 the incident frequency which may be caused by the large amount of stimulated Raman backscattering near and below quarter critical. Another signature of these simulations is the strong self-focusing of the laser beam. The two main mechanisms for this focusing are ponderomotive[21] and relativistic[22] in nature. Initially, we found that because of the relativistic increase in electron mass, the effective plasma density decreases in the center of the beam (where the intensity is highest). As a result, the laser beam focuses down to a diameter of about a wavelength of the laser light, resulting in intensities several times greater than its original intensity. In addition, large transverse ponderomotive force begins to expel ions from the channel on a longer time scale. This complication creates uncertainties as to the true intensity of the light once it reaches the critical surface. Clearly, the interaction can be quite complicated because instabilities that arise can make an exact modeling of the experiment difficult. However, the above simulation results have begun to shed light on many important aspects of the experiment.

Summary

We report on the results of a series of computer simulations describing the interaction of ultra-intense laser light with a preformed plasma created on the surface of a solid. The motion of the plasma electrons in

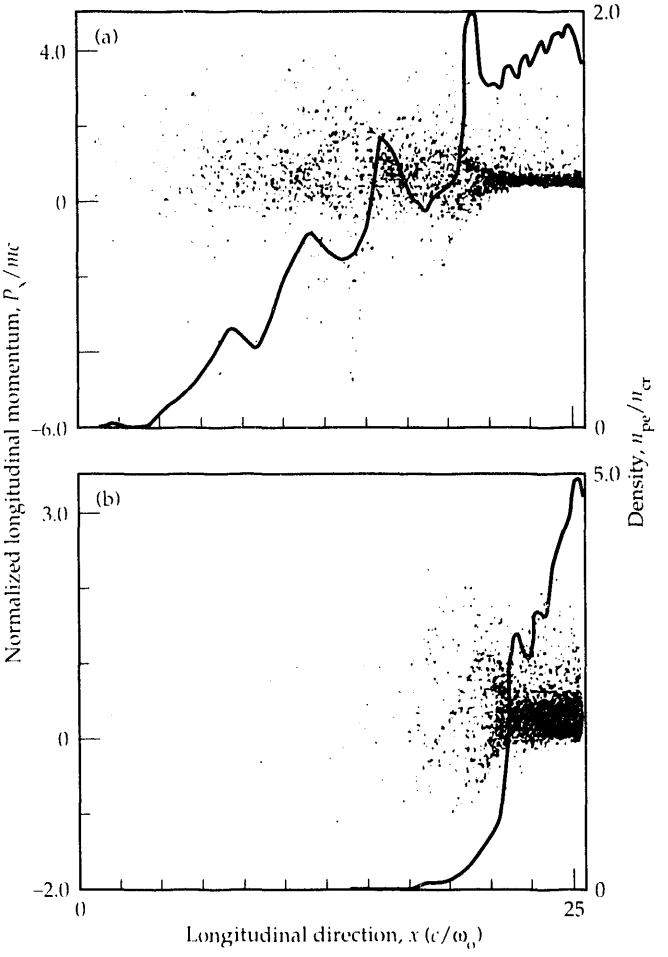

FIGURE 6. Longitudinal momentum p_x, (particles) and density (solid line) vs longitudinal position for (a) scale length of the order of 1 μm, and (b) scale length << 1 μm. For a 1-μm scale length, which occurs early in the interaction, we see that the energy of the electrons is greater than that of the smaller scale length case.

the presence of the laser electric field associated with intensities greater than 10^{18} W · μm^2/cm^2 is extremely relativistic. The 2-D PIC code provides valuable insight into many complex and nonlinear processes that arise in this interaction. We find that there is efficient absorption of laser light (>50%) by the plasma. Most of the energy is absorbed at the critical surface, resulting primarily in the generation of very energetic electrons and ions. The dominant absorption mechanism for the case of normal incidence is **J** × **B** heating of the electrons. The temperature of the hot electrons generated by this mechanism can be estimated by knowing the ponderomotive potential of the laser. Another interesting aspect of the interaction is that a hydrodynamic instability develops on the critical surface due to the large light pressure of the laser. As the laser impinges on the target, the central ripple accelerates into the overdense plasma, which forms a low density channel past the critical surface. The absorption is further enhanced because the laser electric field can now directly drive electrons across the density gradient provided by the channel walls. Finally, the simulations provide insight into recent experimental absorption measurements.

Acknowledgments

We acknowledge useful conversations with K. Estabrook, M. Tabak, C. B. Darrow, D. Klem, M. D. Perry, M. Rosen, W. B. Mori, and J. M. Dawson.

Notes and References

1. R. L. Carmen, D. W. Forslund, and J. M. Kindel, "Visible Harmonic Emission as a Way of Measuring Profile Steepening," *Phys. Rev. Lett.*, **46**, 29 (1981); B. Bezzerides, R. D. Jones, and D. W. Forslund, "Plasma Mechanism for Ultraviolet Harmonic Radiation Due to Intense CO_2 Light," *Phys. Rev. Lett.*, **49**, 202 (1982).

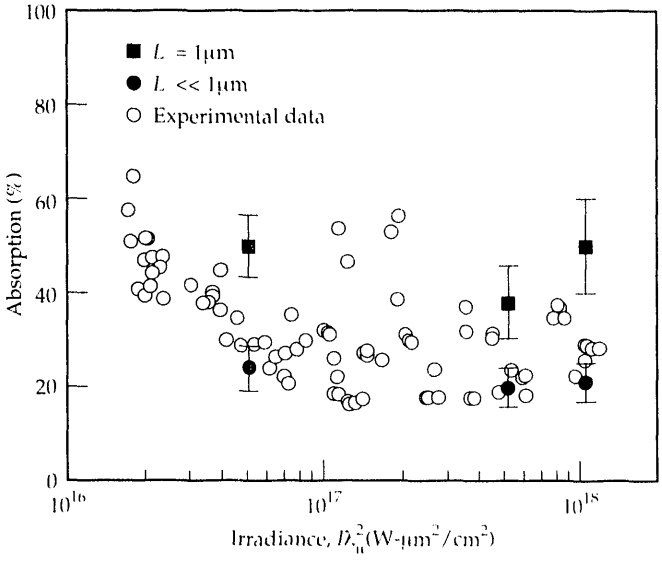

FIGURE 7. Absorption vs irradiance for current experiment at LLNL plotted with simulation points. These results imply a very steep density gradient near the critical surface throughout most of the interaction.

2. D. R Bach, D. E. Casperson, D. W. Forslund, S. J. Gitomer, P. D. Goldstone, A. Hauer, J. F. Kephart, J. M. Kindel, R. Kristal, G. A. Kirala, K. B. Mitchell, D. Van Hulsteyn, and A. Williams, "Intensity-Dependent Absorption in 10.6-μm Laser-Illuminated Spheres," *Phys. Rev. Lett.*, **50**, 2082 (1983).
3. R. Jones, "Surfaces in the Interaction of Intense Longwavelength Laser Light with Plasmas," *Los Alamos National Laboratory Internal Report*, Los Alamos National Laboratory, Los Alamos, NM, LA-UR-85-4318 (1985).
4. D. Strickland and G. Mourou, "Compression of Amplified Chirped Optical Pulses," *Opt. Commun.*, **56**, 219 (1985); P. Maine, D. Strickland, P. Bado, M. Pessot, and G. Mourou, "High Power Chirped Pulse Optical Pulses," IEEE *J. Quantum Electron.*, **24**, 398 (1988).
5. M.D. Perry, and F. Patterson, "Compact, 10 Terawatt Nd:Glass Laser System,"*Opt. Lett.*, **16**, 1107 (1991); A. Sullivan, H. Hamster, H.C. Kapteyn, S. Gordon, W. White, H. Nathel, R.J. Blair, and R. W. Falcone, "Multiterawatt, 100-fs Laser," *Opt. Lett.*, **16**, 1406 (1991).
6. M. M. Murane, H. C. Kapteyn, M. D. Rosen, and R. W. Falcone, "Ultrafast X-Ray Pulses from Laser Plasma Produced Plasmas," *Science*, **251**, 531 (1991).
7. D. C. Eder, P. Amendt, and S. C. Wilks, "Table-Top X-Ray Laser Using a High-Intensity Short-Pulse Driver," *ICF Quarterly Report*, **1**, 114 (1992).
8. S. C. Wilks, W. L. Kruer, and W. B. Mori, "Odd Harmonic Generation of Ultra-Intense Laser Pulses Reflected from an Overdense Plasma," in *IEEE Trans. on Plasma Science*, **12**, 1 (1993).
9. P. Sprangle and E. Esarey, "Laser Wakefield Acceleration and Relativistic Optical Guiding," *Appl. Phys. Lett.*, **53**, 2146 (1988).
10. A. B. Langdon and B. F. Lasinski, "An Electromagnetic Particle in Cell Code," *Methods in Computational Physics* Vol. 16, J Killeen et al., Eds. (Academic Press, New York, N. Y., 1976).
11. W. L. Kruer and K. Estabrook, "**J** × **B** Heating by Very Intense Laser Light," *Phys. Fluids*, **28**, 430 (1985).
12. F. Brunel, "Anomalous Absorption of High Intensity Subpicosecond Laser Pulses," *Phys. Fluids*, **31**, 2714 (1988); F. Brunel, "Not-So-Resonant, Resonant Absorption," *Phys. Rev. Lett.*, **59**, 52 (1987).
13. D. Klem, C. Darrow, S. Lane, and M. D. Perry "Absorption of Intense Subpicosecond 1.06-μm Laser Light by Solid Targets," *Bull. Am. Phys. Soc.* **37**(6) 1382 (1992).
14. J. D. Kmetec, C. L. Gordon, III, J. J. Macklin, B. E. Lemoff, G. S. Brown, and S. E. Harris, "MeV X-Ray Generation with a Femtosecond Laser," *Phys. Rev. Lett.*, **68**, 1527 (1992).
15. X. Liu and D. Umstadter, "Competition between Ponderomotive and Thermal Forces in Short-Scale-Length Laser Plasmas," *Phys. Rev. Lett.*, **69**, 1935 (1992).
16. K. Estabrook, "Resonant Absorption in Very Steep Density Gradients," *Laser Program Annual Report 1986*, 2-87 (1986).
17. E. J. Valeo and K. G. Estabrook, "Stability of the Critical Surface in Irradiated Plasma," *Phys. Rev. Lett.*, **34**, 1008 (1975); K. Estabrook, "Critical Surface Bubbles and Corrugations and Their Implications to Laser Fusion," *Phys. Fluids*, **19**, 1733 (1976).
18. J. M. Kindel, C. H. Aldrich, J. U. Brackbill, D. W. Forslund, and L. Mascheroni, "Modeling of CO_2 Laser Plasma Interaction at High Laser Intensity," *Los Alamos Internal Report.*, Los Alamos National Laboratory, Los Alamos, NM, LA-UR-82-1086 (1982); B. Bezzerides, D. F. DuBois, D. W. Forslund, and E. L. Lindman, "Magnetic Field Generation in Resonance Absorption of Light," *Phys. Rev. Lett.*, **38**, 495 (1977).
19. D. W. Forslund, J. M. Kindel, Kenneth Lee, E. L. Lindman, and R. L. Morse, "Theory and Simulation of Resonant Absorption in a Hot Plasma," *Phys. Rev. A.*, **11**, 679 (1975).
20. K. G. Estabrook, E. J. Valeo, and W. L. Kruer, "Two-dimensional Relativistic Simulations of Resonance Absorption," *Phys. Fluids*, **18**, 1151 (1975).
21. W. L. Kruer, "Ponderomotive and Thermal Filamentation of Laser Light," *Comments on Plasma Physics and Controlled Fusion*, **IX**, 63 (1985).
22. C. E. Max, J. Aarons, and A. B. Langdon, "Self-modulation and Self-focusing of Electromagnetic Waves in Plasmas," *Phys. Rev. Lett.*, **33**, 209 (1974).

Neutron Detectors for Measuring The Fusion Burn History of ICF Targets

T. J. Murphy
R. A. Lerche

Introduction

In ICF experiments, spherical targets filled with deuterium (DD) or a deuterium-tritium (DT) mixture are compressed and heated to conditions at which thermonuclear fusion can occur. Our experimental goals are to achieve 1000× liquid density and temperatures of about 10 keV[1] for confinement time on the order of 100 ps. During confinement, the fuel atoms undergo fusion, releasing energetic charged particles, neutrons, and photons. We are interested in measuring the fusion rate as a function of time relative to the incident drive radiation. These measurements characterize the implosion and hydrodynamics of the target, and are a sensitive indicator of our ability to accurately model energy transport between laser and target.

Reactions of interest in ICF experiments are

$$\begin{aligned} &D + D \rightarrow {}^3He\ (0.82\ MeV) + n\ (2.45\ MeV) \\ &D + D \rightarrow T\ (1.01\ MeV) + p\ (3.02\ MeV) \\ &D + T \rightarrow {}^4He\ (3.52\ MeV) + n\ (14.05\ MeV)\ , \end{aligned} \tag{1}$$

where the quantity in parentheses is the energy of the particles produced in the reaction. Thermal velocity of the reacting plasma ions causes a small energy spread in the otherwise monoenergetic spectra for the fusion products in these reactions. The charged particles are slowed by coulomb interactions with plasma ions and electrons before exiting the fuel. The neutrons, however, are largely unaffected and most escape the target without collision. Therefore, the neutron temporal distribution at a point outside the fuel preserves burn history information with a time-of-flight delay. Thus, the burn history may be measured with fast neutron detectors located some distance from the target. Since confinement times for ICF targets are on the order of 100 ps,[1] diagnostics with time resolution better than this are highly desirable.

The thermal motion of the reacting ions causes a Doppler broadening that produces a spread in the neutron energy, given by[2]

$$\Delta E = \begin{Bmatrix} 82.5 \\ 177 \end{Bmatrix} \sqrt{T} \quad \begin{Bmatrix} DD \\ DT \end{Bmatrix}\ , \tag{2}$$

where T is the ion temperature (keV) and ΔE is the FWHM of the neutron energy distribution (keV). From this, we find

$$\Delta t_T = \begin{Bmatrix} 0.778 \dfrac{ns}{m\ keV^{1/2}} \\ 0.122 \dfrac{ns}{m\ keV^{1/2}} \end{Bmatrix} \sqrt{T} \times d \quad \begin{Bmatrix} DD \\ \\ DT \end{Bmatrix}\ , \tag{3}$$

where Δt_T is the FWHM of the temporal signal, and d is the distance between the target and the neutron detector. For neutrons born at the same time in the target, the velocity spread associated with the neutron energy distribution causes a smearing of their arrival times at a detector. To keep smearing small we must place the detector close to the target. For example, to keep the smearing to below 20 ps, the detector distance d must be less than

$$\begin{aligned} d \le &\begin{cases} 2.6\ cm & DD \\ 16.4\ cm & DT \end{cases} \quad \text{for } T = 1\ keV \\ d \le &\begin{cases} 0.8\ cm & DD \\ 5.2\ cm & DT \end{cases} \quad \text{for } T = 10\ keV\ . \end{aligned} \tag{4}$$

The penetrating nature of neutrons allows substantial shielding against debris without introducing substantial loss of neutron signal. This makes small distances from the target practical.

Due to the finite velocity of the neutrons, we must keep the thickness of the detectors small to maintain the temporal resolution. A thick detector leads to an uncertainty in the exact neutron detection point. Again, for 20-ps resolution, the thickness l of the detector must be less than

$$l \leq \begin{cases} 0.4 \text{ mm} & \text{DD} \\ 1.0 \text{ mm} & \text{DT} \end{cases} . \quad (5)$$

The less stringent requirements for DT-filled capsules on target-detector distance and detector thickness demonstrate the advantages of using them for burn history measurements. In addition, the greater fusion cross section for DT compared to DD neutron yields is greater by about a factor of 100, thereby greatly reducing statistical uncertainty in measurements.

Often, "bang time" and "burn width" are reported instead of a full burn history because of limited detector temporal resolution. Detectors with relatively poor temporal resolution can determine average neutron emission time (bang time) by measuring relative to some feature of the signal, such as the time of peak value or constant fraction of peak value. Since these detectors usually have larger volumes, they also have greater sensitivity. Faster detectors with marginal resolution for a detailed burn history can often provide an estimate for the burn duration of the fuel (burn width).

This article describes three detectors used to measure target burn history. The first is the low-resolution neutron emission time microchannel plate (NET-MCP), which measures the average emission time of fusion neutrons relative to the laser pulse. The second is the gallium arsenide radiation-induced conductivity (GaAs RIC) detector, which measures burn history with fair resolution and sensitivity. The third detector is the sensitive, 25-ps resolution neutron temporal diagnostic (NTD), a streak camera-based instrument. In addition to the instruments currently in use, other proposed detectors are mentioned.

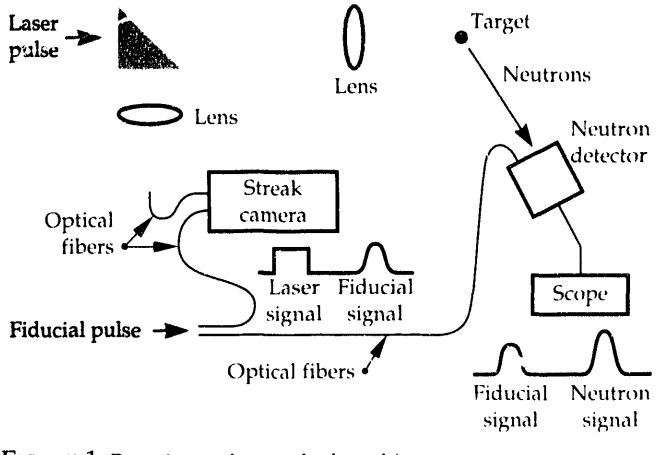

FIGURE 1. Experimental setup for burn history measurements showing how a fiducial pulse is used to relate the neutron signal to the laser pulse.

Detectors for Burn History Measurements

Neutron Emission Time Microchannel Plate

The neutron emission time is a sensitive indicator of implosion physics, and is therefore a good quantity for comparison of experiment with detailed modeling of implosions.

Neutron emission time t_n relative to a reference point on the laser power history t_l can be determined by using the equation[3]

$$t_n - t_l = \Delta t_{nf} - \Delta t_{lf} + \Delta t_{cal} - \Delta t_{tof} \quad (6)$$

where Δt_{nf} is the time between the neutron signal and the fiducial pulse recorded on the neutron detector, Δt_{lf} is the time between the laser signal and the fiducial pulse recorded on a streak camera, Δt_{tof} is the difference between neutron and x-ray time-of-flight (calculated from the measured distance of the detector from the center of the chamber), and Δt_{cal} is a calibration constant determined experimentally by irradiating a gold disk with a short laser pulse, resulting in a short burst of hard x rays. The x rays are produced at the laser-irradiation time and interact with the detector to produce a signal that yields timing information. This method can be used for any neutron detector sensitive to x rays. Figure 1 shows the setup for neutron emission time measurements.

The NET-MCP detector consists of a fast plastic scintillator optically coupled to a microchannel plate photomultiplier tube (PMT). The scintillator used is a 46-mm-diam disk of BC-422[4] plastic, quenched with 2% benzophenone to reduce the scintillation light decay time. We use two different configurations depending on the expected neutron yield. The more sensitive configuration consists of a 15-mm-thick scintillator coupled to a three-stage MCP PMT. The less sensitive detector consists of a 5-mm-thick scintillator coupled to a single-stage MCP PMT. The signal is recorded by 500-MHz transient recorders and the detector is located 60 cm from the target. The system's

response to the optical fiducial is 850 ps FWHM. The detector response to DT neutrons is 1000 ps FWHM and 1200 ps for DD neutrons.

This detector is too slow to determine the burn history of our implosions. The neutron emission time can, however, be determined to ±75 ps by timing relative to the 50% point on the leading edge of the signals (constant-fraction timing). In addition, we must correct for the Doppler broadening of the signal. This correction is more important for DD fuel than for DT owing to the larger temporal spread of the Doppler broadened time-of-flight signals in DD implosions (Eq. 3). Figure 2 shows an example of the neutron and fiducial signals recorded on a shot that produced 10^{13} DT neutrons. The relatively large scintillator and the high gain of the PMT make the NET-MCP a relatively efficient detector. By adjusting the gain of the PMT, the instrument can measure yields from 10^6 to 10^{13}. Emission times for even lower yields can be achieved by moving the detector closer to the target.

Radiation-Induced Conductivity in Gallium Arsenide

The NET-MCP is able to measure the average neutron emission time, but we prefer to also have information about the burn history (fusion rate as a function of time). This information requires a detector with better time resolution. One type of detector that provides better resolution measurements of neutron emission uses radiation-induced conductivity[5,6] in gallium arsenide. Neutrons scatter on detector nuclei, which then create electron-hole pairs as they slow down and lose energy to the lattice. An applied bias voltage sweeps the carriers out of the detector, producing a measurable current.

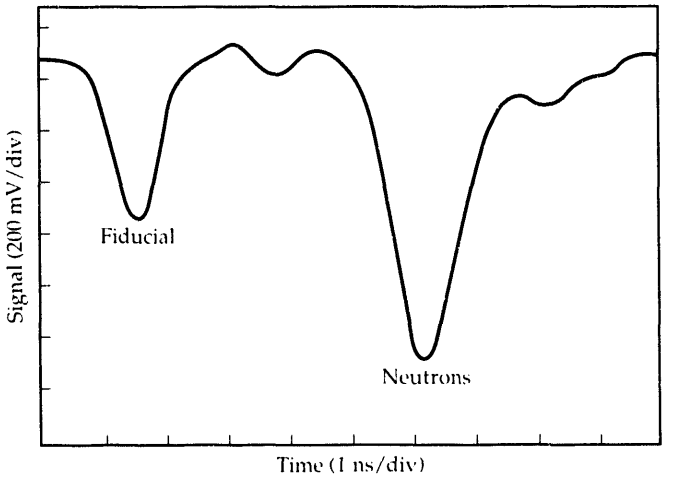

FIGURE 2. Transient recorder data for the NET-MCP showing the optical fiducial and neutron signals for a shot that produced 10^{13} DT neutrons.[3]

To reduce the time response of the detector, trapping sites for charge carriers are introduced by subjecting the material to neutron irradiation.[6] This process reduces the lifetime of the charge carriers, thereby reducing the response time of the detector. If the charge carrier lifetime is made much shorter than the time to sweep the carriers out of the detector, then the response time of the detector will be determined by bulk properties of the material and not by the details of the detector construction.

A GaAs detector has been used to measure burn histories of high-yield neutron-producing shots on Nova.[5] The detector used is a 1 × 1 × 3-mm rectangular parallelepiped, mounted on high-speed transmission line, and connected to a 6-GHz oscilloscope. Figure 3 shows burn histories measured on two shots designed to give different burn widths.[5] The response time (FWHM) of the detector itself to a 2-ps pulse of 0.53-μm laser light was 60 ps. The response of the entire system was estimated to be 130 ps.[5] When placed a few centimeters from a target, the detector can record burn histories for yields as low as 5×10^{10} DT neutrons.

While the GaAs detector has better time response than the NET-MCP, its sensitivity is much lower. A more sensitive detector is necessary to make time-resolved measurements of fusion burn rate on a wide range of targets of interest. A detector with a time response much faster than anticipated burn widths is also desirable.

Neutron Temporal Diagnostic

Plastic scintillators are commonly used as energy-to-light converters in radiation detectors. The temporal

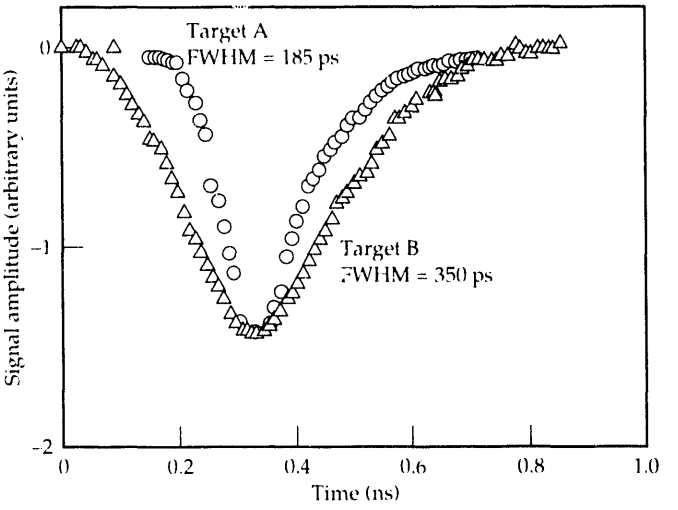

FIGURE 3. Neutron production rate measured using a gallium arsenide detector for two different ICF targets. The amplitudes of the signals have been normalized.[5]

distribution of their light output is typically characterized by a fast, subnanosecond rise time and by an exponential decay measured in nanoseconds. The FWHM for even the fastest conventional plastic scintillator is about 1.3 ns.[7] The speed can be enhanced to a few hundred picoseconds by adding a quenching agent, but only with a significant reduction in total light output.[8,9]

We want to determine burn history with 20-ps resolution for targets producing relatively few (10^8) neutrons. Detectors based on plastic scintillators are attractive because they have relatively high detection efficiency for 14-MeV neutrons. At first glance, the scintillator response appears too slow for such an application. However, for events with a duration much shorter than the scintillator decay rate, it is relatively easy to deconvolve the decay rate from a measured signal. Thus, a detector can be built with a response comparable to the scintillator rise time.

We found that the rise time of the scintillator material BC-422 is less than 20 ps, and we built a fast, sensitive neutron detector for burn history measurements that exploits this property.[10] Figure 4 shows the detector configuration. Neutrons emitted from an ICF target expand radially; some neutrons interact with a small 6-mm-diam, 1.5-mm-thick sample of BC-422 located in a retractable tungsten nose cone. The nose cone shields the scintillator against target x rays and allows the scintillator to be positioned between 1 and 50 cm from the target. The scintillator, whose emission spectrum ranges between 350 and 450 nm, is backed with an aluminized layer to double the light directed towards an $f/2$ achromatic zoom lens system. The lens system images the scintillator through a slit onto a 1-mm-wide active area of the S-20 photocathode of a fast streak camera located 4 m from the target. A light shield prevents laser light scattered from the target from reaching the streak camera.

The streak camera records temporal and spatial modulation of light incident along its input slit. Incident light illuminates a long, narrow region of the streak tube's photocathode to produce photoelectrons. The rate of photoelectron production at any point along the slit is proportional to the instantaneous light intensity at that point. The photoelectrons are accelerated and electrostatically focused to a line at a phosphor output screen. Deflection plates sweep the modulated image of the slit across the output screen. Focusing properties of the streak tube allow us to retain 15-ps response even with wide-slit operation.[11]

Our instrument is capable of recording neutron production rates with less than 25-ps resolution for targets yielding as few as 2×10^8 DT neutrons. Figure 5(a) shows an image for a target shot producing 6×10^8 neutrons. The image was recorded with a CCD camera coupled to the output of the streak camera. Images are corrected for streak camera flat field and time base nonlinearities. The axes of a processed image represent spatial position along the input slit and time. Shown on this image are the neutron-induced signal and a fiducial signal. The fiducial signal is formed by passing a 100-ps, 0.53-μm laser pulse through an etalon to create a series of uniformly spaced pulses. The first pulse allows us to relate the time base of this instrument with those of instruments recording the incident laser beam signals. The pulse train provides a check on the sweep speed of the camera. A lineout of the neutron signal

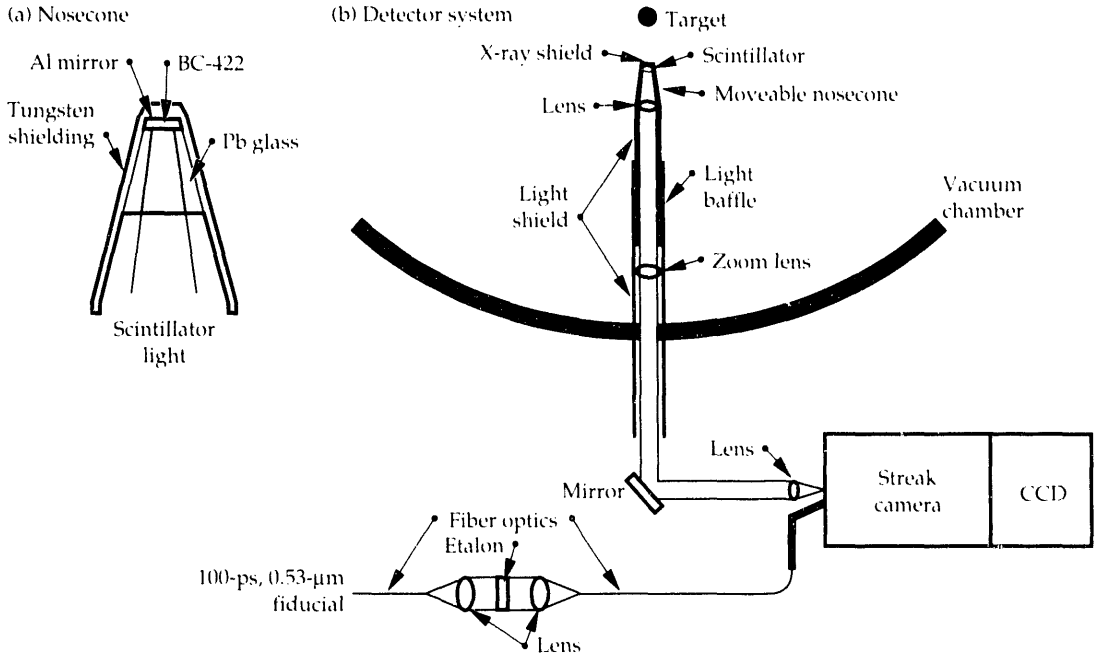

FIGURE 4. Schematic of the neutron temporal diagnostic showing the major components of the system.

[Fig. 5(b)] integrated over the spatial direction shows a fast rise time followed by the characteristic decay of the scintillator. Deconvolution of the exponential decay rate of the scintillator from the signal gives the neutron interaction rate in the detector and the production rate in the target to within a constant factor [Fig. 5(c)]. This factor may be determined by comparing the integral of the neutron production signal with the total neutron yield determined from other instruments (i.e., neutron activation samples).

The deconvolution of the signal is an iterative procedure in which a trial solution is incremented and then convolved with the response function of the detector. This convolution is then compared to the actual measured signal; the trial solution is then incremented in a manner suggested by the comparison. In this way, a neutron production rate is built up such that the convolution of this rate with the response function of the detector agrees with the measured signal.

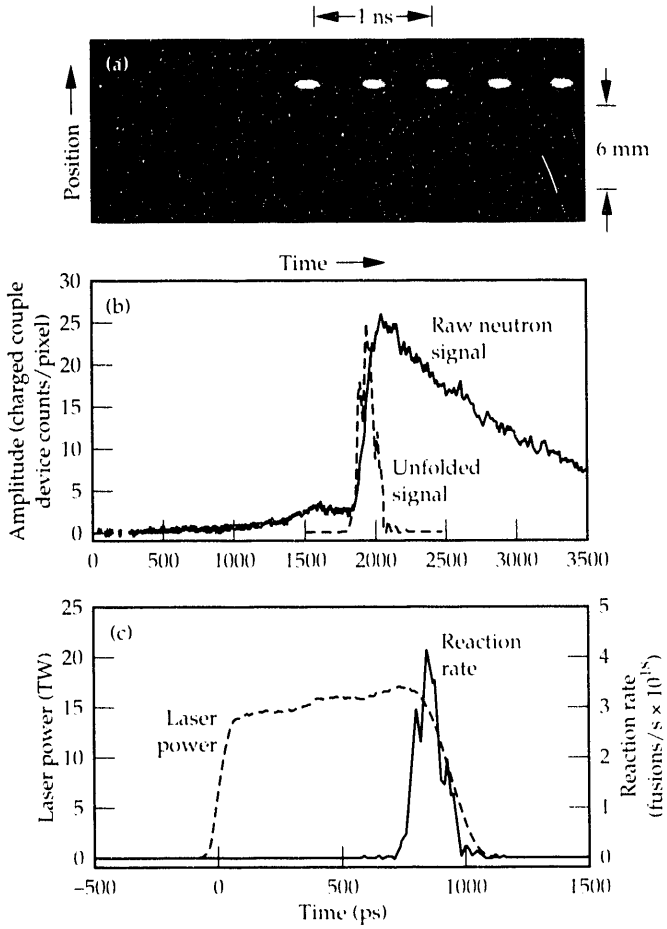

FIGURE 5. Example of burn history data recorded with the NTD: (a) Streak camera image shows neutron-induced signal and an optical fiducial signal used to establish timing relative to the laser pulse, (b) lineout of the raw neutron signal in (a) and the unfolded signal showing burn history, and (c) fusion reaction rate and laser power versus time. Beam focus for this direct drive shot was selected to produce a yield of 5×10^8 DT neutrons.

We conducted a set of short pulse experiments at the Nova laser facility that demonstrates the speed of BC-422. In each experiment, a burst of x rays was produced by focusing 35 to 70 J of light at a wavelength of 0.53 μm in a 20-ps FWHM Gaussian laser pulse onto a gold disk target. A beryllium input window replaced the tungsten shielding allowing x rays with energies greater than 2 keV to excite the scintillator. Excitation by gold M-band x rays whose energies fall between 2 and 4 keV primarily takes place in the first millimeter of the scintillator. Figure 6 shows a typical signal with the exponential tail deconvolved. This signal represents the convolution of the x-ray pulse with both the streak camera response and the scintillator excitation function. From this we have deduced the rise time of the scintillator to be less than 20 ps, indicating that the instrument can potentially measure neutron signals with a time resolution on the order of 20 ps.

Table 1 summarizes the burn history diagnostics presently used on Nova, showing the minimum useful DT yield, time resolution, and absolute timing ability of the three diagnostics.

TABLE 1. Summary of neutron burn history detectors used on Nova, along with the minimum neutron yield allowing a statistically meaningful measurement and the time resolution possible with each.

Detector	Minimum yield (DT)	Time resolution (ps)	Timing relative to laser pulse (ps)
NET-MCP	10^6	1000	75
GaAs	5×10^{10}	130	25
NTD	2×10^8	<30	10

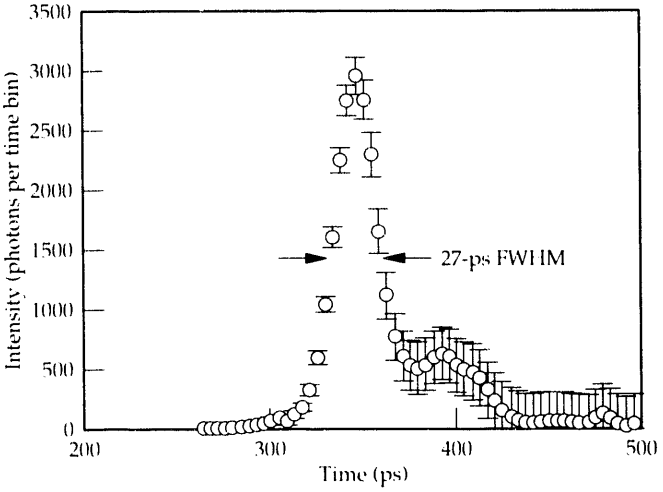

FIGURE 6. NTD response to a 20-ps x-ray pulse. The signal from a 20-ps laser pulse is focused onto a gold disk target to produce a 20-ps burst of x rays for testing the time response of the BC-422 scintillator. This data, with the known response of the streak camera, demonstrates that the rise time of BC-422 is less than 20 ps.

Other Detectors

Several other neutron detectors have been proposed.[12–16] They include the neutron diode, neutron streak camera, and transmission-line neutron diode.

The neutron diode[13] would be similar to an x-ray diode, however the cathode would be coated with ^{238}U. Fission fragments produced by the interaction of fast neutrons with the uranium cathode would then drag large numbers of secondary electrons out of the cathode to produce the electrical signal measured.[12]

The use of uranium as the cathode for a neutron streak camera has also been suggested.[12, 14–16] The interaction of neutrons with the cathode would be the same as for the neutron diode, but in this case the secondary electrons would be focused and streaked onto a phosphor screen.

The transmission-line neutron diode adds temporal resolution to the neutron diode design by shaping the cathode and phosphor screen as long parallel plates to which a voltage pulse may be applied.[14] The pulse acts as a gate, allowing the electrons to leave the cathode only as the pulse passes over the region of interaction. This is similar in operation to gated x-ray imaging cameras used on Nova.[17]

These techniques have not been pursued on Nova, primarily because of the success of scintillator and solid-state detectors for measuring the quantities of interest with sufficient time resolution and sensitivity.

Acknowledgments

The authors gratefully acknowledge the contributions of R. Ellis, R. Griffith, D. Kumpf, G. Mant, D. Phillion, N. Selchow, G. Tietbohl, J. Waldrep, and J. Wass to the development of the NTD.

Notes and References

1. John D. Lindl, Robert L. McCrory, and E. Michael Campbell, "Progress Toward Ignition and Burn Propagation in Inertial Confinement Fusion," *Phys. Today* **45**, 32 (1992).
2. H. Brysk, "Fusion Neutron Energies and Spectra," *Plasma Phys.* **15**, 611 (1973).
3. R. A. Lerche, D. R. Kania, S. M. Lane, G. L. Tietbohl, C .K. Bennett, and G. P. Baltzer, "Neutron Emission Time Measurements for ICF Targets," *Rev. Sci. Instrum.* **59**, 1697 (1988).
4. Bicron Corp., Newbury, OH.
5. D. R. Kania, S. M. Lane, and S. G. Prussin, "Measurement of Single 14-MeV Neutron Bursts with 100-ps Time Resolution," *Appl. Phys. Lett.* **53**, 1988 (1988).
6. D. R. Kania, "Radiation-Induced Conductivity: High-Speed Detection of X Rays and Neutrons," *Laser Part. Beams* **9**, 91 (1991).
7. Glenn F. Knoll, *Radiation Detection and Measurement* (John Wiley & Sons, New York, 1989) p. 225.
8. P. B. Lyons, S. E. Caldwell, L. P. Hocker, D. G. Crandall, P. A. Zagarino, J. Cheng, G. Tirsell, and C. R. Hurlbut, "Subnanosecond Plastic Scintillators," *IEEE Trans. Nucl. Sci.* **NS-24**, 177 (1977).
9. J. C. Cheng, K. G. Tirsell, G. R. Tripp, E. M. Lent, and R. A. Lerche, "Streak Camera Measurement of Subnanosecond Plastic Scintillator Response," *Rev. Sci. Instrum.* **49**, 650 (1978).
10. R. A. Lerche and D. W. Phillion, "Rise Time of BC-422 Plastic Scintillator <20 ps," *Conference Record of the 1991 IEEE Nuclear Science Symposium and Medical Imaging Conference, Vol. 1* (IEEE, Piscataway, NJ, 91CH3100-5, 1991).
11. R. A. Lerche and R. L. Griffith, "Resolution Limitations and Optimization of the LLNL Streak Camera Focus," *Proceedings of SPIE High Speed Photography, Videography, and Photonics V* (SPIE-The International Society for Optical Engineering, Bellingham, WA, 1987; *Proc. SPIE* **832**) p. 266.
12. C. L. Wang, R. Kalibjian, and M. S. Singh, "Design of Neutron Streak Camera for Fusion Diagnostics," *15th International Congress on High-Speed Photography and Photonics* (SPIE-The International Society for Optical Engineering, Bellingham, WA, 1982; *Proc. SPIE* **348**) p. 276.
13. C. L. Wang, D. E. Campbell, G. R. Leipelt, D. G. Nilson, and V. W. Slivinsky, "50-ps Neutron Diode," *Laser Program Annual Report 83*, Lawrence Livermore National Laboratory, Livermore, CA, 1983, UCRL-50021-83, p. 5.
14. C. L. Wang, R. Kalibjian, M. S. Singh, J. D. Wiedwald, D. E. Campbell, E. M. Campbell, M. D. Cable, W. R. Graves, S. M. Lane, R. A. Lerche, R. H. Price, D. G. Stearns, G. A. Mourou, and S. G. Prussin, "Approaches to Ultrafast Neutron Detectors," *Rev. Sci. Instrum.* **56**, 1096 (1985).
15. Toshiyuki Iida, Tatsuya Araki, Chie Miyake, Kenji Sumita, Tatsuhiko Yamanaka, Masanobu Yamakaka, Noriaki Miyanaga, and Takayoshi Yamamoto, "Measurement of Yield and Energy Spectrum of Secondary Electrons Emitted by Fission from Uranium Oxide Cathode for Neutron Streak Tube," *J. Nucl. Sci. Tech.* **25**, 780 (1988).
16. N. Miyanaga, H. Oida, M. Yamanaka, T. Yamanaka, S. Nakai, T. Yamamoto, T. Iida, T. Araki, T. Ohga, and C. Miyake, "Gated Neutron Streak Camera with a Uranium Cathode," *Rev. Sci. Instrum.* **61**, 3592 (1990).
17. J. D. Kilkenny, "High-Speed Proximity Focused X-Ray Cameras," *Laser Part. Beams* **9**, 49 (1991).

THE RECIRCULATOR

J. J. Barnard
F. Deadrick
A. Friedman
D. P. Grote
L. V. Griffith
H. C. Kirbie
V. K. Neil
M. A. Newton
A. C. Paul
W. M. Sharp
H. D. Shay
*R. O. Bangerter**
*A. Faltens**
*C. G. Fong**
*D. L. Judd **
*E. P. Lee**
*L. L. Reginato**
*S. S. Yu**
T. F. Godlove†

Introduction

Heavy ion fusion (HIF) has been identified by several recent advisory studies (e.g. Fusion Policy Advisory Committee Final Report,[1] National Academy of Sciences Review of the Department of Energy's ICF Program[2], and the Department of Energy's National Energy Strategy[3]) as the leading candidate for an inertial fusion energy (IFE) power plant driver. Some advantages of HIF include the high efficiency and high repetition rate inherent to particle accelerators, the use of a magnetic lens in the final focus to assure its survivability, and the favorable target illumination geometry arising from the small solid angle subtended by the beams at the target. The induction accelerator is the leading U.S. candidate for HIF. Induction accelerators can inherently transport more current than rf-accelerators, and systems studies suggest favorable costs for induction linac drivers.

Recirculating induction accelerators, referred to here as recirculators, are circular induction accelerators that reuse the components up to 100 times for each beam pulse. Because they require fewer components, they offer the possibility of a large cost savings. The length of a linear induction accelerator is determined by the maximum average accelerating gradient achievable, which is about 1 MV/m. To accelerate a heavy ion to an energy of 10 GeV requires a length of about 10 km/q, where q is the charge state of the heavy ions. In contrast, the circumference of the recirculator is determined by the bending radius of a 10-GeV ion (atomic mass of approximately 200) in an average bending magnetic field of about 1 T. This suggests a minimum ring size of about 1.3 km/q for the highest energy ions. Since the components are used repeatedly, the accelerating gradient may be reduced by an order of magnitude. This reduced gradient results in induction cores which are smaller than the linear accelerator. The combination of smaller cores and fewer components has a major impact on reducing the driver cost. However, the requirements for ramped magnetic dipoles, increased induction core pulser repetition rates, and longer path lengths traversed by the beam are all more demanding; these issues must be carefully considered in designing a recirculator.

The potential to reduce the cost of an HIF driver motivated a two year study.[4] The goal of the study was to produce a few design examples, from which concrete cost and efficiency estimates could be determined. In addition, the study helped to resolve some of the major physics and engineering issues of the recirculator.

In this article, we discuss some of the major findings,[4] and results of later investigations, an overview of a recirculator design, the considerations which led to the conceptual design of the three major systems of the accelerator: the acceleration modules, the bending magnets, and the focusing magnets, cost and efficiency estimates, and the major engineering and physics issues. The cost and efficiency estimates confirm our initial belief that a cost reduction is possible. Surprisingly, despite the introduction of energy losses in the dipole magnets, the overall efficiency of the recirculator is at least as large as a comparable linear accelerator.

Overview of the Recirculator Configuration

For this report, we adopted a number of parameters that were primarily dictated by target and reactor physics and power plant economics. An end-to-end optimization including target and reactor chamber considerations may well yield a somewhat different set of requirements.

* Lawrence Berkeley Laboratory, Berkeley, CA
† FM Technologies, Inc., Fairfax, VA

We adopted 200 as the atomic mass of the heavy ion, which, together with a stopping range of 0.15 gcm^{-2}, gives a required heavy ion energy of 10 GeV.[5] By choosing the largest ion mass, we maximize allowed ion energy (for a given stopping range) and thus minimize the current. For a charge state of +1 and a required pulse energy of 4 MJ, this translates into a total beam charge of 400 μC.

At a range of 0.15 g cm^{-2}, a spot radius r_{spot} of 2 mm, and a pulse energy W of 4 MJ, the gain curves for indirectly driven targets yield a gain of approximately 57 and a required peak power level of approximately 350 TW. These parameters imply a pulse length of approximately 11 ns. The fusion energy per burst would be 230 MJ. Assuming a thermal efficiency ε of 41%, a blanket multiplication factor M of 1.15, a repetition rate of 10 Hz, and an accelerator efficiency η of 35%, the net electric power, $P_e = \nu_{rep} W(\varepsilon M G - 1/\eta)$, is approximately 1 GW.

Figure 1 shows a schematic of the recirculator. The injection energy is 3 MeV. Upon exiting the injector, the beam passes through three rings [the low energy ring (LER), medium energy ring (MER), and high energy ring (HER)] and makes 100 laps through each ring. Three rings were chosen to restrict the dynamic range in energy in each ring to about 20. There are four beamlines throughout, and at each longitudinal position the beamlines pass through a single induction core. Pulse compression occurs continuously throughout the three rings. On exiting the HER, the beams receive an additional velocity tilt in a linear bunching section, and drift-compress to the target reaching their final pulse duration as they hit the target. Table 1 lists ring characteristics.

Design Considerations

Each ring consists of a number of lattice elements, arranged in a large circle, interrupted only by the linear injection/extraction/transition sections. The lattice arrays consist of induction modules for acceleration, dipole magnets for bending the beam, and quadrupole magnets for focusing the beam. Additional space is allotted for vacuum, control, and diagnostics.

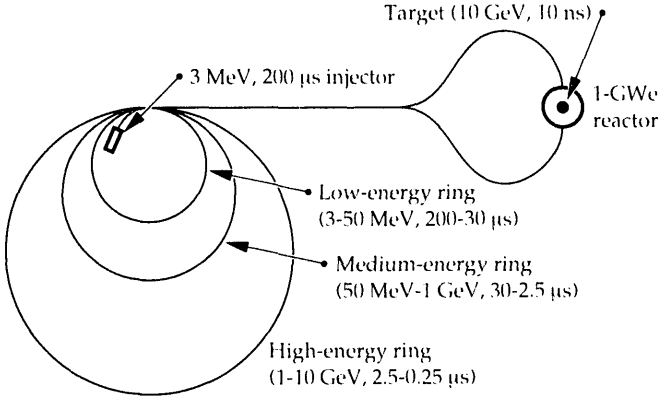

FIGURE 1. Schematic layout of a recirculating induction accelerator.

The induction cores are composed of annular cylinders of ferromagnetic material enclosed by a conducting shell to which a voltage pulse is applied. The changing magnetic flux induces an electric field which appears across the acceleration gap. Each core provides a voltage increment V_c for a duration τ satisfying:

$$V_c\tau = \Delta B A_c , \quad (1)$$

where ΔB is the magnetic flux swing in the ferromagnetic material and $A_c = (R_o - R_i)L_c$. R_i and R_o are the inner and outer radii of the core material and L_c is the length of the core. We chose the ferromagnetic material METGLAS 2605-S2 for cost and efficiency considerations.[6] Its maximum flux swing in this material before saturation is approximately 2.9 T. Because of the low voltage gradient in the recirculator, the voltage on each cell can be reduced from that of a linear accelerator. Equation 1 indicates that the low voltages allow pulse

TABLE 1. Summary of ring parameters.

	LER	MER	HER
Ion energy (GeV)	0.003–0.05	0.05-1	1–10
Pulse duration (μs)	200–30	30–2.5	2.5–0.25
Circumference (m)	700	921	1976
Current/beam (A)	0.5–3.3	3.3–40.0	40.0–400.0
No. of beams	4	4	4
No. of corelines	1	1	1
No. of laps	100	100	100
Pipe radius (m)	0.078	0.064	0.061
Lattice half period (m)	0.85	1.56	3.51
Induction modules:			
Inner radius (m)	0.313	0.255	0.243
Outer radius (m)	0.455	0.554	0.363
Length (m)	0.403	0.837	0.895
No. of cores	785	551	1068
Cell voltage (kV)	0.60	17.4	85
Bends (ramped magnetic dipoles):			
Effective length (m)	0.15	0.41	1.15
No. of bends	2680	1796	1919
Maximum B-field (T)	0.90	0.85	0.81
Super-conducting magnetic quadrupoles/dipoles:			
Length (effective length) (m)	0.47(0.23)	0.92 (0.73)	1.94 (1.76)
No. of quadrupoles	3139	2201	2133
Maximum quadrupole field (T)	2.0	1.25	1.0
Maximum dipole field (T)	-	0.75	1.01
Maximum total bending field (T) (averaged over lattice period)	0.16	0.58	0.77

durations to be lengthened and/or core cross-sections to be reduced. Longer pulse durations are used in the low energy ring and permit the transport of 400 μC of charge in only four beams. Smaller cores in the HER provide cost savings.

Two types of dipole bending magnets are used: time-steady superconducting (for high efficiency) and temporally ramped (to accommodate the increasing energy of the beam). The magnetic rigidity $[B\rho]$ of a heavy ion is given by

$$[B\rho] = \frac{\gamma A m_u \beta c}{qe} \quad . \tag{2}$$

Here, q is again the heavy ion charge state, γ is the Lorentz factor of the heavy ion, β is the heavy ion velocity in units of c, A is the atomic weight of the heavy ion, e is the proton charge, and m_u is an atomic mass unit. The recirculator circumference C is then given by

$$C = \frac{2\pi[B\rho]\max}{\eta_d B_d} \tag{3}$$

Here, $[\beta_\rho]$max is the rigidity at the maximum energy achieved in a ring, $\eta_d B_d$ is the product of the dipole magnetic field and the effective length of the dipole divided by the lattice half period, summed over the time steady field component and maximum of the temporally ramped component. For a fixed ratio of ramped to superconducting dipole field, the energy stored in the field is linear in B_d because the energy density is proportional to B_d^2 but the volume of field energy is proportional to C and hence to $1/B_d$. Since the dipole energy losses are approximately proportional to the total ramped field energy, the dipole losses are roughly proportional to $1/C$, favoring larger rings. On the other hand, the use of the superconducting component allows us to design a relatively small ring (and thus reduce costs) without substantially sacrificing efficiency.

The superconducting quadrupoles comprise the third major element in a lattice period. In our conceptual design, the superconducting quadrupoles and dipoles are combined into a combined function magnet, so that the occupancy factor is the same for both. We could also place them sequentially with half the occupancy and twice the field strength with minimal effects on the design. The quadrupoles are placed within the induction cores to reduce the overall circumference of the recirculator. The requirements on the quadrupoles can be illustrated by the use of the "envelope" equation in the smooth approximation where an average over a complete lattice period is used in calculating the focusing strength. For a more complete treatment[7], which includes the effects of the finite length of the magnetic quadrupoles, see Ref. 4.

$$\frac{d^2a}{dz^2} \cong -\frac{\sigma_0^2 a}{4L^2} + \frac{K}{a} + \frac{\varepsilon^2}{a^3} \quad . \tag{4}$$

Here, σ_0^2 is the phase advance per lattice period of a centroid oscillation in the focusing field of the quadrupoles and a is the average beam radius. The perveance $K = 2q I_b/(I_0\gamma^3\beta^3 A)$ is a dimensionless measure of the current, where I_b is the current in each beam ($I_0 = m4\pi E_0 m_u c^3/e$ = 31 MA), E_0 is the free space permittivity, and ε is the unnormalized emittance, which is a measure of the transverse phase space occupied by the beam, and L is one half of a lattice period. The phase advance is given approximately as

$$\sigma_0 \cong \frac{\eta_q B' L^2}{[B\rho]} \quad , \tag{5}$$

where B' is the magnetic field gradient in the quadrupole ($\cong B/r_p$), η_q is the occupancy fraction of the quadrupole, and r_p is the pipe radius.

The beam current increases as the velocity increases and the pulse duration decreases, causing the average beam radius to increase slightly in each ring. In Eq. (4), the first term on the right hand side $-\sigma_0^2 a/4L^2$ (arising from the focusing quadrupoles) must balance the second term K/a (due to the space charge of the beam) and to a lesser extent the third term ε^2/a^3 (arising from the thermal forces). But there are constraints that limit the choices of r_p, L, B', η_q, and $\eta_d B_d$.

Some of these constraints are: the requirement that the beam radius remain considerably less than the pipe radius, the requirement (for stability reasons) that the phase advance σ_0 remain less than 80°, and the requirement that the ratio of the lattice half period to the pipe radius be greater than about 10 (to minimize nonlinearities in the focusing field). In addition, the often conflicting requirements of low cost and high efficiency required several iterations to develop sensible example designs.

Cost and Efficiency Results

A systems code was developed which used the design equations to determine the specifications of each component and calculate the total cost of components (quadrupoles, dipoles, induction modules, etc.), based on the material quantities and assumed manufacturing costs. As the parameters changed, the systems code rescaled the amount of materials required and recalculated cost. Some cost assumptions were: $5/kg for the induction cores, $0.12/kW peak power (per induction cell) for the induction core pulsers, $122/kg for insulator material, $0.20/J for the magnetic dipole pulsers, $300/kg for the superconductor

material (NbTi), $50/kg for the copper in the superconductors, $20/kg for iron in the ramped dipoles, $0.003/J for the quadrupole power supplies, and $5/l/s for the vacuum pumps. After all recirculator component costs were calculated, an allowance was made for some specific additional costs. Based on other accelerator projects, we assumed that administration, engineering, and installation each contributed an additional cost of 10% of the direct component costs. With these assumptions, we arrived at a total cost of just under $500 million. The result is a significant reduction in cost from the conventional linac, which was estimated in the Heavy Ion Fusion System Assessment studies[8] to be about $1000 million. Other recent studies[9,10] suggest similar cost reductions through a variety of cost saving techniques, including using a higher charge state, using different materials for superconductors, and using a multipulsed linac with storage rings. In collaboration with W. J. Schafer Associates,[11] we are now comparing linear accelerators and recirculators using identical costing algorithms. In addition, both the linacs and recirculators are being optimized from injector to target, so that a fair comparison can be made between the two concepts.

In addition to estimating costs, we calculated the energy requirement of each component and summed it over all components. The energy budget was divided among three major elements: the beam consumed 35% of the supplied electrical energy, losses in the acceleration modules accounted for another 31%, and losses in the ramped dipole magnets accounted for another 24% of the energy. An additional 10% was lost in miscellaneous sources such as vacuum, refrigeration, and beam injection and extraction. The 35% efficiency compares favorably to linear induction accelerators. This result is, at first glance, surprising since the addition of ramped dipole magnets provides energy consumption that does not occur in the linear machine. However, the lower voltage gradient allows smaller cores with lower individual voltages, making the induction cells much more efficient. In addition, the decomposition of the dipole field into an efficient time-steady component and a temporally ramped, energy-consuming component helps to minimize losses in the dipole magnets.

Engineering Issues

A number of engineering issues emerged as a result of the detailed specification of the design example. We focus on two major issues which are present in a recirculator but not in a linear machine. The first issue is that of energy recovery of the ramped dipole field, and the second is the high repetition rate of the induction core pulsers.

As discussed above, when the beam energy increases from lap to lap in each ring of the recirculator, the dipole field must ramp in time. In the high energy ring, for example, the total dipole field (averaged over a lattice period) changes from 0.24 T to a maximum of 0.77 T during the 3 ms that the beam is within the high energy ring. Part of the field is produced by time-independent superconducting magnets, producing a field of 1.01 T with an occupancy of 0.5. The remainder of the field is produced by temporally ramped conventional magnets, which produce a field from –0.81T to + 0.81T with an occupancy of 0.33. The maximum magnetic field energy stored in the ramped component is 48 MJ, which is much larger than the 4-MJ beam energy. For maximum electrical efficiency of the recirculator, a large fraction of that field energy must be recovered each pulse. One method of recovering the energy is to use the inductance of the ramped dipole magnet, together with storage capacitors to produce an oscillating LC circuit. In this scenario, energy is first stored in capacitors and switched to the magnetic field in the dipole magnets and then recovered in the capacitors. The resulting magnetic field is then sinusoidal in time, and the beam circulates within the recirculator during the interval during which the field increases nearly linearly with time. Eddy current and hysteresis losses in the iron of the magnet, and eddy current and conductive losses in the copper conductors are the sources of energy loss in the ramped dipoles. In a one-quarter scale experiment, L. Reginato found a 90% recovery rate was possible, which was consistent with the energy loss calculations. For the parameters of the HER, we estimate that 94% energy recovery is possible. A second method also being considered uses alternating compulsators.[12] In this method, energy is stored in rotational energy of an alternator, and similar efficiencies should be produced in a reliable and cost effective way. In addition, the flexibility of producing a more triangularly shaped temporal profile (thus reducing the maximum required magnetic field) is also possible with alternating compulsators.

The second major engineering challenge for recirculators is the high repetition rate of the induction modules. As the energy of the beam increases in each ring, the orbital time decreases and the repetition rate of the induction cells increases from 15 to 50 kHz in the high energy ring. In addition, pulse compression occurs during acceleration, so the pulse duration must decrease from 2.5 to 0.25 μs. Field effect transistors (FETs) will act as opening and closing switches to deliver power to the induction cells. FET technology has already been developed for some high-voltage applications, although not to the scale required for the recirculator nor at the desired cost. We are developing an integrated induction core and modulator using FET switches to

deliver the accelerating voltage pulse to the induction cells.[13] The near term objective of this work is to develop a modulator capable of delivering 5 kV, 1–2 μs pulses at 200 kHz to an induction cell, suitable for a small scale (100 m) recirculator. To date, a 2 × 2 array of switches in series and parallel has been tested at 1 kV at 200 kHz. The repetition rate achieved in the experiment exceeds the requirements for all three rings of the driver recirculator. The cost of the switches is uncertain. Our assumption of $0.12 per kW of peak power is a factor of four reduction from the current price of the switch. Ten to fifteen years ago, the cost of this switch was 12.5 times larger than the current price, so we believe that our estimate of a factor of four decrease over the next twenty to thirty years is not unreasonable.

Physics Issues

The total path length traversed by a beam pulse is about 360 km from injector to target. This is about 36 times longer than in an equivalent linear accelerator. The longer path length requires higher vacuum and more demanding control of centroid position and transverse emittance than in the linear accelerator. In addition, attention must be paid to the control of instabilities which can occur in improperly designed induction accelerators.

A number of processes that cause loss of particles from the heavy ion beam have been identified.[14–17] We considered the following: beam-beam charge exchange, stripping, background gas ionization, and beam-induced gas desorption. Beam-beam charge exchange occurs when two of the beam ions interact, transferring an electron from one ion to the other. The result is a neutralized ion and a doubly charged ion. Both particles will hit the beam-pipe wall in a distance that is small compared to the circumference of the recirculator. The particle density and transverse velocity determine the reaction rate. The fractional beam loss $\delta n_b/n_b$ from beam-beam charge exchange is approximately given by

$$\frac{\delta n_b}{n_b} \cong 0.02\left(\frac{A}{200}\right)^{0.62}\left(\frac{\varepsilon_N}{6.3\times10^{-6}\,\pi\ \text{m rad}}\right)^{2.24}\left(\frac{Q_b}{100\,\mu\text{C}}\right) \times\left(\frac{6.1\ \text{cm}}{r_p}\right)^{4.24}\left(\frac{0.46}{\eta_p}\right)^{4.24}\left(\frac{37\ \text{m}}{l_b}\right)\left(\frac{\Delta t}{3.2\ \text{ms}}\right) \quad . \tag{6}$$

Here, we assume the cross-section for a heavy ion to change charge states due to an interaction with another heavy ion σ_{ce} is $2.1\times10^{-16}\,(E_{cm}/10\ \text{keV})^{0.62}\ \text{cm}^2$.[18,19] Also, n_b is the ion-beam number density; ε_N is the normalized emittance; $E_{cm} = A m_u v_{cm}^2/2$; $v_{cm} = \varepsilon_N c/a$; Q_b is the charge in each ion bunch, the beam radius a is a fraction η_p of the pipe radius r_p, l_b is the bunch length, and Δt is the residence time of the bunch within the recirculator. Note the steep dependence of the charge exchange loss on the pipe radius.

Stripping occurs when an electron is removed from a heavy ion through an interaction with a residual gas molecule, and is again lost from the beam. The maximum background gas density n_g can be determined by consideration of the mass continuity equation of the heavy-ion beam, which approximately yields

$$n_g \cong \frac{x_{strip}}{\sigma_s n_{lap} C} \quad . \tag{7}$$

Here, x_{strip} is the fractional beam loss due to stripping, σ_s is the cross section for a background gas molecule to strip an electron off of a heavy ion, n_{lap} is the number of laps of the recirculator of circumference C, satisfying $n_{lap} C = v_i \Delta t$, where v_i is the heavy ion velocity.

Equation (7) indicates that the scaling of the required gas density is approximately inversely proportional to the residence time.

Background gas ionization occurs when a beam ion strips an electron off of a neutral residual gas molecule. Background gas ionization does not lead to beam loss directly, but indirectly through interactions with the walls. Beam-induced gas desorption occurs when an ionized background gas molecule, accelerated by the space-charge of the beam, hits the wall, emitting η_G gas molecules. The background molecule hits the wall at an energy which is typically tens of keV. The desorption coefficient is of order a few; we take $\eta_G = 5$. In addition when doubly-ionized or neutral heavy ions hit the wall, they will desorb η_{HI} gas molecules.

By considering the continuity and momentum equations of the background gas, we obtain the total pumping rate[4,20]

$$S_{lin} C \cong N_b n_{lap} C \times\left\{\frac{\sigma_s Q_o A_{sp}}{x_{strip}} + \frac{\left[(\eta_G - 1)\sigma_i + \eta_{HI}\sigma_s\right]Q_b}{qe\,t_r}\right\} \quad . \tag{8}$$

Here, S_{lin} is the average pump rate per unit distance along the accelerator, Q_o is the intrinsic gas desorption rate per unit area, N_b is the number of beams; η_G is the number of molecules desorbed from the pipe inner wall per incident gas molecule; η_{HI} is the number of molecules desorbed from the pipe inner wall per incident heavy ion; qe is the ion charge; t_r is the repetition time for pulses in the recirculator, and $A_{sp} = 2\pi r_p C$ is the total surface area of a single beam pipe. Equation (8) is approximately true when appropriate averages

are made over cross sections and desorption coefficients, and when the beam induced wall desorption does not undergo exponential growth.

The condition for a logarithmic gain of less than one of the background gas can be expressed as a condition of r_p as:

$$r_p > \left\{ \frac{\left[(\eta_G - 1)\sigma_i + \eta_{HI}\sigma_s\right] Q_b n_{lap}}{\pi q e} \right\}^{1/2} . \quad (9)$$

From Eqs. (8) and (9), we can see that the total pumping rate decreases as r_p decreases (as the intrinsic gas desorption decreases) but then increases with the further decrease of the pipe radius as the beam induced desorption becomes significant. As an example, in the high-energy ring, $N_b = 4$, $n_{lap} = 100$, $C = 2.0 \times 10^3$ cm, $Q_0 = 10^{-11}$ Torr l s^{-1} cm^{-2}, $x_{strip} = 0.015$, $\eta_G = 5$, $\sigma_i = 5 \times 10^{-16}$ cm^2, $\eta_{HI} = 0.01$, $\sigma_s = 6 \times 10^{-17}$ cm^2, $Q_b = 100$ μC, $qe = 1.6 \times 10^{-19}$ C, and $t_r = 0.1$ s, so that S_{lin} C $= 2.4 \times 10^6$ l s^{-1}, which translates into a pumping cost of $12 million, assuming a unit cost of $5 l^{-1} s. The required background gas density would be then be about 2×10^{-10} Torr. The critical pipe radius from Eq. (9) is about 7 cm, indicating that the gas increases by about an e-fold during the residence time of the beam.

Large uncertainty exists in our knowledge of η_G and particularly η_{HI}. Extrapolation of sputtering coefficients at low energy to high energy would suggest that η_{HI} should be less than unity, and the dominant contribution to desorption would then come from ionization. Some data and theory[21,22], however, suggest that η_{HI} is of order 5 for some coarse grain metals, and can be much larger (1000) for fine grained metallic films. In our design, we optimistically assume that beam desorption from ionized background gases makes the dominant contribution to beam induced desorption ($\eta_G = 5 >> \eta_{HI} < 1$). For values of η_{HI} as high as 5, the vacuum system would increase in cost by ~65%, but would still be a relatively small fraction of the total cost. For values of η_{HI} as high as 1000, substantial reoptimization of the recirculator would be required. Measurement of η_{HI} in the appropriate energy range and with appropriate materials is vitally important for a reliable recirculator design.

The second major physics issue which is more demanding in a recirculator is beam centroid control. A beam whose centroid is off axis will oscillate harmonically in the focusing channel. These oscillations are known as betatron oscillations. Misalignments of quadrupoles result in a centroid betatron amplitude x_c, which increases like a random walk, giving

$$x_c^2 \cong C_{rw} N_q \delta x_{rms}^2 . \quad (10)$$

Here, N_q is the number of quadrupoles with rms displacement Δx_{rms} through which the beam passes. C_{rw} has been determined by detailed numerical calculations and has been shown to vary from about 6 to 3 in the HER. The longitudinal distance traveled by the beam $z = N_q L$, where L is the half lattice period (3.5 m in the HER). In addition to quadrupole misalignments, dipole magnetic field errors also contribute to a beam which randomly strays from the axis. For a path length of 200 km in the HER and a maximum beam displacement of 1 mm, this analysis gives a quadrupole alignment requirement of about 10 μm and a dipole field error tolerance of less than 1 part in 5×10^4. These alignment criteria are stringent but not impossible. However, the criteria are considerably relaxed when steering stations are included in the design. If δx_{rms} is 100 μm and the allowed beam displacement is about 1 mm, then impulses steering the beam to $x_c = x_c' = 0$ must occur at an interval along the accelerator of $L\, x_c^2/(C_{rw}\Delta x_{rms}^2)$, which is about 16.7 L for the above parameters. A betatron period is $(4\pi/\sigma_0)\, L$ which has a minimum value of about 9 L, implying a correction would be required once every 2 betatron periods. Since the circumference is about 2 km, there would be about 34 such steering sections in the HER. At the extraction from the HER, since C_{rw} is reduced by a factor of 2, x_c will be reduced to about 0.7 mm. Conceptually, the steering stations would consist of three monitors, to infer the position and transverse velocity of the centroid and the beam energy on a given lap of the acceleration sequence. In addition to the monitors, a pair of dipole kickers would be used to set the centroid displacement to zero from the design orbit and then, second, to set the transverse velocity to zero. These kicks would be constant over the duration of the pulse. In addition, one time-dependent kicker station per ring would be required to prevent phase differences from accumulating between the beam center and the ends. The transverse envelope code and longitudinal Lagrangian fluid code CIRCE[23] is being used to develop optimized steering algorithms.

In addition to centroid control, the emittance growth must be minimized. The normalized emittance is a measure of the transverse phase space occupied by the beam and is an invariant in an ideal focusing system. In order to focus onto a spot at the target, the normalized emittance cannot be too large. We estimate that, from injector to target, a growth in normalized emittance by a factor of order 20 is allowable. Two sources of emittance growth have been identified: the conversion of centroid oscillation energy into thermal energy and the conversion of transition mismatch oscillation energy into thermal energy.

As discussed above, centroid misalignments give rise to betatron oscillations. In the presence of nonlinearities in the focusing fields, some of the transverse

energy associated with oscillation of the beam centroid is converted into thermal energy. Using the approximations of smooth focusing, constant velocity, and total conversion of centroid transverse energy into thermal energy[4, 24] implies that the increased normalized emittance $\Delta\varepsilon_N$ can be approximately written

$$\Delta\varepsilon_N \cong \beta C_{rw}\left(\frac{\sigma_0^2}{\sigma}\right)\left(\frac{\delta x_{rms}^2}{L^2}\right) n_{lap} C \quad . \tag{11}$$

Here, using typical numbers of the high-energy ring, the quantitity $\beta C_{rw}(\sigma_0^2/\sigma)$ is approximately 1.3, lattice half period L = 3.5 m, the number of laps the beam makes in the ring n_{lap} = 100, the circumference C = 2.0×10^3 m. We find a $\Delta\varepsilon_N = 2.0 \times 10^{-6}$ π m rad if the rms alignment error δx_{rms} = 10 μm. This compares to a final normalized emittance of about 7.5×10^{-6} m rad in the design for the high-energy ring. Steering will increase the tolerance on emittance growth by a factor $(L_{pm}/L_s)^{1/2}$, where L_{pm} is the phase mixing distance and L_s is the distance between steering stations. A factor of 10 increase in the alignment tolerance would be a reasonable expectation (yielding a tolerance of ~100 μm). We emphasize that this is a pessimistic estimate based on the assumption that all centroid oscillation energy is converted into emittance growth.

The second source of emittance growth was first observed in 3-D particle-in- cell simulations using the code WARP.[25] When a beam which is in equilibrium in a straight section enters a bend, its equilibrium becomes mismatched for the bend. Physically, particles that initially do not have the design momentum for the bend become spatially separated, creating nonlinear space-charge forces, allowing phase mixing of the coherent mismatch oscillations until a new equilibrium is reached. The simulations showed that if a beam enters a bend from a straight section the emittance initially grows but saturates in a few betatron periods as a new equilibrium is approached. However, in a racetrack configuration composed of 180° bends separated by linear sections, the emittance continues to grow since new mismatches are formed at each transition. The simulations were done for a small-scale recirculator, similar to one proposed for the Induction Linac Systems Experiments, now being planned at Lawrence Berkeley Laboratory. A linear theory[26] was developed in which beam displacement and particle energy spread were both treated as linear quantities. Transverse energy conservation was assumed, as well as complete conversion of mismatch energy into thermal energy. For large energy spreads and highly depressed beams, the theory tracked the simulations closely, with theory overestimating the emittance growth when the assumption of complete conversion of mismatch energy was violated. When the parameters of the beam at the exit of the high-energy ring are used, the theory predicts a factor of two increase in emittance, which is within the allowed emittance budget. The transitions may be made gradual enough that equilibria are reached adiabatically with even less growth in the normalized emittance.

The final physics issues addressed here involve beam instabilities. Three instabilities are discussed: the longitudinal resistive instability, the transverse beam-break-up instability and resonance instabilities.

A major research effort on the subject of the longitudinal resistive instability in HIF induction accelerators has been made over the last few years.[27] In this instability, the beam can become bunched due to the impedance of the induction cavities. However, recent studies show that the growth rates and instability gains obtained in the early 1980s overestimate the instability gain since they neglect the capacitance of the induction modules. Further, feed-forward techniques can be utilized to further control residual growth. In the recirculator, the voltage gradient is reduced from that of the linear machine. For line-type modulators, the impedance of the line must be matched (or nearly matched) to the impedance of the load, which is nearly proportional to the cell voltage divided by the total current. Thus, with a small voltage gradient (for a given current) the resistance is reduced. When opening and closing switches are used to modulate the voltage pulse to the induction cores the matched condition is not necessary and the cell resistance may be reduced further. For these reasons, we find that the instability should be less severe in a recirculator, and that the solutions found in Ref. 27 may also be used for residual growth of the instability.

The second instability known to occur in induction linacs is the beam-break-up instability. In this instability, displacements in the head of the beam excite electromagnetic modes in the cavities formed by the acceleration gaps of the induction cells. The excited fields give kicks (momentum impulses) to the rest of the beam, causing displacements, and more excitation and so forth. In the recirculator (and linear driver) strong focusing (alternating gradient) is used in contrast to the weaker solenoidal focusing used in many electron induction linacs. In addition, at the lower energies, the beam takes a relatively long time to transit the gap so that the electric field oscillates in time, averaging out to give a small net kick. The gain of the instability in the HER is estimated to be unity, provided that the cells can be designed such that the Q of the cavity can be reduced to be of order 3–4. Cell designs using the electromagnetic field code, AMOS[28] or the 3-D version PLATO[29] should make such low values of Q possible.

The final instability which is often brought up in the context of circular machines is the resonance instability.

In a storage ring, the orbital period cannot be an integral number of betatron periods. Otherwise a misalignment would give the beam a kick at the same phase of its betatron oscillation. This would lead to a larger and larger centroid displacement, and ultimately result in losing beam particles to the beam pipe. In a recirculator, however, the focusing field remains constant while the beam accelerates. The betatron period thus increases as the energy increases. In the HER, the number of betatron periods varies from 63 to 20 in 100 laps. The betatron phase changes by an average of 140° per lap, and therefore the kicks given by the misalignments add more randomly than coherently. The machine behaves like a long linear accelerator and the earlier discussion on misalignments in the centroid becomes pertinent.

Summary

We have shown that, using our best estimates of physical parameters and component costs, a 4 MJ recirculator driver, with a 35% efficiency would have a projected cost of approximately $500 million. The cost and efficiency compare favorably with previous estimates of these quantities for linear induction accelerators. Studies are underway to compare recirculators with linear induction machines using identical costing algorithms. The crucial engineering issues identified include the high repetition rate of the induction core pulsers and the efficient energy recovery in the ramped dipole magnets. Small-scale experiments are in progress to validate the engineering solutions to these issues. In addition, a recirculator ring is being planned for the proposed Induction Linac Systems Experiment facility, currently being designed at Lawrence Berkeley Laboratory. This ring would provide an integrated test of the recirculator concept. The crucial physics issues to be tested include the maintenance of the high vacuum, beam centroid and beam emittance control. To date, our studies have not revealed insurmountable hurdles although critical desorption coefficient data are required to validate our assumptions on the vacuum system. In general, we find that a driver based on the induction recirculator is an economically attractive candidate for an HIF power plant which merits further experimental and theoretical research.

Acknowledgments

In addition to the authors of this paper, many people contributed to our recirculator studies. Some of these people include W. A. Barletta, A. L. Brooks, R. Bieri, D. Callaghan, J. P. Clay, F. Coffield, J. DeFord, W. M Fawley, T. J. Fessenden, W. L. Gagnon, A. R. Harvey, J. R. Heim, D. W. Hewett, D. C. Ho, W. J. Hogan, C. A. Hurley, A. B. Langdon, E. J. Lauer, J. L. Miller, R. W. Moir, H. G. Patton, G. E. Russell, C. Shang, S. Shen, D. S. Slack, and L. Smith.

Notes and References

1. National Research Council, National Academy of Sciences, *Second Review of the Department of Energy's Inertial Confinement Fusion Program, Final Report* (National Academy Press, Washington, D. C., 1990).
2. Fusion Policy Advisory Committee, *Final Report* (U.S. Department of Energy, Washington, D. C., 1990).
3. U.S. Department of Energy, *National Energy Strategy, First Edition 1991/1992* (Washington, D.C., 1991).
4. J. J. Barnard, A. L. Brooks, J. P. Clay, F. Coffield, F. Deadrick, L. V. Griffith, A. R. Harvey, D. L. Judd, H. C. Kirbie, V. K. Neil, M. A. Newton, A. C. Paul, L. L. Reginato, G. E. Russell, W. M. Sharp, H. D. Shay, J. Wilson, and S. S. Yu, *Study of Recirculating Induction Accelerators as Drivers for Heavy Ion Fusion*, Lawrence Livermore National Laboratory, Livermore, CA, UCRL-LR-108095 (1991).
5. D. Keefe, "Inertial Confinement Fusion," *Annual Review of Nuclear and Particle Science*, **32**, 391 (1982).
6. METGLAS is the trademark for a metal alloy developed by Allied Signal, Inc., Parsippany, NJ.
7. E. P. Lee, T. J. Fessenden, and L. J. Laslett, "Transportable Charge in a Periodic Alternating Gradient System," *IEEE Trans. Nucl. Sci.* **NS-26**, 2489 (1985).
8. J. Hovingh, V. O. Brady, A. Faltens, D. Keefe, and E. P. Lee, "Heavy-Ion Linear Induction Accelerators as Drivers for Inertial Fusion Power Plants," *Fus. Tech.* **13**, 255 (1988).
9. R. F. Bourque, W. R. Meier, and M. J. Monsier, "Overview of the OSIRIS IFE Reactor Conceptual Design" *Fus. Tech.* **21**,1465, (1992).
10. L. M. Waganer, "Status of the Prometheus Reactor Design Studies," *14th IEEE/NPSS Symposium on Fusion Engineering* (Institute of Electrical and Electronic Engineers, New York, N. Y., 1991).
11. W. J. Shafer Associates, Livermore, CA.
12. W. F. Weldon, W. L. Bird, M. D. Driga, K. M. Tolk, H. G. Rylander, and H. H. Woodson, "Fundamental Limitations and Design Considerations for Compensated Pulsed Alternators," *Proceedings of the 2nd IEEE Pulsed Power Conference*, A. H. Guenther and M. Kristiansen, Eds. (Institute of Electrical and Electronic Engineers, New York, N. Y., 79CH1505-7, 1979).
13. H. C. Kirbie, G. J. Caporaso, M. A. Newton, and S. S. Yu, "Evolution of High-Repetition-Rate Induction Accelerators through Advancements in Switching," *1992 Linear Accelerator Conference Proceedings 1992 August 24-28 Ottawa, Ontario, Canada*, C. R. Hoffman, Ed., AECL-10728, **2**, 595 (1992).
14. Y. K. Kim, *ERDA Summer Study of Heavy Ions for Inertial Fusion*, Lawrence Berkeley Laboratory, Berkeley, CA, LBL-5543 (1976) ps. 11 and 58.
15. G. H. Gillespie, *ERDA Summer Study of Heavy Ions for Inertial Fusion*, Lawrence Berkeley Laboratory, Berkeley, CA, LBL-5543 (1976) p. 59.
16. D. Blechshmidt and H. J. Halama, *Proceedings HIF Workshop Brookhaven National Laboratory, Oct. 17, 1977*, Brookhaven National Laboratory, Yaphank, NY, BNL-50769, 136 (1977).
17. G. H. Gillespie, *Proceedings HIF Workshop Brookhaven National Laboratory, Oct. 17, 1977*, Brookhaven National Laboratory, Yaphank, NY, BNL-50769 (1977) p. 45.
18. F. Melchert, E. Salzborn, I. Hofman, R. W. Muller, R and V. P Shevelko, *Nucl. Inst. Meth. Phys. Res.* **A278** 65 (1989).
19. E. Salzborn, *J. Physique*, **C1** (1) 50 (1989).
20. J. J. Barnard, S. S. Yu, and A. Faltens, "Vacuum Requirements for Recirculators," *Part. Accel.* **37-38** 419 (1992).
21. I. A. Baranov, A. S. Krivokhatskii, and V. V. Obnorskii, *Zh. Tekh. Fiz.* **51**, 2457-2475 (December, 1981); (English translation) *Sov. Phys. Tech. Phys.* **26**, 1455, (1981).
22. D. G. Koshkarev, "The Charge Exchange Instability in Intense Ion Beams," *Part. Accel.* **16** 1, (1984).

23. W. M. Sharp, J. J. Barnard, and S. S. Yu, "Envelope Model for a Heavy Ion Recirculator," *Part. Accel.* **37-38** 205, (1992); W. M. Sharp, J. J. Barnard, and S. S. Yu, "Transport and Error Sensitivity in a Heavy Ion Recirculator," in *Proceedings of the 1991 IEEE Particle Accelerator Conference* (IEEE, Piscataway, NJ, 1991) p. 260.
24. M. Reiser, "Free Energy and Emittance Growth in Nonstationary Charged Particle Beams," *J. Appl. Phys.* **70** 1919 (1991).
25. A. Friedman, D. P. Grote, D. A. Callahan, A. B. Langdon, and I. Haber, "3D Particle Simulations of Axially Confined Heavy Ion Beams Using the WARP code: Transport Around Bends," *Part. Accel.* **37–38** 131, (1992); A. Friedman, D. P. Grote, D. A. Callahan, A. B. Langdon, and I. Haber, "3D and r, z Particle Simulations of Heavy Ion Fusion Beams," *1992 Linear Accelerator Conference Proceedings 1992 August 24-28 Ottawa, Ontario, Canada*, C. R. Hoffman, Ed., AECL-10728, **2**, 784 (1992).
26. J. J. Barnard, H. D. Shay, S. S. Yu, A. Friedman, and D. P. Grote, "Emittance Growth in Heavy-Ion Recirculators," *1992 Linear Accelerator Conference Proceedings 1992 August 24-28 Ottawa, Ontario, Canada*, C. R. Hoffman, Ed., AECL-10728, **1**, 229 (1992).
27. E. P. Lee, "Beam Dynamics and Longitudinal Instabilities in Heavy -Ion-Fusion Induction Linacs," *1992 Linear Accelerator Conference Proceedings 1992 August 24-28 Ottawa, Ontario, Canada*, C. R. Hoffman, Ed., AECL-10728, **2**, 591(1992).
28. J. F. DeFord and G. D. Craig, "Wake Potential and Impedance Calculations Using Stiff Subrelativistic Beams," *Part. Accel.* **37–38**, 111 (1992).
29. J. F. DeFord and C. C. Shang, PLATO, Lawrence Livermore National Laboratory, Livermore, CA.

LASNEX EVOLVES TO EXPLOIT COMPUTER INDUSTRY ADVANCES

L. Busby
P. F. Dubois
S. Wilson

Introduction

Lasnex is a computer program for modeling the physics of ICF targets. Initially created by G. Zimmerman in 1970, Lasnex has evolved through several generations of supercomputer hardware and operating systems. Five years ago, the Lasnex group anticipated the development of low-cost, high-performance UNIX workstations and the demise of Livermore-specific languages and operating systems. Our users were pressing for more power and control over the modeling.

Thus, we embarked on an ambitious project with several specific goals:

- Replace the computer science portion of Lasnex with the Basis program-development system, described below, giving users much more control.
- Run the same Lasnex problem on UNIX workstations and the Crays and obtain essentially the same results.
- Make restart dumps and postprocessing files portable among all computer platforms. That is, these files can be used on any computer without translation no matter where they were written.
- Manage source codes, program compilations, and program releases with a modern, automated system on the workstations.
- Replace the Lasnex graphics library with a widely available commercial or government product.
- Rewrite the Lasnex manual and produce it with a modern desk-top publishing system.

We have realized these goals.

- The users enjoy the power of the Basis system, and the Lasnex group's working conditions are greatly improved with our workstation-centered development system.
- Lasnex produces portable files that may be read on our network of Hewlett-Packard and Sun workstations, and on the Cray machines under both the Cray UNICOS and Livermore NLTSS operating systems.
- We manage Lasnex production runs on workstations with a newly installed batch system.
- We are using the National Center for Atmospheric Research (NCAR) graphics library.
- The Lasnex manual has been completely revised and its production uses commercial, not local, technology.

During October 1992, the Lasnex production runs used more than 65% of the total central processing unit (CPU) cycles on our cluster of 11 HP730 workstations. These machines, with an aggregate cost of about $230,000, provided the equivalent of over 2000 hours of Cray Y-MP time valued at more than $800,000 in only 1 month—in addition to their full-time duty as interactive development and analysis machines.

Where possible our work is shared with other projects. Three major projects in ICF and many other projects at LLNL and outside the Laboratory use all or part of our technology.

Making Lasnex Powerful

Eight years ago, an effort began in LLNL's Magnetic Fusion Program to develop a comprehensive modeling code for mirror machines. We were asked to develop a system for creating such scientific programs. The Basis system was the response to that request. Basis survived the termination of the mirror effort and original modeling project, and has gone on to be used here and at other laboratories for about a hundred other projects ranging from small individual explorations to large team projects.

In this article, we use the term "author" to denote the person(s) creating the modeling program, and the term "user" to denote the consumer(s) using the program. Of course, the author of a program is an important user, too.

Basis Makes Applications Programmable

The heart of the Basis philosophy is a conviction that the most rapidly changing aspect of any scientific computer program is what users want to calculate with it. Therefore, the program itself should be programmable, that is, have the flexibility and power of a programming language. This gives the user a degree of control over the program without intervention by the author or recompilation of the code.

Here is how Basis makes this possible: The author writes some physics subroutines and uses the Basis system to create a full-service program with a user interface that is a programming language. The crucial point is that this language *already contains the permanent variables and subroutines in the physics the author has written*. Therefore, the user can manipulate these variables and subroutines as well as others he or she creates in the Basis language itself. Thus the application becomes "user" programmable. The user can plot, print, or change any variable, any time.

Another important advantage of Basis is that its physics "packages" are generally quite modular and reusable. There is an extensive library of existing packages for collecting time histories, reading and writing various file formats, timing, Bessel functions, etc. This modularity makes it relatively easy for users to develop new packages and add them to the code for special projects.

Physicists Use the Power

Lasnex users immediately began to take advantage of this power, and we made it easy for new users to use the new Lasnex:

- Basis resembles a Fortran array language, so that physicists can learn it quickly.
- We wrote a translator to convert old input files to new ones.
- We were able to implement most of the old input commands unchanged using a command-creating facility in the Basis language.

Users can simply translate their old input and use the new program in the same way they used the old. In fact, they tend to make only a few runs this way, and then begin to use the new power available to them. Their creativity has been astounding. One physicist adds a random variation to the laser input each cycle to make it more realistic. Others calculate simulated experimental diagnostic output for comparison to experiment, rezone while running, make customized dumps, and activate actions when certain events are detected. This confirms the Basis philosophy. The authors of a program cannot imagine what the users want to do with it; they must view their job as empowering users.

Other major projects in ICF using Basis and leveraging off the Lasnex effort are: the WARP ion-beam modeling code and the F3D filamentation code. In addition, most of the fusion studies in M-Division use Basis.

Making Lasnex Portable

We want Lasnex to be as portable as possible. By this we mean:

- Have a source code as close to industry standards as possible.
- Get the same answer, or nearly so, on each different type of computer platform.
- Be able to start a problem on one type of platform and continue it on another.
- Have essentially one source code, not a different source code for different platforms.

Most of Lasnex was originally written in a Livermore dialect of Fortran called LRLTRAN. It contained hundreds of special statements called *macros*, which are application-dependent extensions of LRLTRAN. These macros were an intelligent response to a slow central computer running a line editor, where brevity can outweigh clarity of expression, but they are counterproductive today. They add complexity, decrease reliability, and greatly increase the learning curve for new authors.

We wrote a one-time tool to remove the macros and help transform the Lasnex source code to nearly standard Fortran. At the end of this step, our first portability goal above had been reached. Yet the other goals remained unfulfilled.

Why Portability is Hard to Achieve

Fortran is a language with a standard. Therefore, if we write programs that conform to this standard, we get a portable program, right? Wrong. From a programmer's point of view, there are two basic problems with the Fortran standard. It lets the Fortan compiler writer decide too many things, and it doesn't cover all the areas a real program has to deal with. Here are some of the things the programmer cannot control:

- How much precision a real variable has.

- What happens if a floating-point or math-routine error occurs.
- What happens to signals such as interrupt and kill signals.
- How to read arguments from the execute line.
- What the linker/loader thinks common blocks and functions are really named, and how arguments are passed to subroutines. This makes it difficult to call another language, say C, from Fortran or vice-versa. Even if we aren't writing physics in C, the graphics package or database package we want to use, or those signal handlers we need to write may be in C.
- How data items are represented. The way character data, logical data, and real data is represented varies widely. This interferes with interlanguage communication and creating portable data files.
- The compiler options and the argument syntax vary, as do the defaults for such things as whether local variables are static. This makes it harder for the programmer to write *Makefiles* or other automatic compilation scripts, which are essential for large projects.

There is also no standard provision in Fortran for operating on bits, and compilers vary widely in the operations and syntax they provide.

Preprocessor Provides Portability

A *preprocessor* is a program that changes the original source text of a program into a form that is ready for the compiler on a given target machine. A good preprocessor is the key to solving several of the problems discussed above, but the Fortran standard does not specify a preprocessor. However, having one is a practical necessity in order to achieve the goals we've set for ourselves, since the one source code we wish to maintain cannot be correct for all environments.

As part of the Basis project, we wrote the preprocessor MPPL (More Productive Programming Language). It accepts a language that is upwardly compatible with Fortran 77. We enhanced this preprocessor to solve the precision problem for the Lasnex project.

After studying the alternatives, we adopted the syntax of the new Fortran 90 standard for controlling precision and doing bit manipulations. Our preprocessor changes this syntax into a suitable form for the Fortran 77 compilers we actually use. Figures 1–3 show some simple original text and the output of the preprocessor for a Cray and a workstation, showing how we are able to produce compiler-ready output with full control of the precision. Note that it does not suffice to simply make everything double-precision for the workstation; our graphics package, for example, requires single-precision input.

FIGURE 1. Preprocessor input.

```
real(Size4) x,y
real(Size8) z1,z2,z3
real w
x = 1.3_Size4
y = 1.4
z1 = x + y
z2 = 2._Size8 + real(x,Size8)
z3 = max(z1,z2)
```

FIGURE 2. Preprocessor output for a 64-bit Cray.

```
real x,y
real z1,z2,z3
real w
x = 1.3
y = 1.4
z1 = x + y
z2 = 2. + real(x)
z3 = max(z1,z2)
```

Making Portable Output Files

Lasnex creates a large variety of binary output files, including restart files and input files for other postprocessors. We have standardized its output on the portable binary database format created by S. Brown, also of LLNL. This means that we can generate a problem on the workstation, run it for a few cycles to make sure it is running correctly, and then move the restart dump to a Cray to finish it overnight. Likewise, we can make a run on one machine and then postprocess the output on another, or take a Cray job that has run out of time and finish it on a workstation.

How We Got Out of The Graphics Business

We created a Basis-language interactive interface to the NCAR graphics package. The NCAR package is freely available and contains sufficient power to satisfy our needs in the medium term. We combined this

FIGURE 3. Preprocessor output for a 32-bit workstation.

```
real x,y
doubleprecision z1,z2,z3
doubleprecision w
x = 1.3
y = 1.4d0
z1 = x + y
z2 = 2.d0 + dble(x)
z3 = max(z1,z2)
```

with a commercial device driver to make graphics output via X-windows and other output devices. The interface we wrote closely models the graphics commands in the old Lasnex generator decks. We no longer have to maintain our own graphics library.

How We Work Together

When many software developers work together on the same project, their efforts must be coordinated. This coordination is part of a source-code management. We tried a commercial product for source-code management but found it too elaborate for our needs. Eventually we settled on a public domain solution called the Concurrent Version System (CVS). CVS is being widely adopted at the Laboratory, and we have contributed suggestions to its authors that have improved it. It allows each of our program developers to work independently in parallel, and helps them resolve any conflicts that might arise with other developers.

How We *Make* Lasnex

The authors of Basis and Lasnex must create different program versions for many different computer systems, and these systems have different compilers, loaders, and file system layouts. It was a real challenge to automate the "build" process. Ideally, the author should be able to build two or more versions simultaneously. To do this, we created a program called **mmm**. It takes a small description file as input and creates files called *Makefiles* that are input to the UNIX utility **make**. It creates these *Makefiles* using only the common features of the various **make** utilities supplied with each UNIX system. The program **make** in turn carries out the building of the program.

Previously, using the Cray-based system, a developer who wished to rebuild the Lasnex program from the ground up needed to monitor a process that took, on average, 2 to 3 days. Now, this can be done in less than 3 hours on an HP workstation using the following commands:

```
cvs checkout lasnex
mmm
make all lasnex
```

to get the source program, construct the Makefiles, build all the packages, and reload Lasnex. If the target computer is a Cray, one more simple step is required on it.

An author who only needs to change one or two physics packages can usually remake the program in under 10 minutes since the system stores and reuses the binaries from the other unchanged packages.

When the Laboratory's Computer Center began changing the operating system on the Crays to UNICOS, we were ready. We did the UNICOS port while we were finishing the workstation effort. We also added special production details peculiar to UNICOS and solved many mysteries of the batch production system. For the most part, we are able to treat the Crays as just another kind of workstation.

Looking to the Future

We expect that our experience in producing a portable code will be invaluable towards creating a "Lasnex21" to run on the computers of the next century. We are looking forward to tripling the CPU capacity of our network next year and to increasing online data storage by a factor of 10. In the software area, we are beginning a 3-D hydrodynamics project for Lasnex, and we are beginning to study possibilities for parallelizing sections of the code. We plan to continue to make the Basis system easier to use and more portable.

Summary

We have completely modernized Lasnex to be more portable and more powerful.

By use of a preprocessor that changes original source-program text into a code that will compile on any target computer, Lasnex runs on many platforms. Therefore, Lasnex is adaptable and useful for many more applications.

By use of our newly developed Basis system, Lasnex itself is programmable by the user, and therefore, the user can readily manipulate the permanent variables and routines in the physics the author has written, as well as those varibles he or she creates in the full-service interface created by Basis.

Project Team Members

This project was directed by P. F. Dubois. The project was the result of the work of E. W. Alley, R. A. Allsman, D. S. Bailey, L. Busby, Y. H. Chiu, A. Edwards, R. H. Hanscom, J. A. Harte, D. S. Kershaw, S. Langer, M. Prasad, A. I. Shestakov, S. H. Taylor, J. Takemoto, S. Wilson, G. Zimmerman, and M. Zollinger.

Acknowledgments

We also gratefully acknowledge the contributions of C. C. Benedetti [student, Department of Applied Science (DAS)], B. Bonnlander (student, DAS), S. Brown, L. Chase, F. L. Karmitz, A. B. Langdon, Z. Motteler (California Polytechnic State University), D. Munro, C. Rhoades, J. Rathkopf, D. Sinck [student, University of California, Davis], and A. Springer.

FACILITY REPORT OCTOBER–DECEMBER 1992

G. Hermes
Nova Operations Group
Nova Experiments Group
Laser Science Group

During this quarter, Nova Operations fired a total of 282 system shots, resulting in 319 experiments. These experiments were distributed among ICF experiments, Defense Sciences experiments, X-ray Laser experiments, Laser Sciences, and facility maintenance shots.

Beginning this quarter, several operations technicians are starting work one hour earlier (6:00 A. M.) in order to get a head start on the first shot of the day. Many things may be set up prior to the start of the main shift at 7:00 A. M.

The final KDP array of the rework project was installed. This project was undertaken as a result of decreased conversion efficiency, due to KDP coating degradation causing poor transmission and increased scatter. We have increased the 3ω energy delivered to the target by about 17.5% as a result of the KDP refurbishment project.

Five chamber lenses were removed and recoated with the new uniform 1% reflective coating required for the 3ω diagnostic upgrade. Only three lenses are left to recoat. During the lens removals, we discovered a broken and several deformed couplings used on the focus lens drives to move the lens in the Z-axis. Analysis showed that these couplings were being overstressed. A new coupling was designed and the old couplings are being replaced as the lenses are removed for recoating and maintenance.

We are converting from 80-cm debris shields to 65-cm debris shields. The smaller shields are easier to handle for maintenance purposes and are less costly to manufacture. The hardware for these debris shields has arrived and is being installed on the 10-beam chamber. We will begin the design and fabrication of small aperture phase plates next quarter.

The vacuum control system for the 10-beam chamber was replaced with the new programmable controller. This system is much more reliable than the old LSI-11 based system and is easily modified or expanded. With the installation of this system and a new variable vent valve, the chamber (vacuum to air to vacuum) cycle time is only 20 min compared to the old 90 min cycle time. The diagnostic vacuum systems will be transferred to the new system during the remainder of the year.

The installation and activation of the "top off supplies" used to regulate the voltage of the flash lamps for the disk amplifiers has been completed. This project was part of the Precision Nova effort to increase laser power balance and repeatability. The remaining work of seismically securing the capacitors was also completed.

To demonstrate Precision Nova operation and repeatability, the Nova system was operated, on two occasions, continuously for more than 36 hours. This demonstration was very successful.

Construction of the petawatt master oscillator room has begun. We intend to occupy this room in April of 1993.

The Big Sky beam diagnostic system was expanded to 28 cameras. This digitization and analysis system in now fully operational and used on every shot.

PUBLICATIONS

A

Abare, A. C., Keane, C. J., Perry, M. D., Lee, R. W., Da Silva, L. B., and Falcone, R. W., *Analysis of Soft X-Ray Spectra from Short-Pulse Laser-Produced Plasmas that are Candidates for a Recombination X-Ray Laser*, Lawrence Livermore National Laboratory, Livermore, CA, UCRL-MI-111373 (1992). Prepared for the 34th Annual Meeting of the American Physical Society Division of Plasma Physics, Seattle, WA, November 16–20, 1992.

Albritton, J. W. and Liberman, D. A., *On the Distribution of Bound Levels of Ions in Dense Plasmas: The Plasma Polarization Shift*, Lawrence Livermore National Laboratory, Livermore, CA, UCRL-JC-111911 ABS (1992). Prepared for the 5th International Workshop on Radiative Properties of Hot Dense Matter, Santa Barbara, CA, November 2–6, 1992.

Amendt, P., London, R. A., and Strauss, M., *Effects of Plasma Fluctuations on X-Ray Laser Coherence*, Lawrence Livermore National Laboratory, Livermore, CA, UCRL-MI-111162 (1992). Prepared for the 34th Annual Meeting of the American Physical Society Division of Plasma Physics, Seattle, WA, November 16–20, 1992.

B

Back, C. A., Da Silva, L. B., Fenske, J., Montgomery, D. S., Kornblum H. N. Jr., Kauffman R. L., and Lee, R. W., *X-Ray Flux from Burn-Through Au Foils*, Lawrence Livermore National Laboratory, Livermore, CA, UCRL-MI-112145 (1992). Prepared for the 5th International Workshop on the Radiative Properties of Hot Dense Matter, Santa Barbara, CA, November 2–6, 1992.

Back, C. A., Da Silva, L. B., MacGowan, B. J., Montgomery, D. S., Kornblum H. N. Jr., Glendinning S. G., Fenske, J., Kauffman R. L., and Lee, R. W., *X-Ray Flux from Burn-Through Au Foils*, Lawrence Livermore National Laboratory, Livermore, CA, UCRL-JC-111950 ABS (1992). Prepared for the 5th International Workshop on the Radiative Properties of Hot Dense Matter, Santa Barbara, CA, November 2–6, 1992.

Baldis, H. J., Baton, S., Moody, J. D., Labaune, C., Jalinaud, T., Estabrook, K. G., and Dixit, S. N., *Space- and Time-Resolved Backscattered SBS Light from Preformed Plasmas*, Lawrence Livermore National Laboratory, Livermore, CA, UCRL-MI-111149 (1992). Prepared for the 34th Annual Meeting of the American Physical Society Division of Plasma Physics, Seattle, WA, November 16–20, 1992.

Baldis, H. J., Moody, J. D., Batha, S. H., Labaune, C., Montgomery, D. S., Estabrook, K. G., Berger, R. L., Williams, E. A., and Kruer, W. L., *Laser-Plasma Instabilities and Coherence Control*, Lawrence Livermore National Laboratory, Livermore, CA, UCRL-MI-110329 (1992). Prepared for the 14th International Conference on Plasma Physics and Controlled Nuclear Fusion Research (IAEA), Wurzburg, Germany, September 30–October 7, 1992.

Barnard, J. J., Caporaso, G. J., and Yu, S. S., *One Dimensional Simulations of Transients in Heavy Ion Injectors*, Lawrence Livermore National Laboratory, Livermore, CA, UCRL-JC-112343 ABS (1993). Prepared for the 1993 Particle Accelerator Conference, Washington, DC, May 17–20, 1993.

Barnard, J. J., Deadrick, F. J., Griffith, L. V., Grote, D. P., Friedman, A. Kirbie, H. C., Neil, V. K., Newton, M. A., and Paul, A. C., *Recirculating Induction Accelerators as Drivers for Heavy Ion Fusion*, Lawrence Livermore National Laboratory, Livermore, CA, UCRL-MI-111379 (1992). Prepared for the 34th Annual Meeting of the American Physical Society Division of Plasma Physics, Seattle, WA, November 16–20, 1992.

Barnard, J. J., Miller, J. L., and Haber, I., *Emittance Growth in Displaced, Space-Charge-Dominated Beams With Energy Spreads*, Lawrence Livermore National Laboratory, Livermore, CA, UCRL-JC-112340 ABS (1993). Prepared for the 1993 Particle Accelerator Conference, Washington, DC, May 17–20, 1993.

Bell, P., Kilkenny, J. D., Wiedwald, J. D., Ress, D. B., Landen, O. L., Bradley, D. K., Oertel, J., and Watt, R., *High Speed X-Ray Gating Cameras for ICF Imaging Applications*, Lawrence Livermore National Laboratory, Livermore, CA, UCRL-JC-112256 (1992). Prepared for the 20th International Congress on High-Speed Photography and Photonics, Victoria, Canada, September 21–25, 1992.

Berger, R. L., Lasinski, B. F., and Williams, E. A., *Parametric Instability Driven by a Random-Phase-Plate Laser Beam*, Lawrence Livermore National Laboratory, Livermore, CA, UCRL-MI-110763 (1992). Prepared for the 34th Annual Meeting of the American Physical Society Division of Plasma Physics, Seattle, WA, November 16–20, 1992.

Bibeau, C., Payne, S. A., and Powell, H. T., *Direct Measurements of the Terminal-Level Lifetime For Nd^{3+}-Doped Laser Materials*, Lawrence Livermore National Laboratory, Livermore, CA, UCRL-JC-111853 ABS & SUM (1992). Prepared for the Advanced Solid State Lasers 8th Topical Meeting, New Orleans, LA, February 1–3, 1993.

Bibeau, C., Speck, D. R., Kyrazis, D. T., Laumann, C. W., Ehrlich, R. B., Henesian, M. A., Lawson, J. K., Perry, M. D., and Wegner, P. J., "Power, Energy, and Temporal Performance of the Nova Laser Facility with Recent Improvements to the Amplifier System," *Appl. Opt.* **31** (7), 5799–5809 (1992).

Bieri, R. L., *Inertial Confinement Fusion Driver Enhancements: Final Focusing Systems and Compact Heavy-Ion Driver Designs*, Lawrence Livermore National Laboratory, Livermore, CA, UCRL-ID-107986.

Britten, J. A. and Thomas, I. M., *Sol-Gel Multilayers Applied by a Meniscus Coating Process*, Lawrence Livermore National Laboratory, Livermore, CA, UCRL-JC-110152 REP (1992). Prepared for the Materials Research Society 1992 Spring Meeting, San Francisco, CA, April 27–May 1, 1992.

Buckley, S. R., Overturf, G. E., and Cook, R. C., *Brominated Polystyrene at Preselected Atom %*, Lawrence Livermore National Laboratory, Livermore, CA, UCRL-JC-107949 (1991). Prepared for the 8th Target Fabrication Specialists' Meeting, Albuquerque, NM, September 23–25, 1991.

C

Cable, M. D., Hatchett, S. P., and Nelson, M. B., *Neutron Spectroscopy with a Large Neutron Time-of-Flight Detector Array (LaNSA)*, Lawrence Livermore National Laboratory, Livermore, CA, UCRL-JC-109284 REP (1992). Prepared for the 9th Topical Conference on High Temperature Plasma Diagnostics, Santa Fe, NM, March 15–19, 1992.

Callahan, D. A., Langdon, A. B., Haber, I., and Friedman, A., *Longitudinal Beam Dynamics for Heavy Ion Fusion Using WARPRZ*, Lawrence Livermore National Laboratory, Livermore, CA, UCRL-JC-112247 ABS (1992). Prepared for the Computational Accelerator Physics Conference 1993, Pleasanton, CA, February 22–26, 1993.

Callahan, D. A., Langdon, A. B., Haber, I., and Friedman, A., *Longitudinal Beam Dynamics for Heavy Ion Fusion*, Lawrence Livermore National Laboratory, Livermore, CA, UCRL-JC-112341 ABS (1992). Prepared for the 1993 Particle Accelerator Conference, Washington, DC, May 17–20, 1993.

Callahan, D. A., Langdon, A. B., Haber, I., and Friedman, A., *Simulations of the Longitudinal Wall Impedance Instability*, Lawrence Livermore National Laboratory, Livermore, CA, UCRL-MI-111190 (1992). Prepared for the 34th Annual Meeting of the American Physical Society Division of Plasma Physics, Seattle, WA, November 16–20, 1992.

Campbell, E. M., Hogan, W. J., and Lowdermilk, W. H., *Nova Upgrade Mission and Design*, Lawrence Livermore National Laboratory, Livermore, CA, UCRL-JC-110035 (1992). Prepared for the Tenth Topical Meeting on the Technology of Fusion Energy 1992, Boston, MA, June 7–12, 1992.

Campbell, E. M., *Summary of Recent Progress in Indirect Drive ICF and Design of the Nova Upgrade System for Ignition Fusion Experiments*, Lawrence Livermore National Laboratory, Livermore, CA, UCRL-MI-112122 (1992). Prepared for the 14th International Conference on Plasma Physics and Controlled Nuclear Fusion Research (IAEA), Wurzburg, Germany, September 30–October 7, 1992.

Caporaso, G. J. and Barnard, J. J., *Analysis of Beam Loading in Electrostatic Columns*, Lawrence Livermore National Laboratory, Livermore, CA, UCRL-JC-112342 ABS (1992). Prepared for the 1993 Particle Accelerator Conference, Washington, DC, May 17–20, 1993.

Chen, Y.-J., Hewett, D. W., Yu, S. S., and Brandon, S. T., *Simulation of the LBL HIF Ion Injector*, Lawrence Livermore National Laboratory, Livermore, CA, UCRL-MI-111156 (1992). Prepared for the 34th Annual Meeting of the American Physical Society Division of Plasma Physics, Seattle, WA, November 16–20, 1992.

Chen, Y.-J. and Hewett, D. W., *Simulation of Transient Effects in the Heavy Ion Fusion Injectors*, Lawrence Livermore National Laboratory, Livermore, CA, UCRL-JC-112344 ABS (1992). Prepared for the 1993 Particle Accelerator Conference, Washington, DC, May 17–20, 1993.

Chow, R., Falabella, S., Stolz, C. J., Rainer, F., Loomis, G. E., and Kozlowski, M. R., *Reactive Evaporation of Low Defect Density Hafnia*, Lawrence Livermore National Laboratory, Livermore, CA, UCRL-JC-112202 (1992). Submitted to *Applied Optics*.

Collins, G. W., Mapoles, E. R., and Magnotta, F., *Magnetization and Optical Emission Studies of Tritiated Solid Deuterium*, Lawrence Livermore National Laboratory, Livermore, CA, UCRL-JC-112358 ABS (1992). Prepared for the American Physical Society Meeting, Seattle, WA, March 22–26, 1993.

Collins, G. W., Mapoles, E. R., and Unites, W. G., *Surface Structure of Solid Hydrogen Films*, Lawrence Livermore National Laboratory, Livermore, CA, UCRL-JC-112359 ABS (1992). Prepared for the American Physical Society Meeting, Seattle, WA, March 22–26, 1993.

Collins, G. W., Mapoles, E. R., and Unites, W. G., *Density Profile of Thick H_2 Films*, Lawrence Livermore National Laboratory, Livermore, CA, UCRL-MI-110460 (1992). Prepared for the 39th American Vacuum Society National Symposium and Topical Conference, Chicago, IL, November 9–13, 1992.

Collins, G. W., Sanchez, J. J., and Fearon, E. M., "DT and D_2 Retention in Plastic Shells," *J. Vac. Sci. Technol. A* **10** (4), 1158–1163 (1992).

Collins, G. W., "Deuteron NMR in Solid DT," *Phys. Rev. B* **46** (2) 695–701 (July 1, 1992).

Cook, R. C., Bernat, T. P., McEachern, R., Letts, S. A., Collins, G. W., Overturf, G. E., and Turner, R. E., *Production and Characterization of ICF Capsules*, Lawrence Livermore National Laboratory, Livermore, CA, UCRL-MI-111722 (1992). Prepared for the 14th International Conference on Plasma Physics and Controlled Nuclear Fusion Research (IAEA), Wurzburg, Germany, September 30–October 7, 1992 (paper IAEA-CH-56/G-3-5).

Crane, J. K., Perry, M. D., Falcone, R. W., and Herman, S., *High-Field Harmonic Generation in Helium at 526 μm*, Lawrence Livermore National Laboratory, Livermore, CA, UCRL-JC-110090 (1992). Submitted to *Journal of Optics Letters*.

Crane, J. K., Perry, M. D., Nguyen, H., Herman, S., Falcone, R. W., Adams, B., and Glover, E., *High-Order Harmonic Generation in Neutral and Singly Ionized Rare Gases*, Lawrence Livermore National Laboratory, Livermore, CA, UCRL-MI-111943 (1992). Prepared for the NATO Advanced Research Workshop, Super-Intense Laser-Atom Physics, Han-Sur-Lesse, Belgium January 8–14, 1993.

Crane, J. K., Perry, M. D., Nguyen, H., and Herman, S., *High-Order Sum and Difference Frequency Generation in Rare Gases*, Lawrence Livermore National Laboratory, Livermore, CA, UCRL-JC-112629 ABS & SUM (1993). Prepared for Short Wavelength V: Physics with Intense Laser Pulses, Second Topical Meeting, San Diego, CA, March 29–31, 1993.

Crane, J. K., and Perry, M. D., *High-Order Harmonic Generation in Neutral and Singly Ionized Rare Gases*, Lawrence Livermore National Laboratory, Livermore, CA, UCRL-JC-111943 ABS (1992). Prepared for the NATO Advanced Research Workshop, Super-Intense Laser-Atom Physics, Han-Sur-Lesse, Belgium January 8–14, 1993.

D

Da Silva, L. B., Trebes, J. E., Anderson, E., Mrowka, S., Balhorn, R. L., Attwood, D. T., Barbee, T. W., Brase, J. M., and Corzett, M. H., "X-Ray Laser Imaging Microscopy of Rat Sperm Nuclei," *Science* **258**, 269–271 (October 9, 1992).

Da Silva, L. B., Trebes, J. E., Koch, J. A., MacGowan, B. J., Mrowka, S., Matthews, D. L., Barbee, T. W., Balhorn, R. L., and Gray, J., *Progress in Imaging Microscopy with X-Ray Lasers at LLNL*, Lawrence Livermore National Laboratory, Livermore, CA, UCRL-JC-111296 (1992). Prepared for the Third International Colloquium on X-Ray Lasers, Schliersee, Germany, May 18–22, 1992.

Da Silva, L. B., Koch, J. A., Mrowka, S., Matthews, D. L., MacGowan, B. J., Ress, D. B., and Trebes, J. E., *X-Ray Lasers as Diagnostics for High Density Matter*, Lawrence Livermore National Laboratory, Livermore, CA, UCRL-JC-112115 ABS (1992). Prepared for the 5th International Workshop on the Radiative Properties of Hot Dense Matter, Santa Barbara, CA, November 2–6, 1992.

Da Silva, L. B., MacGowan, B. J., Back, C. A., Hammel, B. A., Kania, D. R., Hsieh, E. J., Doyas, R. J., Iglesias, C. A., and Rogers, F. J., "Absorption Measurements Demonstrating the Importance of $N = 0$ Transitions," *Phys. Rev. Lett.* **70** (3), 438–41 (20 July 1992).

Da Silva, L. B., *X-Ray Lasers as Diagnostic Tools for High Density Matter*, Lawrence Livermore National Laboratory, Livermore, CA, UCRL-MI-112136 (1992). Prepared for the 5th International Workshop on the Radiative Properties of Hot Dense Matter, Santa Barbara, CA, November 2–6, 1992.

Darrow, C. B., Coverdale, C., Clayton, C., Mori, W., Perry, M. D., March, K., and Joshi, C., "Strongly Coupled Stimulated Raman Backscatter from Sub-Picosecond Laser-Plasma Interactions," *Phys. Rev. Lett.* **69** (3), 44–45 (20 July 1992).

Darrow, C. B., *Strongly Coupled Stimulated Raman Backscatter from Sub Picosecond Laser Plasma Interactions*, Lawrence Livermore National Laboratory, Livermore, CA, UCRL-ME-110301 (1992). Prepared for the 34th Annual Meeting of the American Physical Society Division of Plasma Physics, Seattle, WA, November 16–20, 1992.

Darrow, C. B., *Observations of MeV Electrons and Scattered Light from Intense, Subpicosecond Laser Plasma Interactions*, Lawrence Livermore National Laboratory, Livermore, CA, UCRL-ME-111151 Rev 1 (1992). Prepared for the 34th Annual Meeting of the American Physical Society Division of Plasma Physics, Seattle, WA, November 16–20, 1992.

Davis, J. L., Campbell, E. M., Storm, E., and Lindl, J. D., *Inertial Confinement Fusion*, Lawrence Livermore National Laboratory, Livermore, CA, UCRL-JC-111721 (1992); *Modern Physics for Scientists and Engineers*.

De Groot, J. S., Estabrook, K. G., Mizuno, K., Drake, R. P., Kruer, W. L., and Cameron, S. M., *Distributed Absorption and Inhibited Heat Transport*, Lawrence Livermore National Laboratory, Livermore, CA, UCRL-JC-109977 (1992). Prepared for the 10th Workshop on Laser-Plasma Interactions and Related Phenomena, Monterey, CA, November 1992.

DeFord, J. F., Hartung, W., and Moffatt, D., *Computing Impedance and Loss Factor of Ferrite Ring HOM Suppressors for Cornell B Factory Superconducting RF Cavity*, Lawrence Livermore National Laboratory, Livermore, CA, UCRL-JC-112374-ABS (1992). Prepared for the 1993 Particle Accelerator Conference, Washington, DC, May 17–20, 1993.

DeFord, J. F., Madsen, N. K., Ryne, R., Rodenz, G., and Shang, C. C., *Calculation of Wake Potentials Using Conforming Grid Time Domain Computer Codes*, Lawrence Livermore National Laboratory, Livermore, CA, UCRL-JC-112262 ABS (1992). Prepared for the Computational Accelerator Physics Conference 1993, Pleasanton, CA, February 22–26, 1993.

DeFord, J. F., Madsen, N. K., Ryne, R., Rodenz, G., and Shang, C. C., *Wake Potential Calculation Using the DSI3D Computer Code*, Lawrence Livermore National Laboratory, Livermore, CA, UCRL-JC-112376 ABS (1992). Prepared for the 1993 Particle Accelerator Conference, Washington, DC, May 17–20, 1993.

Deloach, L. D., Payne, S. A., Krupke, W. F., Kway, W. L., and Smith, L. K., *Laser and Spectroscopic Properties of $Sr_5(PO_4)_3F:Yb$*, Lawrence Livermore National Laboratory, Livermore, CA, UCRL-JC-112130 (1992). Submitted to *Journal of the Optical Society of America B*.

Deloach, L. D., Payne, S. A., Kway, W. L., Smith, L. K., Krupke, W. F., and Tassano, J. B., *Physics of Yb Doped Laser Crystals with the Apatite Structure*, Lawrence Livermore National Laboratory, Livermore, CA, UCRL-JC-111852 ABS & SUM (1992). Prepared for the Advanced Solid State Lasers 8th Topical Meeting, New Orleans, LA, February 1–3, 1993.

Deloach, L. D., Payne, S. A., Morris, R., Krupke, W. F., and Smith, L. K., *Properties of the CaF2Cal Laser Crystal*, Lawrence Livermore National Laboratory, Livermore, CA, UCRL-ME-110040 (1992). Prepared for the Optical Society of America Annual Meeting and 8th Interdisciplinary Laser Science Conference, Albuquerque, NM, September 20–25, 1992.

Dendooven, P. G. and Cable, M. D., *Gamma Ray Diagnostics of the Alpha Shearing Down in ICF Targets*, Lawrence Livermore National Laboratory, Livermore, CA, UCRL-ME-111179 (1992). Prepared for the 34th Annual Meeting of the American Physical Society Division of Plasma Physics, Seattle, WA, November 16–20, 1992.

Ditmire, T. R. and Perry, M. D., *Multiterawatt Femtosecond Cr:LiSrAlF$_6$ Laser System*, Lawrence Livermore National Laboratory, Livermore, CA, UCRL-JC-112267 ABS & SUM (1992). Prepared for the Quantum Electronics and Laser Science Conference 1993, Baltimore, MD, May 2–7, 1993.

Dixit, S. N., Lawson, J. K., Nugent, K. A., Powell, H. T., and Manes, K. R., *Designing Continuous Contour Phase Plates for Beam Smoothing*, Lawrence Livermore National Laboratory, Livermore, CA, UCRL-JC-112270 ABS & SUM (1992). Prepared for Optical Design for Photonics, Palm Springs, CA March 22–April 2, 1993.

Dixit, S. N., *Numerical Modeling of the Suppression of Stimulated Brillouin Scattering Due to Finite Laser Bandwidth*, Lawrence Livermore National Laboratory, Livermore, CA, UCRL-JC-107973 REP (1992). Prepared for the Conference on Nonlinear Optics, Los Angeles, CA, January 19–24, 1992, paper 1626-31, pp. 254–265.

E

Eder, D. C., Scott, H. A., London, R. A., and Maxon, S., "Photon Trapping Models for X-Ray Lasers," *Appl. Opt.* **31** (24), 4962–4968 (20 August 1992).

Eder, D. C., *Optical Field Ionized Plasma X-Ray Laser Status*, Lawrence Livermore National Laboratory, Livermore, CA, UCRL-MI-110083 (1992). Prepared for the Optical Society of America Annual Meeting and 8th Interdisciplinary Laser Science Conference, Albuquerque, NM, September 20–25, 1992.

Eimerl, D., Milam, D., and Yu, J., *Large Bandwidth Frequency Converted Nd:Glass Laser at 527 nm with Av/v ~ 2%*, Lawrence Livermore National Laboratory, Livermore, CA, UCRL-JC-111297 (1992). Submitted to *Physical Review Letters*.

Eimerl, D., *Local Frequencies, the Phase Wind Up Problem, and the Twist Theorem*, Lawrence Livermore National Laboratory, Livermore, CA, UCRL-JC-110860 (1992). Submitted to *Journal of the Optical Society of America*.

Erlandson, A. C., Frank, D. N., McCracken, R. W., Jancaitis, K. S., Gonzales, A. A., Murray, J. R., Rotter, M. D., and Trenholme, J. B., *Performance and Design of Large Aperture Multisegment Nd:Glass Amplifiers*, Lawrence Livermore National Laboratory, Livermore, CA, UCRL-JC-112264 ABS & SUM (1992). Prepared for the Conference on Lasers and Electro-Optics 1993, Baltimore, MD, May 2–7, 1993.

Erlandson, A. C., *Gain Uniformity and Storage Efficiency of a Flashlamp-Pumped Nd:Glass Multisegment Amplifier*, Lawrence Livermore National Laboratory, Livermore, CA, UCRL-ME-112362 (1992). Prepared for the Advance Program, International Conference on Lasers '92, Houston, TX, December 7–10, 1992.

F

Forrest, J. A., Brooks R., J., Schou J., Stenum B., Hunt J. T., Sorensen H., Gartler P., Magnotta, F., and Mapoles, E. R., *Continuum Emission from Irradiated Solid Deuterium*, Lawrence Livermore National Laboratory, Livermore, CA, UCRL-JC-110969 (1992). Submitted to *Physical Review B*.

Friedman, A., Grote, D. P., and Haber, I., *Update on Three Dimensional Particle Simulation of Heavy Ion Fusion Beams*, Lawrence Livermore National Laboratory, Livermore, CA, UCRL-ME-111189 (1992). Prepared for the 34th Annual Meeting of the American Physical Society Division of Plasma Physics, Seattle, WA, November 16–20, 1992.

Friedman, A., Grote, D. P., Langdon, A. B., Haber, I., and Callahan, D. A., *Overview of WARP, a Particle Code for Heavy Ion Fusion*, Lawrence Livermore National Laboratory, Livermore, CA, UCRL-JC-112246 ABS (1992). Prepared for the Computational Accelerator Physics Conference 1993, Pleasanton, CA, February 22–26, 1993.

Friedman, A., *Introduction Second Meeting of FEAC Panel 7 Inertial Fusion Energy*, Lawrence Livermore National Laboratory, Livermore, CA, UCRL-ME-112373 (1992). Prepared for the FEAC Panel 7 Meeting, Berkeley, CA, December 7–8, 1992.

G

Glendinning, S. G., Remington, B. A., Weber, S. V., Munro, D. H., and Haan, S. W., *Analysis Techniques for Directly and Indirectly Driven Hydrodynamic Experiments on Nova*, Lawrence Livermore National Laboratory, Livermore, CA, UCRL-JC-109369 (1992). Prepared for the 9th Topical Conference on High Temperature Plasma Diagnostics, Santa Fe, NM, March 15–19, 1992.

Glendinning, S. G., Remington, B. A., Weber, S. V., Munro, D. H., and Haan, S. W., "Analysis Techniques for Directly and Indirectly Driven Hydrodynamic Experiments on Nova," *Rev. Sci. Instrum.* **63** (10), 5108–5110 (October 1992).

Glendinning, S. G., Weber, S. V.,Wallace, R. J., Kilkenny, J. D. Dixit, S. N., Knauer, J. P., and Verdon, C. P., *Laser Seeded Modulation Experiments on Nova*, Lawrence Livermore National Laboratory, Livermore, CA, UCRL-MI-112137 (1992). Prepared for the 34th Annual Meeting of the American Physical Society Division of Plasma Physics, Seattle, WA, November 16–20, 1992.

Glendinning, S. G., Weber, S. V., Dixit, S. N., Da Silva, L. B., Bell, P., Henesian, M. A., Kania, D. R., Kilkenny, J. D., and Powell, H. T., *Laser-Driven Planar Rayleigh-Taylor Instability Experiments*, Lawrence Livermore National Laboratory, Livermore, CA, UCRL-JC-109991 (1992). Submitted to *Physical Review Letters*.

Glendinning, S. G., Weber, S. V., Dixit, S. N., Da Silva, L. B., Bell, P., Henesian, M. A., Kania, D. R., Kilkenny, J. D., and Powell, H. T., "Laser-Driven Planar Rayleigh-Taylor Instability Experiments," *Phys. Rev. Lett.* **69** (8), 1202–1204 (24 August 1992).

Glinsky, M. E. and Kruer, W. L., *Simple Model of Suprathermal Electron Transport*, Lawrence Livermore National Laboratory, Livermore, CA, UCRL-JC-111436 SUM (1992). Prepared for Short Wavelength V: Physics with Intense Laser Pulses, Second Topical Meeting, San Diego, CA, March 29–31, 1993.

Greiner, G. J., Trent, M. G., Bernat, T. P., and Di Grazia, H. X., *Facility Safety Procedure Building 298 Complex*, Lawrence Livermore National Laboratory, Livermore, CA, FSP-298 (1992).

Grote, D. P., Friedman, A. and Yu, S. S., *3-D Simulations of An Electrostatic Quadrupole Injector*, Lawrence Livermore National Laboratory, Livermore, CA, UCRL-MI-111188 (1992). Prepared for the 34th Annual Meeting of the American Physical Society Division of Plasma Physics, Seattle, WA, November 16–20, 1992.

Grote, D. P., Friedman, A. and Yu, S. S., *3-D Simulations of an Electrostatic Quadrupole Injector*, Lawrence Livermore National Laboratory, Livermore, CA, UCRL-JC-111188 ABS Rev 1 (1992). Prepared for the Computational Accelerator Physics Conference 1993, Pleasanton, CA, February 22–26, 1993.

Grote, D. P., Friedman, A., and Haber, I., *Three Dimensional PIC Simulation of Heavy Ion Fusion Beams: Recent Improvements to and Applications of WARP*, Lawrence Livermore National Laboratory, Livermore, CA, UCRL-JC-112508 ABS (1992). Prepared for the 1993 Particle Accelerator Conference, Washington, DC, May 17–20, 1993.

H

Haan, S. W., *Modeling Hydrodynamic Instabilities for ICF*, Lawrence Livermore National Laboratory, Livermore, CA, UCRL-JC-112167 ABS (1992). Prepared for the 4th International Workshop on the Physics of Compressible Turbulent Mixing, Cambridge, England, March 29–April 1, 1993.

Hammel, B. A., Keane, C. J., Lee, R. W., Kilkenny, J. D. Kania, D. R., and Pasha, R. A., *X-Ray Spectroscopic Measurements of High Densities and Temperatures from Indirectly Driven ICF Capsules*, Lawrence Livermore National Laboratory, Livermore, CA, UCRL-JC-111184 (1992). Submitted to *Physical Review Letters*.

Hammel, B. A., Keane, C. J., Lee, R. W., Kilkenny, J. D. Kania, D. R., and Pasha, R. A., *K- and L-Shell X-Ray Spectroscopic Measurements of Ultrahigh Densities and High Temperatures in Indirectly Driven ICF Capsules*, Lawrence Livermore National Laboratory, Livermore, CA, UCRL-MI-111931 (1992). Prepared for the 5th International Workshop on the Radiative Properties of Hot Dense Matter, Santa Barbara, CA, November 2–6, 1992.

Hammel, B. A., Keane, C. J., Lee, R. W., Kilkenny, J. D. Kania, D. R., and Pasha, R. A., *K- and L-Shell X-Ray Spectroscopic Measurements of Ultrahigh Densities and High Temperatures in Indirectly Driven ICF Capsules*, Lawrence Livermore National Laboratory, Livermore, CA, UCRL-JC-111931 ABS (1992). Prepared for the 5th International Workshop on the Radiative Properties of Hot Dense Matter, Santa Barbara, CA, November 2–6, 1992.

Hammel, B. A., Landen, O. L., Pasha, R. A., and Remington, B. A., "High Energy X-Ray Imaging Diagnostic on Nova," *Rev. Sci. Instrum.* **63** (10) (October 1992).

Hammel, B. A., Remington, B. A., Oades, K., Goldsack, T. J., Kilkenny, J. D. and Thomas, B., *X-Ray Radiographic Measurements of Kelvin-Helmholtz Growth in X-Ray-Driven Solid-Density Materials*, Lawrence Livermore National Laboratory, Livermore, CA, UCRL-JC-112385 ABS (1992). Prepared for the 4th International Workshop on the Physics of Compressible Turbulent Mixing, Cambridge, England, March 29–April 1, 1993.

Hammel, B. A., Ress, D. B.,Kilkenny, J. D. Keane, C. J., Bradley, D. K., Landen, O. L., Bell, P., Pasha, R. A., and Wallace, R. J., *X-Ray Imaging and Spectroscopic Measurements of Implosions*, Lawrence Livermore National Laboratory, Livermore, CA, UCRL-MI-109892 (1992). Prepared for the 14th International Conference on Plasma Physics and Controlled Nuclear Fusion Research (IAEA), Wurzburg, Germany, September 30–October 7, 1992.

Hammel, B. A., *K- and L-Shell X-Ray Spectroscopy of Indirectly Driven Implosions*, Lawrence Livermore National Laboratory, Livermore, CA, UCRL-JC-109253 (1992). Prepared for the 9th Topical Conference on High Temperature Plasma Diagnostics, Santa Fe, NM, March 15–19, 1992.

Hammel, B. A., *K- and L-Shell X-Ray Spectroscopy of Indirectly Driven Implosions*, Lawrence Livermore National Laboratory, Livermore, CA, UCRL-JC-109253 REP (1992). Prepared for the 9th Topical Conference on High Temperature Plasma Diagnostics, Santa Fe, NM, March 15–19, 1992.

Hermes, G. L., Trent, M. G., Casamajor, A., and Burgin, C., *Facility Safety Procedure Building 391—Nova Laser Facility*, Lawrence Livermore National Laboratory, Livermore, CA, UCRL-FSP-391-92 (1992).

Hewett, D. W. and Chen, Y.-J., *Simulation Tests of a New Space Charge Emission Algorithm*, Lawrence Livermore National Laboratory, Livermore, CA, UCRL-JC-112245 ABS (1992). Prepared for the Computational Accelerator Physics Conference 1993, Pleasanton, CA, February 22–26, 1993.

Hewett, D. W., Kruer, W. L., and Bangerter, R. O., *Corona Physics of Heavy Ion Fusion Targets*, Lawrence Livermore National Laboratory, Livermore, CA, UCRL-MI-111708 (1992). Prepared for the European Research Conference on Nuclear Physics: Prospects for Heavy Ion Fusion, Crete, Greece, September 27–October 1, 1992.

Hewett, D. W. and Larson, D. J., *Best of Gymnos: A User's Guide*, Lawrence Livermore National Laboratory, Livermore, CA, UCRL-UR-110499 (1992).

Hjorth, P. G. and Glinsky, M. E., *Helicity in Hamiltonian Dynamical Systems*, Lawrence Livermore National Laboratory, Livermore, CA, UCRL-JC-112520 ABS (1992). Prepared for the SIAM Conference on Applications of Dynamical Systems, Snowbird, UT, October, 1992.

Ho D. D.-M. and Crandall, K., *Sextupole Correction of Second-Order Chromatic Aberrations for High-Current Heavy-Ion Beams*, Lawrence Livermore National Laboratory, Livermore, CA, UCRL-JC-110212 ABS Rev 1 (1992). Prepared for the 1993 Particle Accelerator Conference, Washington, DC, May 17–20, 1993.

Ho, D. D.-M., Crandall, K. R., and Haber, I., *Focusing Beams with Widely Varying Current Using Fixed Strength Quadrupoles for Heavy-Ion Inertial Fusion*, Lawrence Livermore National Laboratory, Livermore, CA, UCRL-JC-112144 (1992). Submitted to *Particle Accelerators*.

Hogan, W. J., Bangerter R. O., and Kulcinski G. L., *Energy from Inertial Fusion*, Lawrence Livermore National Laboratory, Livermore, CA, UCRL-JC-111596 (1992). Submitted to *Physics Today*.

Hogan, W. J., *Remarks of William Hogan*, Lawrence Livermore National Laboratory, Livermore, CA, UCRL-JC-111949 (1992). Submitted to *Journal of Fusion Energy*.

J

Jalinaud, T., Labaune, C., Estabrook, K. G., and Baldis, H. J., *Effect of Spatial Beam Smoothing on Stimulated Brillouin Scattering and Stimulated Raman Scattering*, Lawrence Livermore National Laboratory, Livermore, CA, UCRL-MI-111902 (1992). Prepared for the Societé Française de Physique à Nancy Conference, Nancy, France, October, 1992.

K

Kauffman R. L., Phillion D. W., and Spitzer, R., *X-Ray Production—130 Angstrom from Laser-Produced Plasmas for Projection X-Ray Lithography Applications*, Lawrence Livermore National Laboratory, Livermore, CA, UCRL-JC-110217 (1992). Prepared for the Soft X-Ray Lithography Projection Meeting, Monterey, CA, April, 1992.

Keane, C. J., Hammel, B. A., Kania, D. R., and Osterheld, A. L., *Diagnostics of Electron Temperature and Density in High Density Plasmas Using L-Shell Xenon Emission Spectroscopy*, Lawrence Livermore National Laboratory, Livermore, CA, UCRL-MI-111697 (1992). Prepared for the 4th International Colloquium on Atomic Spectra, Gaithersburg, MD, September 14–17, 1992.

Keane, C. J., Hammel, B. A., Kania, D. R., and Osterheld, A. L., *Diagnostics of Electron Temperature and Density in High Density Plasmas Using L-Shell Xenon Emission Spectroscopy*, Lawrence Livermore National Laboratory, Livermore, CA, UCRL-JC-112496 ABS (1992). Prepared for the 4th International Colloquium on Atomic Spectra, Gaithersburg, MD, September 14–17, 1992.

Keane, C. J., Hammel, B. A., Lee, R. W., Kania, D. R., Osterheld, A. L., Suter, L. J., Mancini, R. C., Hooper, C. F., and Delamater, N. D., *Diagnosis of Fuel Plasma Conditions in ICF Targets Using K- and L-Shell Emission Spectroscopy*, Lawrence Livermore National Laboratory, Livermore, CA, UCRL-JC-111724 ABS (1992). Prepared for the 5th International Workshop on the Radiative Properties of Hot Dense Matter, Santa Barbara, CA, November 2–6, 1992.

Keane, C. J., *X-Ray Spectroscopy of High Energy Density Plasmas*, Lawrence Livermore National Laboratory, Livermore, CA, UCRL-MI-111168 (1992). Prepared for the 34th Annual Meeting of the American Physical Society Division of Plasma Physics, Seattle, WA, November 16–20, 1992.

Keane, C. J., *Diagnosis of Fuel Plasma Conditions in ICF Targets Using K- and L-Shell Emission Spectroscopy*, Lawrence Livermore National Laboratory, Livermore, CA, UCRL-MI-111724 (1992). Prepared for the 5th International Workshop on the Radiative Properties of Hot Dense Matter, Santa Barbara, CA, November 2–6, 1992.

Kershaw, D. S., *LASNEX on Unix Workstations*, Lawrence Livermore National Laboratory, Livermore, CA, UCRL-JC-111693 ABS (1992). Prepared for the Nuclear Explosive Code Developers Conference, Sunnyvale, CA, November 2–6, 1992.

Kilkenny, J. D., Glendinning S. G., Verdon, C. P., Knauer, J. P., and Weber, S. V., *Evaluation of Hydrodynamic Instabilities Induced by Direct Drive Laser Irradiation of Planar Foils*, Lawrence Livermore National Laboratory, Livermore, CA, UCRL-JC-112500 ABS (1992). Prepared for the 4th International Workshop on the Physics of Compressible Turbulent Mixing, Cambridge, England, March 29–April 1, 1993.

Kilkenny, J. D., Munro, D. H., Remington, B. A., Glendinning S. G., Haan, S. W., Weber, S. V., Wallace, R. J., Powell, H. T., and Dixit, S. N., *Experimental Determination of the Hydrodynamic Instability Growth Rates in Indirect and Direct Drive ICF*, Lawrence Livermore National Laboratory, Livermore, CA, UCRL-MI-110277 (1992). Prepared for the 14th International Conference on Plasma Physics and Controlled Nuclear Fusion Research (IAEA), Wurzburg, Germany, September 30–October 7, 1992.

Kilkenny, J. D. Munro, D. H., Remington, B. A., Glendinning S. G., Haan, S. W., Weber, S. V., Wallace, R. J., Powell, H. T., and Dixit, S. N., *Experimental Determination of the Hydrodynamic Instability Growth Rates in Indirect and Direct Drive ICF*, Lawrence Livermore National Laboratory, Livermore, CA, UCRL-JC-110277 (1992). Prepared for the 14th International Conference on Plasma Physics and Controlled Nuclear Fusion Research (IAEA), Wurzburg, Germany, September 30–October 7, 1992.

Kilkenny, J. D., *Recent Diagnostic Developments at Nova*, Lawrence Livermore National Laboratory, Livermore, CA, UCRL-JC-110312 (1992). Submitted to *Review of Scientific Instruments*.

Kilkenny, J. D., *Gating of X-Ray Images in the 30–40 ps Region for Laser Plasma Experiments*, Lawrence Livermore National Laboratory, Livermore, CA, UCRL-MI-109277 (1992). Prepared for the Optical Society of America Annual Meeting and 8th Interdisciplinary Laser Science Conference, Albuquerque, NM, September 20–25, 1992.

Kirbie, H. C., Cravey, W. R., Hawkins, S. A., Newton, M. A., and Ollis, C. W., *FET-Switched Induction Accelerator Cell*, Lawrence Livermore National Laboratory, Livermore, CA, UCRL-JC-112510 ABS (1992). Prepared for the 9th IEEE International Pulsed Power Conference, Albuquerque, NM, June 21–23 1993.

Klem, D. E., Lane, D. S., and Perry, M. D., *Absorption and X-Ray Production by Intense Subpicosecond 1.06-μm Laser Light Striking Solid Targets*, Lawrence Livermore National Laboratory, Livermore, CA, UCRL-MI-112176 (1992). Prepared for the 34th Annual Meeting of the American Physical Society Division of Plasma Physics, Seattle, WA, November 16–20, 1992.

Kobayashi, A., *Integration of IDL Programs into a Large Control System*, Lawrence Livermore National Laboratory, Livermore, CA, UCRL-MI-110473 (1992). Prepared for the CUBE Symposium, Pleasanton, CA, October 27–30, 1992.

Koch, J. A., Barbee, T. W., Da Silva, L. B., Carter, M., Batson, P., MacGowan, B. J., Matthews, D. L., Mrowka, S., and Shimkaveg, G., *Coherence Properties and Multipass Development of X-Ray Laser Sources at LLNL*, Lawrence Livermore National Laboratory, Livermore, CA, UCRL-JC-112116 ABS (1992). Prepared for the 5th International Workshop on the Radiative Properties of Hot Dense Matter, Santa Barbara, CA, November 2–6, 1992.

Koch, J. A., MacGowan, B. J., Underwood. J., Matthews, D. L., Da Silva, L. B., Batson, P., and Mrowka, S., "Observation of Gain-Narrowing and Saturation Behavior in Se X-Ray Laser Line Profiles," *Phys. Rev. Lett.* **68** (22), 3291–3294 (1992).

Kozlowski, M. R., Thomas, I. M., Rainer, F., and Campbell, J. H., *High-Power Optical Coatings for a Megajoule-Class ICF Laser*, Lawrence Livermore National Laboratory, Livermore, CA, UCRL-JC-109735 (1992). Prepared for the International Symposium on Optical Systems Design, Berlin, Germany, September 14–18, 1992.

Kozlowski, M. R., *High-Damage-Threshold Optical Coatings for a Megajoule-Class ICF Laser*, Lawrence Livermore National Laboratory, Livermore, CA, UCRL-MI-111694 (1992). Prepared for the International Symposium on Optical Systems Design, Berlin, Germany, September 14–18, 1992.

Kruer, W. L., Wilks, S. C., and Langdon, A. B., *Laser Plasmas II: Intense Lasers and X Rays*, Lawrence Livermore National Laboratory, Livermore, CA, UCRL-MI-112252 (1992). Prepared for the 34th Annual Meeting of the American Physical Society Division of Plasma Physics, Seattle, WA, November 16–20, 1992.

Kruer, W. L., *Interaction Physics for Laser Fusion*, Lawrence Livermore National Laboratory, Livermore, CA, UCRL-JC-108660 (1992).

Kruer, W. L. and Wilks, S. C., *Introduction to Ultra-Intense Laser-Plasma Interactions*, Lawrence Livermore National Laboratory, Livermore, CA, UCRL-JC-111519 ABS (1992). (Abstract for chapter in a book, *Advances in Plasma Physics*.)

L

Landen, O. L., and Alley, W. E., "Dynamics of Picosecond Laser Plasmas Determined from the Spectral Shifts of Reflected Probe Pulses," *Phys. Rev. A* **46** (8), 5089–5100 (October 15, 1992).

Landen, O. L., and Bell, P. M., *Studies of Gain Uniformity, Linearity, Saturation, and Depletion in Gated Microchannel-Plate X-Ray Framing Cameras*, Lawrence Livermore National Laboratory, Livermore, CA, UCRL-MI-111183 (1992). Prepared for the 34th Annual Meeting of the American Physical Society Division of Plasma Physics, Seattle, WA, November 16–20, 1992.

Landen, O. L., Bell, P., M Bradley, D. K., Satariano, J. J., and Oertel, J., *Gain Uniformity, Linearity, Saturation, and Depletion in Gated Microchannel-Plate X-Ray Framing Cameras*, Lawrence Livermore National Laboratory, Livermore, CA, UCRL-JC-112384 ABS (1992). Prepared for the SPIE 1993 International Symposium on Optical Instrumentation and Applied Science, San Diego, CA, July 11–16, 1993.

Landen, O. L., Hatchett, S. P., Hammel, B. A., Munro, D. H., Glendinning S. G., Nash, J., and Kania, D. R., *Time-Resolved Studies of Indirectly Driven Low-Z Foils*, Lawrence Livermore National Laboratory, Livermore, CA, UCRL-MI-111182 (1992). Prepared for the 34th Annual Meeting of the American Physical Society Division of Plasma Physics, Seattle, WA, November 16–20, 1992.

Landen, O. L., *High-Resolution 2-Dimensional Space- and Time-Resolved X-Ray Imaging of Plasmas at Nova*, Lawrence Livermore National Laboratory, Livermore, CA, UCRL-JC-109094 REP (1992). Prepared for the 9th Topical Conference on High Temperature Plasma Diagnostics, Santa Fe, NM, March 15–19, 1992.

Landen, O. L., *High Resolution Time- and Two-Dimensional Space-Resolved X-Ray Imaging of Plasmas at Nova*, Lawrence Livermore National Laboratory, Livermore, CA, UCRL-MI-109094 Rev. 1 (1992). Prepared for the 34th Annual Meeting of the American Physical Society Division of Plasma Physics, Seattle, WA, November 16–20, 1992.

Lander, S. H. and Keane, C. J., *Modeling Line Ratios for use as Temperature and Density Diagnostics in ICF Targets*, Lawrence Livermore National Laboratory, Livermore, CA, UCRL-MI-111167 (1992). Prepared for the 34th Annual Meeting of the American Physical Society Division of Plasma Physics, Seattle, WA, November 16–20, 1992.

Lane, S. M., Cauble, R., Glendinning S. G., and Da Silva, L. B., *Shock-Wave Transit Time Measurements in Aluminum on the Nova Laser*, Lawrence Livermore National Laboratory, Livermore, CA, UCRL-MI-111191 (1992). Prepared for the 34th Annual Meeting of the American Physical Society Division of Plasma Physics, Seattle, WA, November 16–20, 1992.

Langdon, A. B., *On Enforcing Gauss' Law in Electromagnetic Particle-in-Cell Codes*, Lawrence Livermore National Laboratory, Livermore, CA, UCRL-JC-105059 REP (1991). Submitted to *Computational Physics Communications*.

Lasinski, B. F., Berger, R. L., Kruer, W. L., Williams, E. A., Langdon, A. B., Kaiser, T. B., and Cohen, B. I., *Effect of Beam Smoothing on Filamentation*, Lawrence Livermore National Laboratory, Livermore, CA, UCRL-MI-110759 Rev. 1 (1992). Prepared for the 34th Annual Meeting of the American Physical Society Division of Plasma Physics, Seattle, WA, November 16–20, 1992.

Lawson, J. K., Dixit, S. N., Woods, B. W., Thomas, I. M., Morgan, A. J., Manes, K. R., Powell, H. T., and Nugent, K. A., *Design and Fabrication of Continuous Contour Phase Plates for Beam Smoothing*, Lawrence Livermore National Laboratory, Livermore, CA, UCRL-JC-112268 ABS & SUM (1992). Prepared for the Conference on Lasers and Electro-Optics 1993, Baltimore, MD, May 2–7, 1993.

Lawson, J. K., Dixit, S. N., Woods, B. W., Thomas, I. M., Morgan, A. J., and Powell, H. T., *Production of High Damage Threshold Diffractive Optics for Beam Smoothing*, Lawrence Livermore National Laboratory, Livermore, CA, UCRL-JC-112271 ABS & SUM (1992). Prepared for Optical Design for Photonics, Palm Springs, CA, March 22–24, 1993.

Lawson, J. K. and Payne, S. A., *Excited-State Absorption of Eu^{2+}-Doped Materials*, Lawrence Livermore National Laboratory, Livermore, CA, UCRL-JC-111720 (1992). Submitted to *Physical Review B*.

Lawson, J. K., Speck, D. R., Henesian, M. A., Burkhart, S. C., Bibeau, C., Laumann, C. W., Weiland, T. L., and Wilcox, R. B., "Temporal Shaping of Third-Harmonic Pulses on the Nova Laser System," *Appl. Opt.* **31** (24), 5061–5068 (August, 1992).

Lerche, R. A., Hatchett, S. P., Murphy, T. J., Nelson, M. B., and Cable, M. D., *Plasma Temperatures from First-Hit Neutron Time-of-Flight Spectra*, Lawrence Livermore National Laboratory, Livermore, CA, UCRL-JC-109357 REP (1992). Prepared for the 9th Topical Conference on High Temperature Plasma Diagnostics, Santa Fe, NM, March 15–19, 1992.

Lerche, R. A., Hatchett, S. P., Murphy, T. J., Nelson, M. B., and Cable, M. D., *Plasma Temperatures from LaNSA First-Hit Neutron Time-of-Flight Spectra*, Lawrence Livermore National Laboratory, Livermore, CA, UCRL-MI-111181 (1992). Prepared for the 34th Annual Meeting of the American Physical Society Division of Plasma Physics, Seattle, WA, November 16–20, 1992.

Lerche, R. A. and Murphy, T. J., *Geometry Compensation for Improving Speed and Efficiency of Scintillator-Based Neutron Time-of-Flight Detectors*, Lawrence Livermore National Laboratory, Livermore, CA, UCRL-JC-109285 REP (1992). Prepared for the 9th Topical Conference on High Temperature Plasma Diagnostics, Santa Fe, NM, March 15–19, 1992.

Lerche, R. A. and Phillion, D. W., *Fast (30-ps) Neutron Detector for Fusion Reaction-Rate Measurements of ICF Capsules*, Lawrence Livermore National Laboratory, Livermore, CA, UCRL-MI-111178 (1992). Prepared for the 34th Annual Meeting of the American Physical Society Division of Plasma Physics, Seattle, WA, November 16–20, 1992.

Letts, S. A., Buckley, S. R., Fearon, E. M., Saculla, M. D., Lindsey, E. F., and Moore, C. E., *Preparation of Hollow Shells Using a Depolymerizing Mandrel—Feasibility*, Lawrence Livermore National Laboratory, Livermore, CA, UCRL-MI-110454 (1992). Prepared for the 39th American Vacuum Society National Symposium and Topical Conference, Chicago, IL, November 9–13, 1992.

Liberman, D. A. and Albritton, J. W., *Dense Plasma Equation of State Model*, Lawrence Livermore National Laboratory, Livermore, CA, UCRL-JC-111723 ABS (1992). Prepared for the 5th International Workshop on the Radiative Properties of Hot Dense Matter, Santa Barbara, CA, November 2–6, 1992.

London, R. A., Matthews, D. L., and Suckewer, S., *Applications of X-Ray Lasers*, Lawrence Livermore National Laboratory, Livermore, CA, UCRL-CONF-9206170. Prepared for the Applications of X-Ray Lasers Workshop, San Francisco, CA, January 12–14, 1992.

M

MacGowan, B. J., Barbee, T. W., Matthews, D. L., Koch, J. A., Da Silva, L. B., Mrowka, S., and Trebes, J. E., *Saturated Laboratory X-Ray Lasers*, Lawrence Livermore National Laboratory, Livermore, CA, UCRL-MI-111144 (1992). Prepared for the 34th Annual Meeting of the American Physical Society Division of Plasma Physics, Seattle, WA, November 16–20, 1992.

MacGowan, B. J., Mrowka, S., Eder, D. C., Da Silva, L. B., Barbee, T. W., Koch, J. A., and Underwood, J. H., *Problems in the Implementation of X-Ray Optics with X-Ray Lasers*, Lawrence Livermore National Laboratory, Livermore, CA, UCRL-JC-111376 (1992). Prepared for the Third International Colloquium on X-Ray Lasers, Schliersee, Germany, May 18–22, 1992.

Marcy, H. O., *Second Harmonic Generation in Zinc Tris (Thiourea) Sulfate*, Lawrence Livermore National Laboratory, Livermore, CA, UCRL-JC-105486 REP Cand I (1991). Submitted to *Applied Optics*.

Marshall, C. D., Payne, S. A., Powell, H. T., and Speth, A., *Broad-Band Transient Absorption in KDP Induced by Two-Photon Excitation at 266 nm*, Lawrence Livermore National Laboratory, Livermore, CA, UCRL-JC-112269 ABS & SUM (1992). Prepared for the Quantum Electronics and Laser Science Conference 1993, Baltimore, MD, May 2–7, 1993.

Moir, R. W., Adamson, M., Condit, R. H., Bieri, R. L., Bangerter, R. O., Hartman C. W., House, P. A., Langdon, A. B., and Logan, B. G., *HYLIFE-II Progress Report*, Lawrence Livermore National Laboratory, Livermore, CA, UCRL-ID-21816.

Moir, R. W., Chen, X., Colella, P., Peterson, P., and Schrock, V., *Gas Dynamics in the Central Cavity of HYLIFE-II Reactor*, Lawrence Livermore National Laboratory, Livermore, CA, UCRL-CR-109549 (1992). Prepared for the 10th Topical Meeting on the Technology of Fusion Energy, Boston, MA, June 7–12, 1992 and for submission to *Fusion Technology*.

Moir, R. W., Chen, X., Peterson, P., and Schrock, V., *Hydraulic Analysis of Cylindrical Flibe Jets in a HYLIFE-II ICF Reactor*, Lawrence Livermore National Laboratory, Livermore, CA, UCRL-CR-109547 (1992). Prepared for the 10th Topical Meeting on the Technology of Fusion Energy, Boston, MA, June 7–12, 1992, and for submission to *Fusion Technology*.

Moir, R. W., Chen, X., Peterson, P., and Schrock, V., *Soft-Sphere Equation of State of Liquid Flibe*, Lawrence Livermore National Laboratory, Livermore, CA, UCRL-CR-109690 (1992). Prepared for the 10th Topical Meeting on the Technology of Fusion Energy, Boston, MA, June 7–12, 1992.

Moir, R. W., Chen, X., Schrock, V., and Peterson, P., *Calculation of the Kinetic Rate Constants for LiF and BeF*$_2$, Lawrence Livermore National Laboratory, Livermore, CA, UCRL-CR-109548 (1992). Prepared for the 10th Topical Meeting on the Technology of Fusion Energy, Boston, MA, June 7–12, 1992, and for submission to *Fusion Technology*.

Montgomery, D. S., Baldis, H. J., Estabrook, K. G., Berger, R. L., Moody, H., Lasinski, B. F., Williams, E. A., and Labaune, C., *Effects of Laser Temporal Smoothing on SRS in Exploding-Foil Plasmas*, Lawrence Livermore National Laboratory, Livermore, CA, UCRL-MI-112255 (1992). Prepared for the 34th Annual Meeting of the American Physical Society Division of Plasma Physics, Seattle, WA, November 16–20, 1992.

Montgomery, D. S., Landen, O. L., Baldis, H. J., Estabrook, K. G., Drake, R. P., Batha, S. H., Bradley, K. S., and Procassini, R. J., *Measurements of Radial Heat Wave Propagation in Laser-Produced Exploding-Foil Plasmas*, Lawrence Livermore National Laboratory, Livermore, CA, UCRL-JC-111514 (1992). Submitted to *Physical Review Letters*.

Moody, J. D. Baldis, H. J., Berger, R. L., Labaune, C., Montgomery, D. S., Dixit, S. N., Estabrook, K. G., Kruer, W. L., and Williams, E. A., *Experimental Investigations of Beam Smoothing Effects on Laser-Plasma Instabilities*, Lawrence Livermore National Laboratory, Livermore, CA, UCRL-MI-111148 (1992). Prepared for the 34th Annual Meeting of the American Physical Society Division of Plasma Physics, Seattle, WA, November 16–20, 1992.

Morales, R., Remington, B. A., Hensley, G., and Schwinn, T., *Laboratory Facility for Characterizing the Wölter X-Ray Optics used at Nova*, Lawrence Livermore National Laboratory, Livermore, CA, UCRL-MI-111169 (1992). Prepared for the 34th Annual Meeting of the American Physical Society Division of Plasma Physics, Seattle, WA, November 16–20, 1992.

Murphy, T. J. and Lerche, R. A., *Use of a Geometry-Compensated Neutron Time-of-Flight Detector with Approximately 200-ps Time Response for ICT Applications*, Lawrence Livermore National Laboratory, Livermore, CA, UCRL-MI-111177 (1992). Prepared for the 34th Annual Meeting of the American Physical Society Division of Plasma Physics, Seattle, WA, November 16–20, 1992.

Murray, J. R., Campbell, J. H., and Frank, D. N., *Beamlet Project: Technology Demonstration for a National Inertial Confinement Fusion Ignition Facility*, Lawrence Livermore National Laboratory, Livermore, CA, UCRL-JC-112282 ABS & SUM (1992). Prepared for the Conference on Lasers and Electro-Optics 1993, Baltimore, MD, May 2–7, 1993.

Murray, J. R., *Applications of High-Power Lasers*, Lawrence Livermore National Laboratory, Livermore, CA, UCRL-MI-111928 (1992). Prepared for the IEEE 1992 Nuclear Science Symposium, Orlando, FL, October 25–31, 1992.

N

Nelson, M. B., Cable, M. D., Mant, G., and Bennett, C. K., *LaNSA: A Large Neutron Scintillator Array for Neutron Spectroscopy at Nova*, Lawrence Livermore National Laboratory, Livermore, CA, UCRL-JC-103286 REP (1992). Prepared for the 9th Topical Conference on High Temperature Plasma Diagnostics, Santa Fe, NM, March 15–19, 1992.

Newton, M. A., Cravey, W. R., Ollis, C. W., Kirbie, H. C., and Hawkins, S. A., *Development of FET-Switched Induction Accelerator Cells for Heavy-Ion Recirculators*, Lawrence Livermore National Laboratory, Livermore, CA, UCRL-JC-112375 ABS (1992). Prepared for the 1993 Particle Accelerator Conference, Washington, DC, May 17–20, 1993.

O

Ollis, C. W., Cravey, W. R., Hawkins, S. A., Kirbie, H. C., and Newton, M. A., *SPICE Modeling of a Switched Induction Accelerator Cell*, Lawrence Livermore National Laboratory, Livermore, CA, UCRL-JC-112511 ABS (1992). Prepared for the 9th IEEE International Pulsed Power Conference, Albuquerque, NM, June 21–23, 1993.

Overturf, G. E., Buckley, S. R., and Cook, R. C., *Synthesis and Characterization of Iodinated Polystyrene*, Lawrence Livermore National Laboratory, Livermore, CA, UCRL-ID-107950.

P

Paisner, J. A., *Beamlet Update*, Lawrence Livermore National Laboratory, Livermore, CA, UCRL-MI-111927 (1992).

Payne, A. N., *System Modeling for the Longitudinal Beam Dynamics Control Problem in Heavy Ion Induction Accelerators*, Lawrence Livermore National Laboratory, Livermore, CA, UCRL-JC-112378 ABS (1992). Prepared for the 1993 Particle Accelerator Conference, Washington, DC, May 17–20, 1993.

Payne, A. N., *Modeling Magnetically Switched Pulse Modulators*, Lawrence Livermore National Laboratory, Livermore, CA, UCRL-JC-112509 ABS (1992). Prepared for the 9th IEEE International Pulsed Power Conference, Albuquerque, NM, June 21–23, 1993.

Payne, S. A., Chase, L. L., Krupke, W. F., Kway, W. L., and Smith, L. K., "Infrared Cross Section Measurements for Crystals Doped with Er^{3+}, Tm^{3+}, and Ho^{3+}," *IEEE J. Quantum Electron.* **28** (11), 2619–2630 (November 1992).

Payne, S. A., Krupke, W. F., Tassano, J. B., Smith, L. K., Deloach, L. D., and Kway, W. L., *Optical and Physical Properties of the $LiSrAlF_6$:Cr Laser Crystal*, Lawrence Livermore National Laboratory, Livermore, CA, UCRL-JC-111851 ABS (1992). Prepared for the 8th Topical Meeting on Advanced Solid State Lasers, New Orleans, LA, February 1–3, 1993.

Pennington, D. M. and Harris, C. B., *Dynamics of Photothermal Surface Expansion Using Laser Induced Holographic Gratings*, Lawrence Livermore National Laboratory, Livermore, CA, UCRL-JC-109976 (1992). Submitted to *IEEE Journal of Quantum Electronics*.

Pennington, D. M. and Harris, C. B., "Dynamics of Photothermal Surface Expansion Using Laser-Induced Holographic Gratings," *IEEE J. Quantum Electron.* **28** (10), 2523–2534 (October 1992).

Pennington, D. M., Henesian, M. A., Weiland, T. L., Thompson, C. E., and Powell, H. T., *Bandwidth Effects on Third-Harmonic Frequency Conversion and Beam Smoothing on the Nova Laser*, Lawrence Livermore National Laboratory, Livermore, CA, UCRL-JC-112265 ABS & SUM (1992). Prepared for the Quantum Electronics and Laser Science Conference 1993, Baltimore, MD, May 2–7, 1993.

Pierce, E. L., Overturf, G. E., Moore, C. E., Lindsey, E. F., Hamlow, D. L., Olsen, M., Chen, V., and Hsieh, E. J., *Characteristics of Some Polymer Films by Rf Sputtering and Co-Sputtering with a Metal*, Lawrence Livermore National Laboratory, Livermore, CA, UCRL-JC-110296 EXT ABS (1992). Prepared for the 39th American Vacuum Society National Symposium and Topical Conference, Chicago, IL, November 9–13, 1992.

Powell, H. T., *Recent Improvements to the Nova Laser*, Lawrence Livermore National Laboratory, Livermore, CA, UCRL-JC-111709 ABS (1992). Prepared for the 1992 International Conference on Lasers and Optoelectronics, Beijing, China, October 16–18, 1992.

Powell, H. T., *Recent Improvements to the Nova Laser*, Lawrence Livermore National Laboratory, Livermore, CA, UCRL-MI-111709 (1992). Prepared for the 1992 International Conference on Lasers and Optoelectronics, Beijing, China, October 16–18, 1992.

Powell, H. T., *Beam Smoothing Development for Nova*, Lawrence Livermore National Laboratory, Livermore, CA, UCRL-MI-111918 (1992). Prepared for the Institute of Laser Engineering, Osaka, Japan, October 26, 1992.

Powell, H. T., *Laser Development for the Precision Nova Project*, Lawrence Livermore National Laboratory, Livermore, CA, UCRL-MI-111919 (1992). Prepared for NLHPLP, Shanghai, China, October 22, 1992.

Powers, L. V., *Analysis of Nova Capsule Symmetry Experiments*, Lawrence Livermore National Laboratory, Livermore, CA, UCRL-MI-111166 (1992). Prepared for the 34th Annual Meeting of the American Physical Society Division of Plasma Physics, Seattle, WA, November 16–20, 1992.

Procassini, R. J. and Cohen, B. I., *Comparison of Particle-in-Cell and Fokker-Planck Methods as Applied to the Modeling of Auxiliary-Heated Mirror Plasmas*, Lawrence Livermore National Laboratory, Livermore, CA, UCRL-JC-110791 (1992). Submitted to *Journal of Computational Physics*.

Procassini, R. J. and Cohen, B. I., "Comparison of Particle-in-Cell and Fokker-Planck Methods as Applied to the Modeling of Auxiliary-Heated Mirror Plasmas," *J. Comput. Phys.* **102** (1), 39–48 (1992).

Procassini, R. J. and Knoll, D. A., *Kinetically Motivated Boundary Conditions for Fluid Models of Scrape-off Layer Transport*, Lawrence Livermore National Laboratory, Livermore, CA, UCRL-JC-110317 (1992). Submitted to *Journal of Nuclear Materials*.

Procassini, R. J. and Knoll, D. A., *Development of an Advanced Kinetic Model of Scrape-off Layer Transport*, Lawrence Livermore National Laboratory, Livermore, CA, UCRL-MI-112506 (1992). Prepared for the 34th Annual Meeting of the American Physical Society Division of Plasma Physics, Seattle, WA, November 16–20, 1992.

Procassini, R. J. and Rambo, R. W., *Kinetic and Hydrodynamic Simulations of Interpenetrating Laser-Produced Plasmas*, Lawrence Livermore National Laboratory, Livermore, CA, UCRL-MI-110498 (1992). Prepared for the 1992 CECAM Workshop, Orsay, France, September 5–14, 1992.

R

Remington, B. A., Glendinning S. G., Morales, R. I., Rothman, S., and Wallace, R. J., "Wölter X-Ray Microscope Characterization Measurements on Nova," *Rev. Sci. Instrum.* **63** (10), 5080–5082 (October 1992).

Remington, B. A. and Morales, R. I., *Reflectance Measurements of the Wölter X-Ray Microscope used at Nova*, Lawrence Livermore National Laboratory, Livermore, CA, UCRL-MI-111170 (1992). Prepared for the 34th Annual Meeting of the American Physical Society Division of Plasma Physics, Seattle, WA, November 16–20, 1992.

Remington, B. A., Weber, S. V.,Glendinning S. G., Kilkenny, J. D. Haan, S. W., and Wallace, R. J., *Laser-Driven Hydrodynamic Instability Experiments*, Lawrence Livermore National Laboratory, Livermore, CA, UCRL-JC-111286 (1992). Prepared for the 34th Annual Meeting of the American Physical Society Division of Plasma Physics, Seattle, WA, November 16–20, 1992.

Remington, B. A., Weber, S. V.,Wallace, R. J., Kilkenny, J. D., and Haan, S. W., *Multimode and 3-D Rayleigh-Taylor Experiments on Nova*, Lawrence Livermore National Laboratory, Livermore, CA, UCRL-JC-111171 ABS Rev. 1 (1992). Prepared for the 4th International Workshop on the Physics of Compressible Turbulent Mixing, Cambridge, England, March 29–April 1, 1993.

Remington, B. A., *Laser-Driven Hydrodynamic Instability Experiments*, Lawrence Livermore National Laboratory, Livermore, CA, UCRL-MI-111286 (1992). Prepared for the 34th Annual Meeting of the American Physical Society Division of Plasma Physics, Seattle, WA, November 16–20, 1992.

Ress, D. B., Bell, P., and Bradley, D. K., *Demonstration of a Time-Resolved X-Ray Ring Coded-Aperture Microscope for Inertial Confinement Fusion Applications*, Lawrence Livermore National Laboratory, Livermore, CA, UCRL-JC-112251 (1992). Submitted to *Applied Physics Letters*.

Ress, D. B., Bell, P., and Bradley, D. K., *X-Ray Images of Directly Driven Implosions Using a Time-Resolved Ring Coded-Aperture Microscope*, Lawrence Livermore National Laboratory, Livermore, CA, UCRL-MI-111180 (1992). Prepared for the 34th Annual Meeting of the American Physical Society Division of Plasma Physics, Seattle, WA, November 16–20, 1992.

Ress, D. B., Ciarlo, D. R., Kania, D. R., Bell, P., M, and Stewart, J. E., "A Ring Coded-Aperture Microscope for High-Resolution Imaging of High-Energy X Rays," *Rev. Sci. Instrum.* **63** (10), 5086–5088 (October 1992).

Ress, D. B., Trebes, J. E., Procassini, R. J., Mrowka, S., Da Silva, L. B., V, and London, R. A., *Soft X-Ray Moiré Deflectometer for Characterization of High-Density Plasma*, Lawrence Livermore National Laboratory, Livermore, CA, UCRL-JC-112386 ABS (1992). Prepared for Soft X-Rays in the 21st Century, Provo, UT, February 10–13, 1993.

Rhodes, M. A. and Taylor, J. B., *Pulse Power Requirements for Large Aperture Optical Switches Based on Plasma Electrode Pockels Cells*, Lawrence Livermore National Laboratory, Livermore, CA, UCRL-JC-109579 (1992). Prepared for the 20th International Power Modulator Symposium, Myrtle Beach, SC, June 23–25, 1992.

Rosen, M. D., *Recent Advances in Laser-Plasma Interactions at the Lawrence Livermore National Laboratory*, Lawrence Livermore National Laboratory, Livermore, CA, UCRL-MI-112160 (1992). Prepared for the International Symposium on Laser-Plasma Interactions, Shanghai, China, November 11, 1992.

Rotter, M. D., Doss, S. K., McCracken, R. W., and Erlandson, A. C., *Pump-Induced Wavefront Distortions in Laser Slabs: Experiment and Analytical Model*, Lawrence Livermore National Laboratory, Livermore, CA, UCRL-JC-112257 ABS & SUM (1992). Prepared for the Conference on Lasers and Electro-Optics 1993, Baltimore, MD, May 2–7, 1993.

Rotter, M. D., Erlandson, A. C., and McCracken, R. W., *Analytic Model for Calculating Pump-Induced Wavefront Distortions in Laser Slabs*, Lawrence Livermore National Laboratory, Livermore, CA, UCRL-MI-111193 (1992). Prepared for the Advance Program, International Conference on Lasers '92, Houston, TX, December 7–10, 1992.

S

Sacks, R. A. and Dixit, S. N., *Numerical Modeling of Transverse SRS and SBS in Large-Aperture High-Power Optical Components*, Lawrence Livermore National Laboratory, Livermore, CA, UCRL-MI-111926 (1992). Prepared for the Optical Society of America Nonlinear Optics '92, Maui, HI, August 18, 1992.

Sanchez, J. J., Collins, G. W., and Fearon, E. M., *DT and D_2 Retention in Plastic Shells*, Lawrence Livermore National Laboratory, Livermore, CA, UCRL-JC-108691 (1991). Prepared for the 38th American Vacuum Society National Symposium and Topical Conference, Seattle, WA, November 11–15, 1991.

Sharp, W. M., Barnard, J. J., and Grote, D. P., *How to Hold a Pulse Together*, Lawrence Livermore National Laboratory, Livermore, CA, UCRL-MI-112261 (1992). Prepared for the 34th Annual Meeting of the American Physical Society Division of Plasma Physics, Seattle, WA, November 16–20, 1992.

Sharp, W. M., Barnard, J. J., Yu, S. S., Fessenden, T. J., and Grote, D. P., *Envelope Model of Beam Transport in ILSE*, Lawrence Livermore National Laboratory, Livermore, CA, UCRL-JC-112244 ABS (1992). Prepared for the Computational Accelerator Physics Conference 1993, Pleasanton, CA, February 22–26, 1993.

Sharp, W. M., Callahan, D. A., Fessenden, T. J., and Langdon, A. B., *Correction of Longitudinal Errors in Accelerators for Heavy-Ion Fusion*, Lawrence Livermore National Laboratory, Livermore, CA, UCRL-JC-112377 ABS (1992). Prepared for the 1993 Particle Accelerator Conference, Washington, DC, May 17–20, 1993.

Sharp, W. M., Rangarajan, G., and Sessler, A. M., *Multi-Mode Discrete-Cavity Simulation of a Standing-Wave Free-Electron Laser*, Lawrence Livermore National Laboratory, Livermore, CA, UCRL-JC-112662 ABS (1993). Prepared for the 1993 International Symposium on Optical Applied Science and Engineering, San Diego, CA, July 11–16, 1993.

Shepard, T. D. and Darrow, C. B., *Thomson Scattering Simulations for Nova Experimental Targets*, Lawrence Livermore National Laboratory, Livermore, CA, UCRL-MI-111175 (1992). Prepared for the 34th Annual Meeting of the American Physical Society Division of Plasma Physics, Seattle, WA, November 16–20, 1992.

Shestakov, A. I., Prasad, M. K., Harte, J. A., and Kershaw, D. S., *Point-Centered Finite Element Transport in Lagrangian Codes*, Lawrence Livermore National Laboratory, Livermore, CA, UCRL-JC-111692 ABS (1992). Prepared for the Nuclear Explosive Code Developers Conference, Sunnyvale, CA, November 2–6, 1992.

Smith, L. K., Payne, S. A. Chai, B. H. T., Chase, L. L., and Kway, W. L., "Investigation of the Laser Properties of Cr^{3+}:LiSrGaF$_6$," *IEEE J. Quantum Electron.* **28** (11), 2612–2618 (November 1992).

Smith, L. K , Payne, S. A., Kway, W. L., Deloach, L. D., and Krupke, W. F., *Determination of Laser Efficiencies for Yb-Doped Apatite-Structure Hosts*, Lawrence Livermore National Laboratory, Livermore, CA, UCRL-JC-111850 ABS (1992). Prepared for the Advanced Solid State Lasers th Topical Meeting, New Orleans, LA, February 1–3, 1993.

Sommargren, G. E. and Seppala, L. G., *Condenser Optics, Partial Coherence and Imaging for Soft X-Ray Projection Lithography*, Lawrence Livermore National Laboratory, Livermore, CA, UCRL-JC-110134 Rev. 1 (1992). Submitted to *Applied Optics*.

Spitzer, R. Kauffman R. L., Cerjan, C. J., Phillion, D. W., and Orzechowski, T. J., *Soft X-Ray Production from Laser-Produced Plasmas for Soft X-Ray Projection Lithography*, Lawrence Livermore National Laboratory, Livermore, CA, UCRL-MI-112139 (1992). Prepared for the 34th Annual Meeting of the American Physical Society Division of Plasma Physics, Seattle, WA, November 16–20, 1992.

Swa[illegible]oski, T. L., *Graphical User Interface for AMOS and POISSON*, Lawrence Livermore National Laboratory, Livermore, CA, UCRL-JC-112263 ABS (1992). Prepared for the Computational Accelerator Physics Conference 1993, Pleasanton, CA, February 22–26, 1993.

T

Thomas, I. M., "Method for the Preparation of Porous Silica AR Coatings Varying in Refractive Index from 1.22 to 1.44," *Appl. Opt.* **31** (28), 6145–6149 (October 1, 1992).

Trebes, J. E., Anderson, E., Kern, D., Da Silva, L. B., Brase, K., McNulty, I., Nugent, K. A., Szöke, H, and Yorkey, T. J., *Three Dimensional, High-Resolution Soft X-Ray Imaging*. Lawrence Livermore National Laboratory, Livermore, CA, UCRL-JC-112119 ABS (1992). Prepared for the 1993 International Conference on Confocal and 3-D Image Processing, Sydney, Australia, February 8–11, 1993.

Trebes, J. E., *Imaging in Three Dimensions with Soft X Rays*, Lawrence Livermore National Laboratory, Livermore, CA, UCRL-MI-112118 (1992). Prepared for the Workshop on Scientific Applications of Short Wavelength Coherent Light Sources, Berkeley, CA, October 21, 1992.

Trebes, J. E., *Some Topics in X-Ray Imaging*, Lawrence Livermore National Laboratory, Livermore, CA, UCRL-MI-112143 (1992). Prepared for the Imaging Technologies, Algorithms and Applications Conference, Orlando, FL, October 25–26, 1992.

Trebes, J. E., *X-Ray Laser Deflectometry and Interferometery of Laser-Produced Plasmas*, Lawrence Livermore National Laboratory, Livermore, CA, UCRL-MI-112297 (1992). Prepared for the 34th Annual Meeting of the American Physical Society Division of Plasma Physics, Seattle, WA, November 16–20, 1992.

Tsang, K. T., Ho, D.-M., Siverson, R. J., and Wong, A. Y., *Stratospheric Ozone Conservation by Electron Attachment to Chlorine Atoms*, Lawrence Livermore National Laboratory, Livermore, CA, UCRL-JC-110318 (1992). Prepared for Controlled Active Global Experiments, Piero Caldirola School, Varenna, Italy, September 5–12, 1990.

V

Velsko, S. P., *Strategy and Tactics in the Search for New Harmonic-Generating Crystals*, Lawrence Livermore National Laboratory, Livermore, CA, UCRL-JC-105000 (1991); *Symposium on Nonlinear Materials*, Ch. 23, pp. 343–359.

Vernon, S. P. Stearns, D. G., and Rosen, R. S , *Ion-Assisted Sputter Deposition of Mo/Si Multilayers*, Lawrence Livermore National Laboratory, Livermore, CA, UCRL-JC-109359 (1992); *Physics of X-Ray Multilayer Structures*.

Villeneuve, D. M., Lafontaine, B., Enright, G. D., Dunn, J., Baldis, H. J., Rosen, M. D., Young, P. E., and Matthews, D. L., *Temperature Determination in X-Ray Laser Plasmas by Thomson Scattering*, Lawrence Livermore National Laboratory, Livermore, CA, UCRL-JC-109721 (1992). Prepared for the Fifth Topical Meeting of the Optical Society of America on Short-Wavelength Coherent Radiation: Generation and Applications, Monterey, CA, April 8–10, 1991.

W

Wall, M. A., Barbee, T. W., and Weihs, T. P., *Transmission Electron Microscopy Study of Thick Copper–304 Stainless Steel Multilayers*, Lawrence Livermore National Laboratory, Livermore, CA, UCRL-JC-112054 ABS (1992). Prepared for the Materials Research Society 1993 Spring Meeting, San Francisco, CA, April 12–16, 1993.

Wallace, R. J. and Bernat, T. P., *Surface Perturbation of ICF Capsules by Laser Ablation*, Lawrence Livermore National Laboratory, Livermore, CA, UCRL-MI-112153 (1992). Prepared for the 39th American Vacuum Society National Symposium and Topical Conference, Chicago, IL, November 9–13, 1992.

Webb, M. S., Eimerl, D., and Velsko, S. P., "Wavelength-Insensitive Phasematched Second-Harmonic Generation in Partially Deuterated KDP," *J. Opt. Soc. Am. B* **9** (7), 11118–1127 (July 1992).

Weber, S. V., Glendinning S. G., Krauer, J. P., and Dixit, S. N., *Imprinting of Laser Intensity Fluctuations on Directly Driven Foils*, Lawrence Livermore National Laboratory, Livermore, CA, UCRL-MI-111160 (1992). Prepared for the 34 Annual American Physical Society Meeting of the Division of Plasma Physics, Seattle, WA, November 16–20, 1992.

Wegner, P. J., Henesian, M. A., Ehrlich, R. B., Bibeau, C., Speck, D. R., Laumann, C. W., Lawson, J. K., and Weiland, T. L., "Harmonic Conversion of Large-Aperture 1.05-μm Laser Beams for Inertial Confinement Fusion Research," *Appl. Opt.* **31** (30), 6414–6426 (October 20, 1992).

Wegner, P. J., *Measurements and Modeling of Laser Irradiance in the High-Power Third-Harmonic Nova Focus, Vol. 2: Data Book*, Lawrence Livermore National Laboratory, Livermore, CA, UCRL-ID-110480 Vol. 2 (1992).

Weihs, T. P., Barbee, T. W., and Wall, M. A., *Solid State Amorphization and Crystallization in Cu/Zr Multilayers*, Lawrence Livermore National Laboratory, Livermore, CA, UCRL-JC-112055 ABS (1992). Prepared for the Materials Research Society 1993 Spring Meeting, San Francisco, CA, April 12–16, 1993.

Weihs, T. P., Barbee, T. W., and Wall, M. A., *Correlating the Strength of Cu/Zr Multilayers with Variations in the Structure and Thickness of Individual Layers*, Lawrence Livermore National Laboratory, Livermore, CA, UCRL-JC-112056 ABS (1992). Prepared for the Materials Research Society 1993 Spring Meeting, San Francisco, CA, April 12–16, 1993.

Wilks, S. C., Kruer, W. L., Langdon, A. B., and Estabrook, K. G., "Theory and Simulation of Raman Scattering at Near Forward Angles," *Phys. Fluids B* 4 (9), 2794–2800 (1992).

Wilks, S. C., Kruer, W. L., Langdon, A. B., and Tabak, M., *Absorption of Ultra-Intense Laser Pulses*, Lawrence Livermore National Laboratory, Livermore, CA, UCRL-JC-109745 REP (1992). Submitted to *Physical Review Letters*.

Wilks, S. C., Kruer, W. L., Mori, W., Campbell, E. M., Tabak, M., and Darrow, C. B., *Ultrahigh-Intensity, Short Pulse Laser-Plasma Interactions*, Lawrence Livermore National Laboratory, Livermore, CA, UCRL-MI-111195 Rev. 1 (1992). Prepared for the Optical Society of America Annual Meeting and 8th Interdisciplinary Laser Science Conference, Albuquerque, NM, September 20–25, 1992.

Wilks, S. C., Kruer, W. L., Mori, W., and Langdon, A. B., *Simulations of Ultra-Intense Laser-Plasma Interactions*, Lawrence Livermore National Laboratory, Livermore, CA, UCRL-MI-112253 (1992). Prepared for the 34th Annual Meeting of the American Physical Society Division of Plasma Physics, Seattle, WA, November 16–20, 1992.

Wilks, S. C., Kruer, W. L., and Mori, W., *Harmonic Generation of Ultra-Intense Laser Pulses Reflected from an Overdense Plasma*, Lawrence Livermore National Laboratory, Livermore, CA, UCRL-JC-111509 (1992). Submitted to *IEEE Transactions on Plasma Science*.

Williams, E. A., *Action Transfer in Three-Way Coupling*, Lawrence Livermore National Laboratory, Livermore, CA, UCRL-MI-111153 (1992). Prepared for the 34th Annual Meeting of the American Physical Society Division of Plasma Physics, Seattle, WA, November 16–20, 1992.

Z

Ze, F., Kauffman R. L., Bell, P., Wiedwald, J. D., Kilkenny, J. D., Hanks, R. L., Stewart, J., Dean, D., and Bower, J., *A New Multichannel Soft X-Ray Framing Camera for Fusion Experiments*, Lawrence Livermore National Laboratory, Livermore, CA, UCRL-JC-110094 (1992). Prepared for the 9th Topical Conference on High Temperature Plasma Diagnostics, Santa Fe, NM, March 15–19, 1992.

Ze, F., Kauffman R. L., Suter, L. J., Kilkenny, J. D., Ress, D. B., Wiedwald, J. D., Wallace, R. J., Cray, M., and Bocher, J. L., *Investigation of Electron Energy Transport and Spatial Dependence of X-Ray Emission in Laser-Driven Plasmas*, Lawrence Livermore National Laboratory, Livermore, CA, UCRL-MI-110973 (1992). Prepared for the 34th Annual Meeting of the American Physical Society Division of Plasma Physics, Seattle, WA, November 16–20, 1992.

DATE
FILMED
9/8/93

END